UNIVERSITÀ
DEGLI STUDI
DI PADOVA

**UNIVERSITY OF PADUA**

**Department of Industrial Engineering DII**

Master degree in Materials Engineering (LM-53)

# HYDROGEL MATERIALS FOR BIOMEDICINE: MECHANOBIOLOGY STUDIES AND INJECTABLE SCAFFOLDS FOR VACCINES

*Supervisor:* Giovanna Brusatin, *Associate Professor*

*Co-supervisor:* Alessandro Gandin, *Engineer*

*Graduating student:* Elisa Pozzebon 1179199

ACADEMIC YEAR 2019 / 2020

# Abstract

Mechanobiology is an emerging field which is fundamental in the study of cellular and tissue behaviour and crucial to understand the emergence and evolution of diseases. Materials that can be used as cell-culture substrates and induce different mechanical stimuli are fundamental for these biological studies. For this, hydrogels materials have shown to be suitable as they adequately mimic the natural environment of cells, tissues and organs. Nowadays standardized synthesis methods of hydrogels aren't available on a commercial level. This study is focused on the development and optimisation of standardized and reproducible protocols, for the synthesis of hydrogels and their mechanical characterisation. These methods allowed to synthetize polyacrylamide and polyethylene glycol-based hydrogels with a gradient of elastic moduli and a good control of the cell-adhesion type and properties. These 2D substrates were tested as cell-culture substrates, showing that a gradient of increasing mechanosensitive behavior nicely matches hydrogel rigidity gradient. Two simple and cheap methods were also developed for the mechanical characterization of hydrogels, macroindentation and micropipette aspiration tests, which allowed to measure the elastic moduli of synthetized hydrogels. About the macroindentation method, an analytical equation for the experimental calculation of elastic moduli of hydrogels was developed based on Finite Element Method simulations and mathematical correlations, that implemented and optimized theoretical models suggested in literature. This equation considers all boundary effects and can be applied in the case of large deformations and non-linearity of the material. In addition, hydrogels can be used in a new promising frontier, which is the development of cancer vaccines in a personalized medicine perspective. In this work protocols which allows the preparation of cryogels, highly porous and adhesive for cells, were developed.

# Index

# Introduction

Mechanobiology is an emerging field, which can be defined as the study of how cells perceive physical forces and how they translate them into biochemical and biological responses. Nowadays, it is fundamental in the study of cellular and tissue behaviour and it is very useful to understand the emergence and evolution of diseases. Biological substrates are fundamental tools which allows mechanobiology studies. In order to be effective, these materials must provide a substrate for cell cultures and to transmit them mechanical stimuli. For decades and still nowadays, cell biology studies have been performed on plastic or glass cell culture substrates. However, these materials proved to be inadequate to study the behaviour of cells and tissues because they could not adequately mimic the natural environment of cells, tissues and organoids, in particular their rigidity and complexity. In fact, their stiffness is significantly higher than the one of physiological tissues, so they induce different behaviours on cells cultured on them. In recent years, different substrates have emerged to be cell cultures substrates. One of them are hydrogels which provide an environment to cells that allows to adequately mimic the natural environment of cells. These materials are able to simulate a wide range of chemicals and physical physiological properties and to induce different mechanical stimuli to cells. However, nowadays standard protocols to synthetize these materials are not available on a commercial level. Many studies are reported in literature, but these protocols are difficult to standardize, being long and complex[1,2], and don't offer the synthesis of ready to use hydrogels. In addition, hydrogels can be used in a new promising frontier, which is the personalized medicine. In fact, hydrogels can be used to create materials that are capable of recapitulate disease environment or applied for disease treatments. For example, they can be used in the screening of drugs, to regenerate tissues and, as in the present study, to develop cancer vaccines. In this thesis work, standardized and reproducible protocols have been developed and optimised, which are able to produce hydrogels for biological studies and cryogels for vaccines development.

Two types of synthetic hydrogels for cell cultures were optimized to achieve variable and controlled values of their elastic moduli, in order to induce different mechanical stimuli to cells. These methods allow to obtain and characterize hydrogels for cell cultures with high reproducibility, using common equipment which can be found in any biological laboratory.

Connected to this, two standardized, easy and cheap methods have been designed and developed to determine the elastic modulus of hydrogels: macroindentation and micropipette aspiration. In both cases theoretical models reported in literature are used to interpret data. They are based on Hertzian contact theory, improved for large/non-linear deformations and for geometrical features (finite height of the hydrogels for macroindentation). On top of that, for macroindentation a case-specific model taking into account also the finite dimension of the samples was developed, using finite element simulations and mathematical correlations that allowed to formulate an improved analytical equation for the elastic modulus calculation.

Concerning cryogels, they are a special type of porous hydrogels, synthetized during this thesis for the realization of cell-based cancer vaccine. They are able to support specific antigen presenting cells and thanks to their porosity are accessible to the immune system cells. These materials were characterized by scanning electron microscopy, which was fundamental to study their microstructure. A preliminary evaluation of the biological applications of both hydrogels and cryogels was done. The hydrogels with variable stiffness were seeded with cells in order to verify their capability to be used as cell culture substrates for mechanobiology studies. Immunofluorescence analysis were used to analyse the localization of two specialized proteins, transcription factors, that are mechanosensors, YAP and TAZ, inside the nuclei and in the cytoskeleton. In addition, hydrogels for cancer vaccines were seeded with antigen presenting cells and implanted under skin in a mouse, to study the stimulated immunity response.

Chapter one describes the basic concepts of mechanobiology and of the key actors involved. Chapter two describes some basic knowledge about the immune system and cancer vaccines. Chapter three is related to biomaterials, in particular natural and synthetic hydrogels, which well mimic cell microenvironment and living tissues, and cryogels. Chapter four illustrated the mechanical properties of hydrogels and the main techniques that are normally used to characterize them. Chapter five delineates the methods implemented and optimised in this study. Chapter six describes the theoretical models implemented and developed to calculate the elastic modulus of hydrogels for the macroindentation method and chapter seven illustrates main experimental results: the synthesis, mechanical and biological characterizations results of hydrogels and cryogels. This thesis work has been made in close collaboration with the laboratory of Prof. Stefano Piccolo of the Department of Molecular Medicine in Padua. In addition, some results have been carried out with the collaboration of Prof. Lucia Nicola (DII), Prof. Paolo Netti and Maurizio Ventre (IIT Laboratory of Napoli), Prof. Paolo Sgarbossa (DII) and Prof. Katia Brunelli (DII).

# Chapter 1

# Mechanobiology

Complex living organisms are composed by many cells that are kept together by interactions between cells and the extracellular matrix (ECM). Cells can sense and respond, at cellular level, to mechanical signals that comes from the environment around them: they interact to each other and with the extracellular matrix with physical forces and this determine their macroscopic form which, in turn, gives a function to the cell. These phenomena are studied by mechanobiology that can be defined as the study of how cells perceive physical forces and how they translate them into biochemical and biological responses[3]. But these are not the only signals that affect cells: the microenvironment around them is composed by several factors that influence the normal cell function such as growth, migration, proliferation and differentiations of stem cells. In general, these factors can be divided into two categories: soluble cues, such as growth factors, metabolites and dissolved gases, that are characterized by physical, chemical and mechanical properties, and insoluble cues that are architectural features of the microenvironment, for example the composition and the mechanical properties of the extracellular matrix[3].

Mechanotransduction is the major challenge in mechanobiology and it is an emerging field at the interface of biology, physics and engineering. It focuses on how the mechanics of cells or tissue and physical forces influence the behaviour of cells[4]. The mechanotransduction involves intra- and extracellular components. Cells translate inputs into a cascade of biochemical events that leads to gene expression regulators[5]. For example, it has been observed, in response to different stiffness of ECM, the differentiation of mesenchymal stem cells (MSC), promoting osteogenesis rather than adipogenesis[6]. The mechanotransduction is also involved in many different diseases, such as muscular dystrophies and metastasis[6]. The key components in mechanotransduction are: integrins that regulate cell-cell interaction, extracellular matrix (ECM) and intracellular cytoskeleton (CSK). These elements keep cells in shape, regulate cell proliferation, differentiation and stemness, migration and cell death[7]. Many intracellular signalling pathways combine mechanical forces and biochemical responses[4], the one

considered in this study involves YAP/TAZ co-activators. All these key components involved in mechanobiology phenomena are shortly described in the following paragraphs

## 1.1 Cytoskeleton

Cytoskeleton is a network of protein filaments present in the cytoplasm of a cell. It develops from the nucleus to the cell membrane and it defines the shape and the mechanical behaviour of the cell. These proteins are also fundamental to form adhesions within cells and between cells and ECM. The mammalian CSK is composed by three types of protein filaments: actin filaments, microtubules (MTs) and intermediate filaments (IFs). The first two are polar filaments with two different ends, that are capable to generate pushing and pulling forces by coupling polymerization to nucleotide hydrolysis. IFs are non-polar and more stable [4]. Some of the major proteins that form the three filaments are: actin, vinculin and talin.

Actin is a protein existing in most eukaryotic cells, that can have two forms: the monomeric one is called G-actin and the filamentous one, F-actin. The filaments are formed by the spontaneous polymerization of G-actin monomers, forming a double-strained right-hand helical filament. The monomers are globular and dense. The polymerization and de-polymerization of F-actin is regulated by the local concentration of G-actin, the presence of F-actin binding proteins, the concentration of ions in the environment. Mechanical forces applied play a fundamental role in F-actin polymerization[8].

Vinculin is a membrane-cytoskeletal protein that is involved in the connection of F-actin fibers to integrin adhesion molecules in focal adhesion sites. For this reason, it plays an important role mediating the link between the cytoskeleton and cell-ECM adhesion sites.

Talin is a high molecular weight protein, it is very important because it is involved in the connection of actin filaments of cytoskeleton with integrin receptors, by the interaction with vinculin and α-actinin[8]. It is present in high concentration in focal adhesion sites. In his native state, talin has a conformation that hides several binding sites for actin, vinculin and integrins. The activation of this protein is required to stabilize the adhesion between cell and ECM. The activation mechanism is supposed to be induced by the application of a force because the mechanical stretching of talin promotes the bound with vinculin. This makes it a fundamental protein in mechanotransduction[8].

Actin filaments, microtubules and intermediate filaments can be classified as semiflexible polymers because they remain straight under the influence of thermal fluctuations over a length

scale comparable to their 'persistence length'. Actin filaments and IFs are considered the main actors to provide cell stiffness while MTs, that are more rigid, can provide resistance to compression forces. Under the influence of mechanical shear forces, the networks of F-actin and IFs increases their stiffness. This phenomenon allows cells to increase the stiffness of their cytoskeleton when are in contact with hard substrates[4].

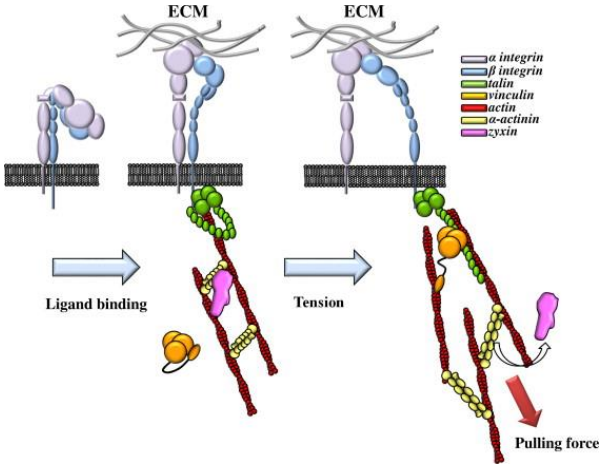


**Figure 1.1.** *Schematic of the integrated mechanotransduction at the integrin-mediated adhesion site subjected to an external force*[9].

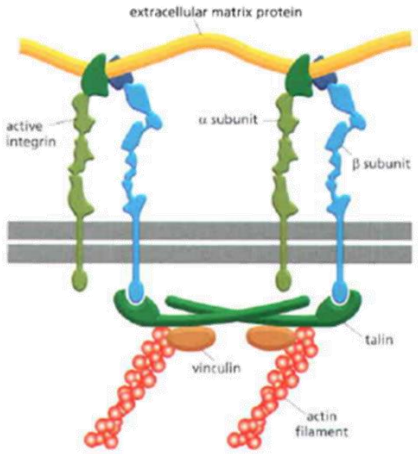


**Figure 1.2.** *Integrin-mediated adhesion site.*

In cellular mechanosensing, more attention is paid to the contribution of actin, because it is responsible for traction force generation. In response to mechanical or chemical stimuli, cells are able to migrate thanks to the presence of stress fibers, which are contractile bundles of actin and myosin. In general, within the cell, actin filaments can be arranged to form multiple structures. Stress fibres are large assemblies of actin filaments that can span the length of the cell. The presence of myosin in stress fibres enables contractility.

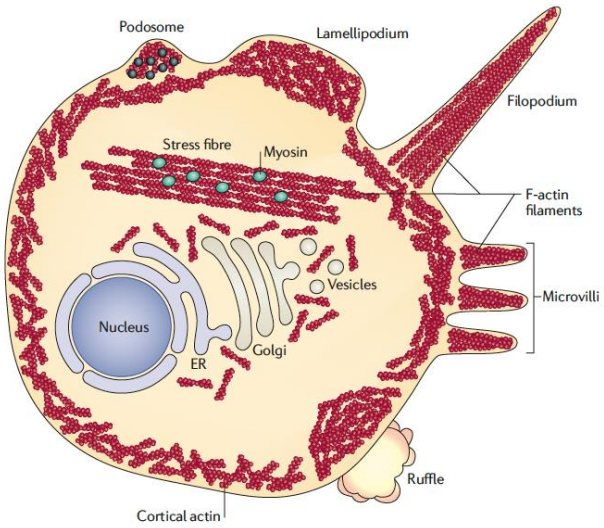


**Figure 1.3.** *Actin organization in cell cytoplasm*[10].

For example, in the migrating cell, there are three main types of stress fibers: ventral stress fibers, transverse arcs, and dorsal stress fibers. These are represented in figure 1.4. Ventral stress fibers usually extend almost the entire cell length and are anchored at both ends to focal adhesions (FAs). They are located on the ventral surface of the cell and they are involved in the adhesion and the contraction. Dorsal stress fibers are shorter and only connected to a focal adhesion at one end. They are located at the leading edge of the cell where they attach to focal adhesions and extend dorsally, towards the cell centre to attach to transverse arcs. Transverse arcs are not directly linked to focal adhesions, and typically flow from the leading edge of the cell, back towards the cell centre. With the increase of the stiffness of the substrate, the degree of actin crosslinking and bundling increases. For example, fibroblasts cells, thanks to this behaviour, can adapt their stiffness to that of the substrate[4].

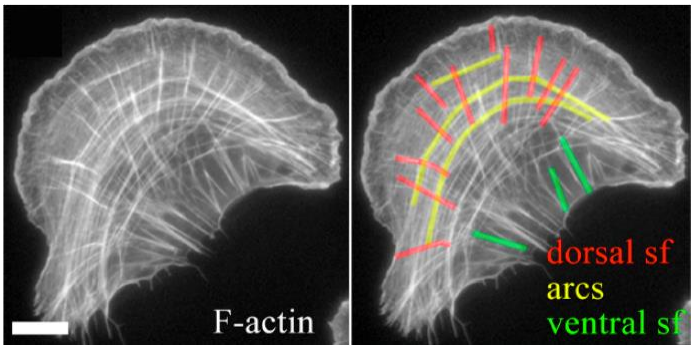


**Figure 1.4.** *Schematic representation of stress fibers of a cell cultured on a stiff two-dimensional substrate.*

## 1.2 Extracellular Matrix (ECM)

The extracellular matrix is a complex and organized network composed by proteins that forms the scaffold to which cells adhere. Its composition and structure varies with the tissue or organism taken into account, but it is composed by the same types of macromolecules. Its main functions are: give mechanical support to cells and tissues, and act as a supply for growth factors, cytokines and proteolytic enzymes. There are two main types of ECM: the basement membrane and the interstitial connective tissue matrix.

The first one is a thin structure that provides a two-dimensional substrate, where polarized cells can adhere such as epithelial and endothelial cells. Its function is to separate the epithelium from the surrounding stroma. It is composed of two layers, the basal lamina and the underlying layer of reticular connective tissue. The underlying connective tissue attaches to the basal lamina with collagen anchoring fibrils and fibrillin microfibrils. Interstitial matrix surrounds animal cells and it is composed by polysaccharides gels and fibrous proteins. Its function is to act as a compression buffer against the stress placed on the ECM. Interstitial matrix and cells form the connective tissue: one of the four types of animal tissue that provides a fibrous 3D scaffold.

The proteins that composes ECM can be divided into fibrous proteins and glycosaminoglycans (GAGs). The main component of ECM is collagen, a fibrous protein that consists of a triple helix of elongated fibril formed by amino acids bound together. The diameter and organization of its fibers are tailored to the biomechanical function of each tissue. Under influence of force, ECM proteins could also act as a mechano-transducer by exposing cryptic sites and growth factors. Collagen is used as a biomaterial for in vitro studies and tissue engineering, thanks to its biocompatibility and physiological scaffold role; but it isn't able to mimic the full tissue-specific context, the architecture and the chemical composition, of the ECM, because, during the progression of diseases and the aging, the characteristics of the in vivo ECM changes[4].

Fibronectin is a dimeric glycoprotein, with a molecular weight of about 220'000 kDa, produced by many cells and tissues, present in loose and dense connective tissue. Its amino acid composition allows it to bind both proteins of the plasma membranes of the connective cells and components of the extracellular matrix, such as collagen fibers. For this reason, it is fundamental for cell attachment and migration. Its monomer is composed by approximately 30 Fn domains, two monomers can bind each other by a disulphide bond. Dimes can bind together with other dimers, collagen and proteoglycans[4]. A human fibronectin molecule is formed by

two very similar polypeptide chains, joined by disulphide bonds in the C-terminal site. Each of the chains has a length of 60-70 nm and a thickness of 2-3 nm. The main role of fibronectin is to make cells adhere to all types of extracellular matrices; it is in fact called 'adhesion molecule'. It can interact with ECM's proteins, forming an interconnected network, and with cells thanks to the presence of Arg-Gly-Asp (RGD) cell-binding site. In addition, external mechanical forces can induce the stretching of fibrous protein and consequently the exposition of cryptic binding sites. It also influences the shape and organization of the cytoskeleton; it is essential during cell migrations and in the cell differentiation processes that take place during embryogenesis. Fibronectin is also important in wound healing processes, since it facilitates the migration of macrophages and other cells of the immune system towards the injured part; it is crucial during the early stages of blood coagulation as well, since allows adhesion of platelets to the damaged area of the wall of blood vessels.

Another type of proteins that are present in the ECM are proteoglycans that are composed by a core protein which binds glycosaminoglycans (GAGs), that are linear anionic polysaccharides (carbohydrate polymers) that absorbs divalent cations and water via osmosis. And so, they are able to keep the ECM and the resident cells lubricated and hydrated. Proteoglycans may also help to trap and store growth factors within the ECM[4].

The extracellular matrix (ECM) is characterized by physical properties that provides mechanical cues to the cells. In the case of abnormal changes in the stiffness of ECM, various diseases start and progress, such as cancer and fibrosis. The stiffness of tissues subjected to cancer is up to ten time higher than a healthy tissue, and so allows the survival and the proliferation of tumor cells[4]. In mechanobiology the ECM plays a central role due to the many factors that acts on cell behaviour such as global and local stiffness, matrix topography, porosity and dimensionality.

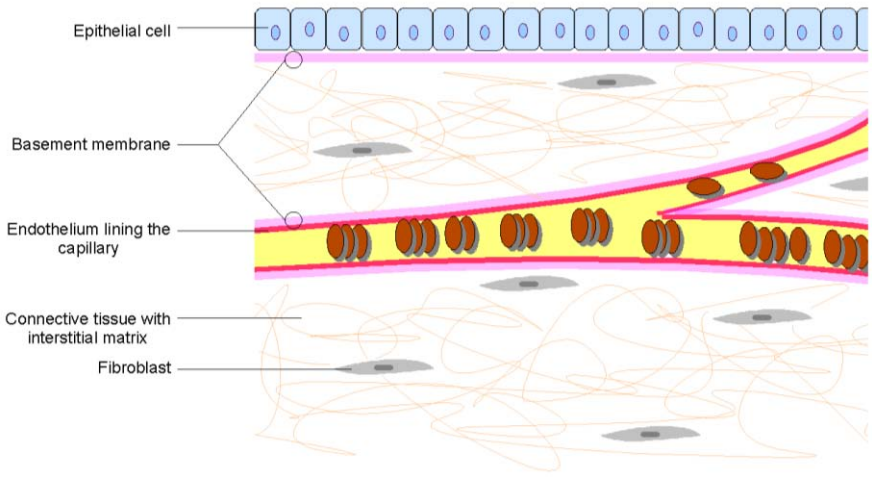


**Figure 1.5.** *Illustration of extracellular matrix in relation to epithelium, endothelium and connective tissue.*

## 1.3 Integrins and focal adhesion

Integrins are heterodimeric transmembrane proteins that physically connect the ECM to the CSK and act as a bidirectional signalling receptor. For these reasons they are one of the major players in mechanotransduction[4]. The connection with ECM ligands is allowed because most of integrins can recognize multiple ligands containing the same binding motifs, for example RGD motif. On the other side, the cytoplasmic tail of integrins can links to the cytoskeleton, in particular, with talin, α-actin and vinculin[8]. Integrins are composed by two subunits: α and β heterodimers. 24 different heterodimers have been discovered which are formed combining 18 different α subunits and β subunits. The integrin αvβ3 can bind vitronectin, fibronectin and fibrogen through the RGD-binding motif. Integrin adhesions can be classified as slip or catch-bond adhesion molecules according to their bond lifetime under applied force. Integrins can assume an inactive conformation, and they can be activated by two types of signals[4]:

- Inside-out signals: intracellular proteins bind to the tail region of integrins, and this led to conformational changes in the head region, increasing the affinity for its extracellular ligands.
- Outside-in signals: the binding of ligand led to conformational changes that activate intracellular signals.

Very important, integrins activation can then trigger F-actin fibre polymerization[8]. In addition, ligand binding also promotes integrin clustering, essential for cell spreading. The connection, in fact, occurs typically in clusters of integrins, called focal adhesions (FAs). A focal adhesion is the adhesion between cell and matrix that is usually associated with actin stress fibers. The

form of focal adhesions is elongated and are found at the front, rear and periphery of the cell [2]. These structures are discrete and dynamic, and can transmit intracellular myosin-generated contractile forces and extracellular signals. For this reason, focal adhesions act as mechano-sensors. They are one of the most mature ECM-cell contact type, besides fibrillar adhesions, and are therefore associated with a larger variety of proteins from the adhesion[4]. When mechanical forces are applied to focal adhesions, talin can be stretched and so other binding sites can be exposed, activating a wide range of signalling pathways and genetic programs to control cell survival, fate and behaviour.

## 1.4 Mechanotransduction from a molecular perspective: YAP/TAZ

During the normal life of cells many types of forces interact with them, for example they are subjected to shear stresses during breathing and blood flow, or compression and tension due to the contraction of muscles. The sensitivity of cells to forces applied on them and to the substrate has been used as a very important tool in tissue engineering. If the design of biomaterials is optimal, the cells can be guided towards generating a functional tissue. For example, stem cells differentiation can be programmed for regenerative medicine applications[4]. Some of the physical stimuli that can be exerted on cells and organs are heart pumping, muscle contraction, cytoskeletal tension and ECM rigidity. Since the whole system must be kept in equilibrium, cells react translating properly external mechanical cues into intracellular biochemical signals[11]. Some studies showed that multiple types of mechanical inputs in different cellular settings can influence the regulation of two transcriptional co-factors: YAP and TAZ[12].

The adhesion between cells and ECM is performed by more than 150 proteins, some of them are integrins that create the interaction. Each protein has a specific pathway. Mechanosensing mediated by integrins regulate gene transcription by activating various downstream signalling cascades connected to gene expression. A network that links integrin-mediated mechanosensing is the Hippo network. Its functioning is similar to the path that suppresses cancer in vertebrates. The most important components involved are transcription co-activators YAP (Yes-Associated Protein) and TAZ (Transcriptional co-Activator with PDZ-binding motif or WWTR1)[4]. There are proteins that bind themselves with transcription factors and drive the transcriptional program that specifies cell growth, proliferation and cell fate decisions: in the nucleus YAP and TAZ bind to the DNA through TEAD complex and control the expression of genes involved in cell cycle, regulation, replication and repair, cycling gene expression and mitotic kinases[12].

They are also highly mechanosensitive transduction regulators that act as a molecular switch and represent the explanation on how the external forces to the cell could be connected to the genes within its nucleus. Each cell type reacts differently to the activation and deactivation of specific genes. For example, if the amount of YAP / TAZ is increased, the cells stop differentiating and go back to the proliferation phase. Since the molecular structure of these two mechanotrasductors is very similar and perform superimposable functions, these two proteins are referred to as one: YAP / TAZ. Their activity needs integrity of the actin cytoskeleton but doesn't depend on the ratio between F-actin and G-actin, since the co-activators are inhibited and confined in the cytoplasm in rounded cells even if there is a high amount of F-actin. Instead, the activation of YAP/TAZ is influenced by the organisation of F-actin in the cytoskeleton and by its ability to perceive tension.

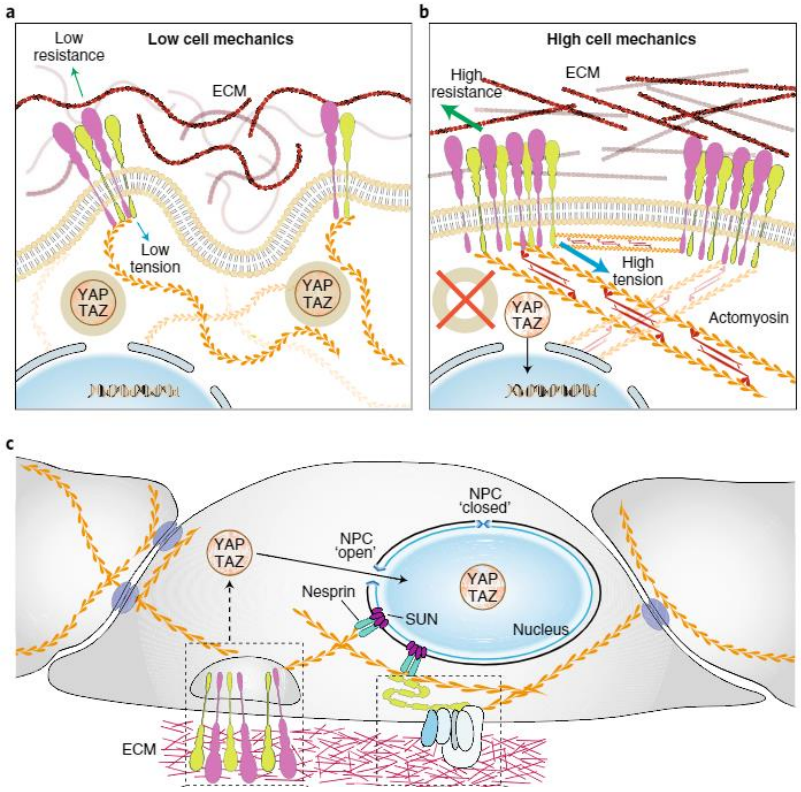


**Figure 1.6.** *Representation of YAP7TAZ mechano-regulation by ECM tension*[12].

In figure 1.6 can be seen the schematic representation of YAP/TAZ mechano-regulation by ECM tension. In a cell not subjected to external stimuli YAP / TAZ are located in the cytoplasm of the cell, but when the cell is pulled or deformed, these proteins translocate from the cytoplasm to the nucleus. These stimuli can be generated increasing the stiffness of the substrate. In fig. 1.6a, ECM has a low resistance and so, focal adhesion maturation is reduced, actomyosin cytoskeleton is relaxed and YAP/TAZ are confined in the cytoplasm, in an inactive

state. In fig.1.6b, the ECM has a high resistance and consequently there is a high tension on integrins, that aggregates in clusters to form focal adhesions. FAs induce the contraction of cytoskeleton and the translocation of YAP/TAZ inside the nucleus. In fig.1.6c is represented the pathway of mechano-transduction inside the cell. The mechanical strain is transferred from the ECM to the cytoskeleton, through integrins and cell-cell adhesion proteins. The physical signal is then transduced to the nucleus by Nesprin and SUN complexes. The traction force that arrives to the nucleus, open nuclear pores, allowing the permeation of YAP/TAZ inside it. In turn, they can co-operate as transcription factors[12].

If the cells are seeded on stiff substrate YAP/TAZ localize in the nucleus, while if cell substrate is soft YAP/TAZ are inactive in the cytoplasm. Inside the cell, YAP / TAZ activates the transcription of genes that induce cell growth and proliferation. This is the mechanism by which molecular disruption works. If, on the other hand, the cells are seeded on a compliant substrate, the two mechanotransducers remain in the cytoplasm, where they degrade[11]. In fig. 1.7 can be observed a scheme that represents the influence of YAP/TAZ on subcellular localization and activity. In the A part of the figure, is displayed the regulation of gene expression inside the cell: YAP and TAZ bind to TEAD in the nucleus, when mechanistically activated. In the B parts of the figure 1.7, are compared the inhibited condition on the left, to the activated one on the right. In this case nuclei are painted red[11].

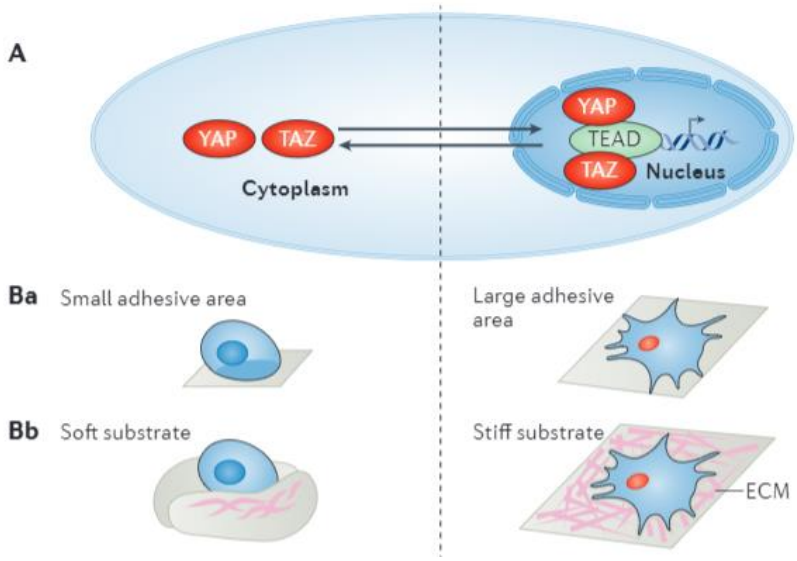


***Figure 1.7:*** *schematic representations of the mechanical stimuli that influence YAP and TAZ subcellular localization and activity*[11].

In addition, the activity of these co-activators can be influenced by the confluence and the degree of cell spreading, in fact cells plated in a small confined area inactivate YAP/TAZ and

cells seeded in large fibronectin island, with the same substrate stiffness, presents nuclear YAP/TAZ.

The mechanical regulation of YAP/TAZ is important in many physiological and pathological responses. For example, YAP and TAZ are essential for tissue repair, trophoblast development in embryos, they are also involved in preventing human embryonic stem cells (hESC) differentiation during development. These proteins can also mediate pathological effects, being involved in atherosclerosis, fibrotic diseases, cancer development and metastasis[11].

# Chapter 2

# Cancer vaccines

This chapter describes some basic knowledge about the immune system, that is able to defend the human body from pathogens, and vaccines with particular regards to cancer vaccines, that recently has attracted interest as promising cure that allows to instruct the immune system to fight cancer.

## 2.1 Immune System

Immunology is the study of the physiological mechanisms that humans and other animals use to defend their bodies from invasion by all sorts of other organisms. The interest to this subject started observing that people, that survived from epidemic disease, were untouched when faced with that same diseases again, becoming immune to the infection. Infections are caused by microorganisms that are able to reproduce and evolve much more rapidly than their human hosts. The human body reacts using cells dedicated to its defence, which forms the immune system, that is crucial to the survival of humans. Without these cells, all type of infections can become fatal. However, the response of the immune system takes time to fully develop and this causes suffering for the patient because microorganisms in the meantime can multiply and cause disease. The best triumph in immunology is vaccination or immunization, which is a procedure that prevents disease by exposing the body to the infectious agent in a form that cannot result in disease. This mild exposure offers the immune system the opportunity to fight disease and develop a protective response by running a low risk of getting sick. A deeper understanding of immunity mechanisms is generating new ideas for vaccines against infectious diseases and even against other types of diseases such as cancer. Nowadays, knowledge on the molecular and cellular components of the immune system is vast. The objectives that guide the studies and research are aimed at understanding the contribution of immune components to fight against infections in the world in general. New knowledge is also being used to find better ways to manipulate the immune system to prevent unwanted immune responses that cause allergies, autoimmune diseases and organ transplant rejection. Main actors involved in immune responses

are leukocytes, one of the five groups in which can be classified white blood cells (WBCs). In turn, they can be classified into B cells, T cells and NK cells. B and T cells are the cells that are more numerous in the adaptive immune system, that develops by recognition of antigen by specific receptors on T and B lymphocytes. Adaptive immunity, in turn, can be divided in two arms: humoral immunity (mediated by antibody secreted by terminally differentiated B cells that directly bind the pathogen) and cell-mediated immunity (driven by T cells that recognize antigen processed at the surface of infected cells). B and T cells recognize and bind specific antigens, during an antigen presentation, and then they generate specific responses in order to eliminate them: B cells generate many antibodies, some T cells (T helper cells) produce cytokines and other T cells (cytotoxic T cells) release enzymes that induce the death of infected cells. After the extinction of pathogens, B and T cells store information on how to deal with the antigens encountered in the form of memory cells. During the lifetime these cells will be able to provide a strong and rapid response if the same pathogen is detected again[13] .

Recently, immunotherapy has gain attention for cancer treatment, being alternative to treatments that directly kill cancer cells as chemo- or radio- therapies and that have more off-target effects. Cancer immunotherapy aim to improve immune responses using agents that activate or boost the activation of the immune systems to attack cancer cells through natural mechanisms.

## 2.2 Cancer

A neoplasm or tumor is defined, in pathology, as: "a mass of tissue that grows excessively and in an uncoordinated way compared to normal tissues, and that persists in this state after the cessation of the stimuli that induced the process". The cause that determines the uncontrolled and uncoordinated growth of a group of cells is due to alterations in their genetic patrimony, and this is the basis of many different tumors. They can be classified according to the original histological type of cells, in tumor of the epithelial, mesenchymal, blood or nerve tissue; and according to aggression in benign or malignant tumors (cancerous, or cancer). Oncology is the branch of medicine that deals with studying tumors. The onset of cancers can be attributed for the 90-95% to environmental factors, and only 5-10% to genetic factors. One of the most impacting factors in the beginning of a tumor is pollution, followed by smoking, nutrition, obesity, ionizing radiation and stress. Cancer is a genetic disease of somatic cells, and a cell turn into a tumor cell when it has accumulated a lot of damage to its playback control system and start an uncontrolled proliferation. The carcinogenesis process is shown in figure 2.1[14].

Unfortunately, the ability of the immune system to fight cancer on its own is limited. In fact, sometimes it can't detect cancer cells because they are apparently not different from normal cells and other times the response of the immune system might be not strong enough to stop the invasion[15].

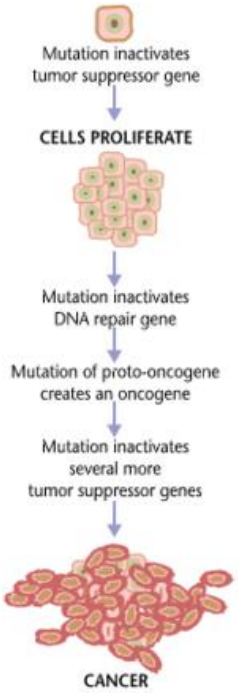


**Figure 2.1.** *Carcinogenesis process.*

## 2.3 Cancer Vaccines

Chemotherapy and radiotherapy are largely used to treat cancer, but these are partially affective and lead to other serious side effects because they kill also healthy cells. New immune therapies have been developed and studied in the last decades. These are based on stimulating the response of tumor specific humoral and cytotoxic T lymphocytes, in order to make them effective in targeting and eliminating the patient's cancer cells. Cancer immunotherapy is able to identify more specifically cancer cells modulating the functions of specific immune cells and producing milder side effects. Cancer treatment vaccines, also called therapeutic vaccines, are a type of immunotherapy under study these days. It can help people already diagnosed with cancer to instruct the immune system in order to prevent the cancer from coming back, to destroy any cancer cells still in the body after other treatments have ended or to stop a tumor from growing or spreading. Some vaccines are "autologous", because are prepared from cells taken from the patient. For this reason, the treatment is specific to the patient.

Cancer immunotherapy is based on the fact that cancer cells have tumor antigens (specific proteins attached to their surface) and these can be identified by cell-receptors of the immune system. Thanks to the bound with tumor antigens, the immune system is able to identify cancer cells, and then inhibit or kill them.

One type of cell-based cancer immunotherapy is based on stimulation of macrophages and dendritic cells (DCs) that activate anti-tumor responses by the presentation of tumor antigens to lymphocytes. Activated lymphocytes act as messengers for antigens associated to tumors (TAAs): they migrate to the lymph nodes where present them on the cell surface to the T cells. Specific T cells then migrate to tumor tissues and recognize the antigen on the surface of tumor cells, starting the killing process, also helped by pro-inflammatory cytokines, releases by other T cells[16]. Target of cell-based cancer vaccines is the activation of DCs using autologous tumor lysates or short peptides, that are small parts of protein that correspond to the protein antigens on cancer cells. These peptides are often given in combination with adjuvants that helps to increase the immune and anti-tumor responses.

# Chapter 3

# Biomaterials

Biomaterials are material that well mimic and/or interface with living tissues, organisms, or microorganisms. Among different biomaterials, this study is focussed on hydrogels, thanks to the fact they closely mimic natural tissues and their behaviour. This chapter deals with hydrogels that are used for cell culture and for the synthesis of cryogel.

## 3.1 Hydrogel biomaterials

The best material to mimic natural environment of cells are hydrogels: they are made of 3D networks of cross-linked polymers that can absorb a large amount of water. This absorption doesn't compromise their structural integrity, which depends on their cross-linked bonds formed by covalent polymer chains and physic interactions. Their capability of retaining water is due to the presence of hydrophilic groups in the polymeric chains. An increase of the number of these groups and a decrease of the crosslinking density, lead to an increased capability of absorbing water. Increasing the crosslinking density, on the contrary, leads to a decrease of the stretchability of the polymer network. These materials are exploited as scaffolds for tissue engineering applications, thanks to their similarities with native soft tissue, and as soft materials in biomedical applications, such as cell culture, cell encapsulation, controlled delivery of therapeutic agents, and medical device fabrication. Their structural and mechanical properties are very similar to those of many tissue's ECM. The network structure of hydrogels has typically nanoporous geometry and this provides an increased surface area for cell attachment and interaction. Many techniques have been exploited to produce microporous hydrogel scaffolds. Some of these are: fiber bonding, gas foaming, microemulsion formation, phase separation, freeze-drying, and porogen leaching. Cryogelation is another technique that allows to produce cell adhesive gels with large size pores, accessible to cells of the immune system [4].

Hydrogels can be obtained from natural and/or synthetic polymers, and they can be classified by the mechanism by which they are formed, obtaining chemical crosslinked (chemical gelation) or physical crosslinked (physical gelation) hydrogels.

The substantial difference between chemical and physical hydrogels lies on their different behaviour in aqueous solutions: the physical ones become soluble in water and the chemical ones are insoluble. This behaviour is related to the different strength of cross-linking bonds between chains. The polymerization reaction that leads to the formation of proper hydrogels can be spontaneous or can be triggered by external agents. For example, the crosslinking can be activated by a photopolymerization under a laser exposal at 514 nm.

In this study chemical crosslinked hydrogels are mainly used. The hydrogels and cryogels synthetized and used in this study are made by polyacrylamide and polyethylene glycol.

## 3.1 Natural hydrogels

Natural biomaterials are materials that originate from living organisms and haven't been chemically modified. These are advantageous for some factors, such as cell recognition, presence of adhesion sites, biodegradability by enzymatic action and often a better biocompatibility compared to non-natural materials. Hydrogels derived from natural polymers are physically crosslinked or reversible gels, where the network is held together by molecular entanglements, and or secondary forces including ionic, hydrogen bonding or hydrophobic interactions. Physical crosslinking is often achieved with temperature. No chemical agents are involved in the synthesis reaction. A disadvantage of natural hydrogels is the scarce reproducibility, due to batch-to-batch variation, biocompatibility, due to possible immune reactions. For this reason, great effort is made to substitute them with synthetic biomaterials.

The natural biomaterials used in tissue engineering to produce hydrogels are mainly components that belong to the extracellular matrix, such as proteins and polysaccharides. Some of them are collagen, fibrin, alginate, gelatine and hyaluronic acid. These molecules provide a starting point in the construction of hydrogels to be used *in vitro*. They can be classified into hydrogels with a protein structure, for example collagen, and hydrogels with a polysaccharide nature, such as hyaluronic acid. These materials are not always suitable to guarantee biocompatibility, because of their low purity. Impure proteins or polysaccharides can lead to the activation of an immune response that recognize those impurities as antigens. There are other disadvantages related to these structures. The range of their mechanical properties is very limited, and they can't be always modified or optimized. In addition, their composition can't be totally controlled because they are generally taken from human or animal tissues and this therefore can lead to differences in composition and mechanical properties in the same gel. Furthermore, the use of biological tissues involves a potential presence of pathogens and a

limited availability of their quantity [17]. For these reasons, natural biomaterials are rarely used. There have been synthetized other biomaterials that allows a better control in their different properties [17].

### 3.1.1 Collagen

Collagen is the main structural protein in extracellular matrix in connective tissues and this makes it the most abundant protein in the body. It can be found in the form of elongated fibrils in fibrous tissues such as tendons, ligaments and skin. Collagen is also abundant in corneas, cartilage, teeth, bones and blood vessels, and gives strength and elasticity to skin. In fact, its main function is to determine the shape, organization and architecture of tissues. It is formed by three polypeptide chains, that are organized in a triple helical structure, called collagen helix and represented in figure 3.1 [4]. The chains are composed of amino acids and are bound together by hydrogen and covalent bonds. There are forty six distinct type of collagen chains, assembled to form twenty eight different collagen types that can be classified into: fibril-forming, network-forming and fibril-associated collagens, and others [4]. Figure 3.2 shows the formation process of fibril-forming collagen. The most abundant types of collagen are type I, II and III. The most common cells that create collagen in bodies are fibroblast. Collagen is also used in food and industry in the form of gelatine, that consists on collagen irreversibly hydrolysed, and in many medical treatments to cure bones and skin complications.

Collagen mechanical properties are strongly influenced by the degree of mineralization, that is the concentration of minerals inside the material, and crosslinking, typically occurring in diseased or aged tissues. In fact, crosslinking or high mineral concentration increases the stiffness of collagen tissues. For example, in bones there are rigid collagen tissues and in tendons flexible one. Mechanical properties of collagen fibers and scaffolds can artificially be improved introducing chemical cross-linkers, such as formaldehyde, or performing on them physical treatments such as UV irradiation, freeze-drying and heating [4].

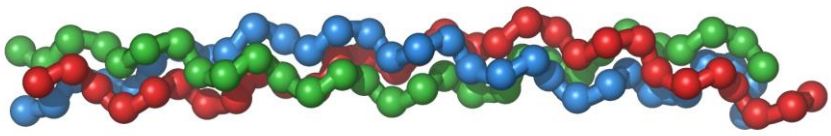

**Figure 3.1.** *A triple helical tropocollagen molecule.*

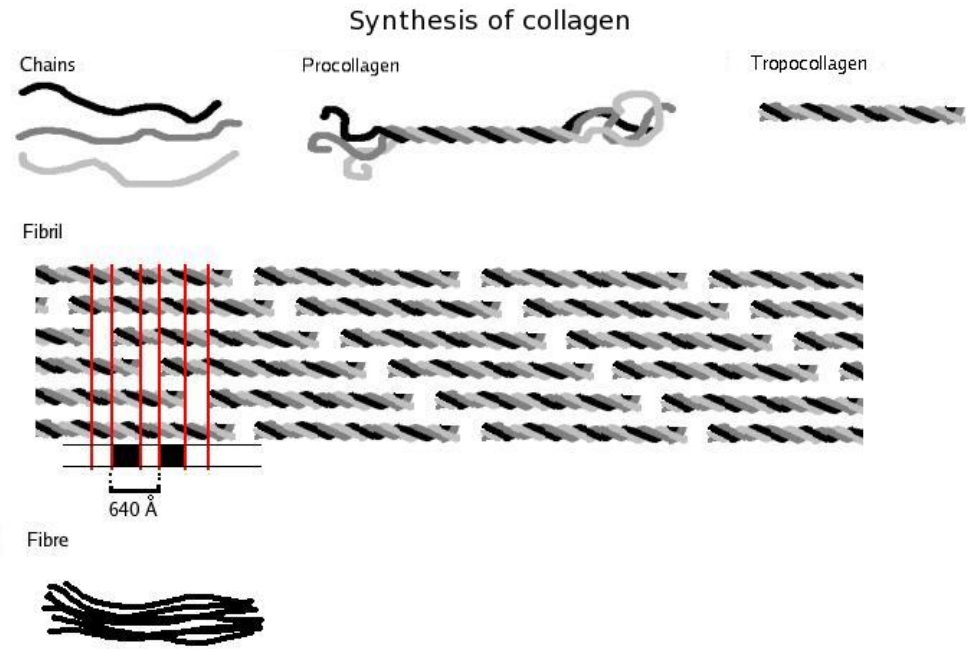


**Figure 3.2.** *Formation of collagen fibers starting from single chains.*

## *3.1.2 Alginate*

Alginates are calcium, magnesium, and sodium salts of alginic acid, a natural polymer obtained from brown algae [18]. Alginate is composed by a block copolymer of (1–4) linked b-D-mannuronic acid and a-L-guluronic acid, as shown in figure 3.3 [19]. This natural polymer can form gels through ionic crosslinks between the carboxylic acid on the polymer backbone and divalent cations [18]. $Ca^{+2}$ ions are commonly used and the hydrogel mechanical properties can be varied by changing the amount of calcium ions [20]. However, the formation of hydrogel is reversible if a cation scavenger is added such as EDTA or sodium citrate [19]. Alginate has been used in many biomedical applications, including drug delivery, cell delivery and tissue engineering [20]. For example, ionically crosslinked alginate hydrogels can be used to encapsulate cells, preserving their differentiated phenotype. It has been observed that calcium alginate loses their structural integrity in long-term static culture, due to the diffusion of calcium ions into the culture medium [21]. Furthermore, calcium ions can be exploited for their role in regulating immune responses, their presence promotes inflammatory innate immunity and pathogen-specific humoral immunity [20]. In addition, the use of these polymers is limited by the fact that impurities present from the isolation procedure have to be removed and its final chemical composition have to be determined [19].

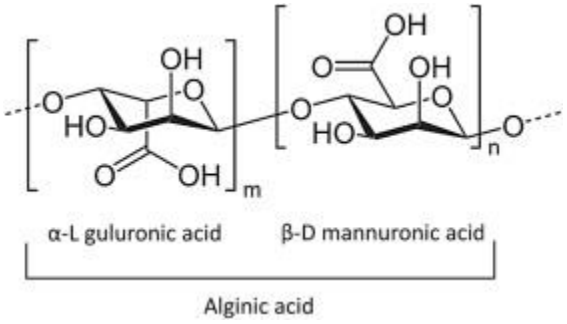


**Figure 3.3.** *Chemical structure of alginic acid* [18].

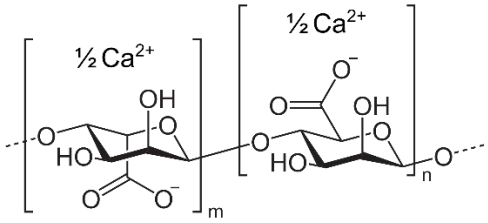

**Figure 3.4.** *Chemical structure of calcium alginate.*

## *3.1.3 Gelatine*

Gelatine is a translucent, colourless and flavourless food ingredient, derived from collagen. It is commonly used as a gelling agent in food, medications, drug and vitamin capsules, photographic films and papers, and cosmetics. Gelatin is an irreversibly hydrolyzed form of collagen, wherein hydrolysis reduces protein fibrils into smaller peptides, denaturing the tertiary structure of collagen[22]. Gelatine contains many arginine-glycine-aspartic acid (RGD) sequences that promote cell attachment, since it is produced from collagen [22]. Depending on the physical and chemical methods of denaturation, the molecular weight of the peptides falls within a broad range. This smaller molecules are more soluble and less antigenic compared to collagen [22]. In addition, the hydrolysis process reduces the structural variations of collagen due to their different sources [22]. A gelatine solution has the unique property of gelation at low temperatures, forming a physically crosslinked hydrogels, without external stimuli [22]. In addition, in order to control the polymerization reaction of gelatine, several chemical reactions have been applied to covalently crosslink it [22]. This allowed to control physical and chemical properties of gelatine hydrogels, providing ideal platforms to engineer tissues and to study cellular behaviour. For example, methacryloyl substituent groups are often introduced in gelatine, obtaining a product called GelMA [22].

GelMA is also called methacrylated gelatine and is a gelatine containing a majority of methacrylamide groups and a minority of methacrylate groups. A schematic representation of

the synthesis of GelMA is represented in figure 3.5. This molecule can polymerize under UV light exposure with the presence of a photoinitiator, forming covalently crosslinked hydrogels. The reaction occurs throw a radical polymerization of the methacryloyl substituents and at mild conditions (room temperature, neutral pH, in aqueous environments, etc). The good cell adhesive properties of gelatine is retained in GelMA, because the RGD motifs don't contain groups that will react with MA, and this allow cells to proliferate and spread in GelMA-based scaffolds [22]. Thanks to these suitable biological properties and tunable physical characteristics, GelMA hydrogels have been widely used for various biomedical applications. GelMA is also versatile from a processing perspective because it can be microfabricated using different methodologies including micromolding, photomasking, bioprinting, selfassembly, and microfluidic techniques to generate constructs with controlled architectures. These hydrogels can also be produced introducing carbon nanotubes, graphene oxide or other polymers, obtaining networks with desired combined properties and characteristics for specific biological applications[22].

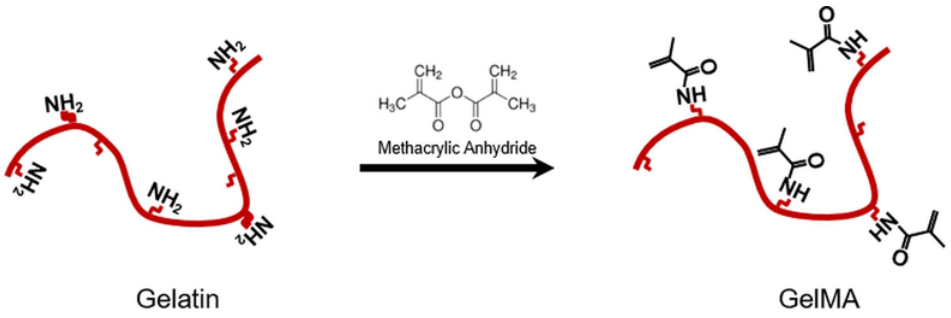


**Figure 3.5.** *Radical polymerization reaction between gelatin and methacrylic anhydride* [23].

## *3.1.4 Hyaluronic acid*

Hyaluronic acid (HA) is a natural polysaccharide found abundantly in the body, represented in figure 3.6 [24]. It can be found in connective, epithelial, and neural tissues, such as cartilage. HA is one of the main components of extracellular matrix and it contributes significantly to cell proliferation and migration. It has many desirable properties for application as a biomaterial for tissue engineering [24]. Hyaluronic acid is an anionic, non sulfated glycosaminoglycan formed by a linear polysaccharide of alternating D-glucuronic acid and N-acetyl-D-glucosamine, shown in figure 3 [24]. This copolymer degrades in the presence of hyaluronidases and free radicals [24]. HA plays a role in cellular processes including cell proliferation, morphogenesis, inflammation, and wound repair. In addition, HA can be modified through both its carboxyl and hydroxyl groups [24]. These properties make HA a desirable choice for the fabrication of

biomaterials in cartilage regeneration [24]. In fact, some applications of HA are in viscosurgery and arthritis treatment. In addition, it is under investigation for drug delivery and wound healing [19].

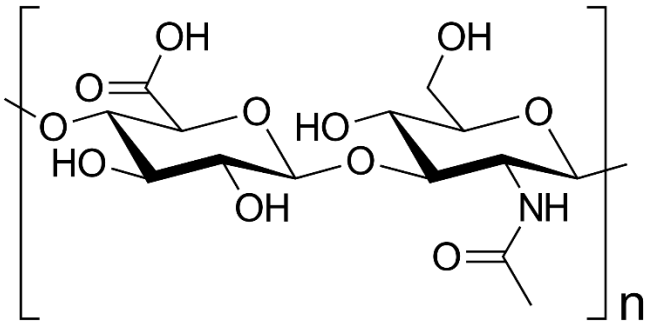


**Figure 3.6.** *Chemical structure of hyaluronic acid unit.*

## 3.2 Synthetic hydrogel

Synthetic hydrogels are generally chemically crosslinked. They are mostly irreversible gels, due to the formation of covalent bonds in their structure, forming a covalently crosslinked network. After the synthesis, these types of gels absorb a large amount of water and reach an equilibrium swelling state, stable in time. Various methodologies are used, in order to obtain these hydrogels, such as reactions induced by chemical reagents and ultraviolet radiation which guarantee short and precise cross-linking times. Synthetic hydrogels are largely used in tissue engineering, because their chemical and physical properties are easily controlled and reproducible. They can be produced with specific molecular weights, degradable bonds, and so on. Choosing these parameters, can be defined the way gels form, the density of cross-linked bonds, the mechanical properties and how much they are degradable. There are many materials that can be used to form synthetic polymers, some of them are polyacrylamide and polyethylene glycol, largely used in this study.

The growth, migration and differentiation of cells are deeply linked to the cell's adhesion to its substrate. The adhesion process of a cell can be stimulated in vitro by the presence of many different proteins as for example fibronectin and collagen. Since these hydrogels don't have any cell-binding moieties themselves, they have to be properly functionalized, in order to allow cell adhesion.

### *3.1.1 Polyacrylamide hydrogels*

Polyacrylamide hydrogels (PAAs) are synthetic, non-ionic, hydrophilic, chemically inert and biocompatible materials. They can be tailored in many ways for several applications. Linear polyacrylamide polymers can be obtained polymerizing acrylamide monomers (AA). High molecular weight PAA hydrogels can be obtained by the polymerization of both acrylamide and crosslinker molecules, such as bis-acrylamides (BIS). These monomers are soluble in water. Acrylamide (AA) is a monofunctional monomer, displayed in figure 3.7. The polymerization of AA to form linear PAA chains occurs throw vinyl groups. Acrylamide can be obtained from the condensation reaction of acrylic acid with ammonia or by the hydrolysis of acrylonitrile. Acrylamide is a strong neurotoxin, easily absorbed throw the skin, that promotes the formation of cancer.

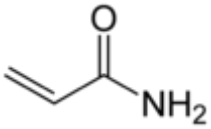


**Figure 3.7.** *Molecular structure of monomer of Acrylamide.*

Bis-acrylamide, also called N, N'-Methylene-bis-acrylamide, is a bifunctional monomer used to crosslink acrylamide polymer chains, to create a highly hydrophilic three-dimensional network. Bis-acrylamide molecule is displayed in figure 3.8.

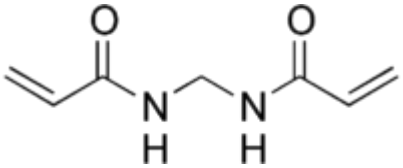


**Figure 3.8.** *Molecular structure of bis acrylamide monomer.*

The copolymerization reaction takes place when radical initiators are added to the solution and it occurs through a radical-mediated chain-grow mechanism. In this study it has been used ammonium persulfate, APS, and N, N, N', N'-tetramethyl ethylenediamine, TEMED. The chemical formulas of these initiators are displayed in figures 3.9 and 3.10 [25]. TEMED catalyses the decomposition of persulfate ions, which produced free radicals. The decomposition reaction of ammonium persulfate is the following:

$$[O_3SO - OSO_3]^{2-} \leftrightarrow 2\,[SO_4]^{\cdot -}$$

Sulphate radicals then add to the alkene of acrylamide to give a sulphate ester radical, catalysing the polymerization of acrylamide. APS acts as an oxidizing agent and as a source of radicals.

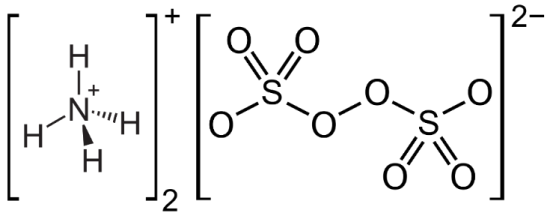

**Figure 3.9.** *Chemical formula of ammonium persulfate.*

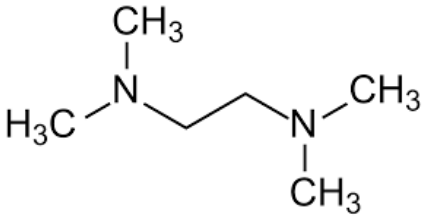

**Figure 3.10.** *Chemical formula of TEMED.*

The polymerization is a time effective technique and it occurs within minutes at room temperature. An increase of the reaction time increases the molecular weight of the final polymer. The resulting crosslinked gel, showed in figure 3.11, is composed of long acrylamide chains bounded together by some bis-acrylamide molecules. This polymer can retain a large amount of water, thanks to the formation of hydrogen bonds between water and amide groups[25].

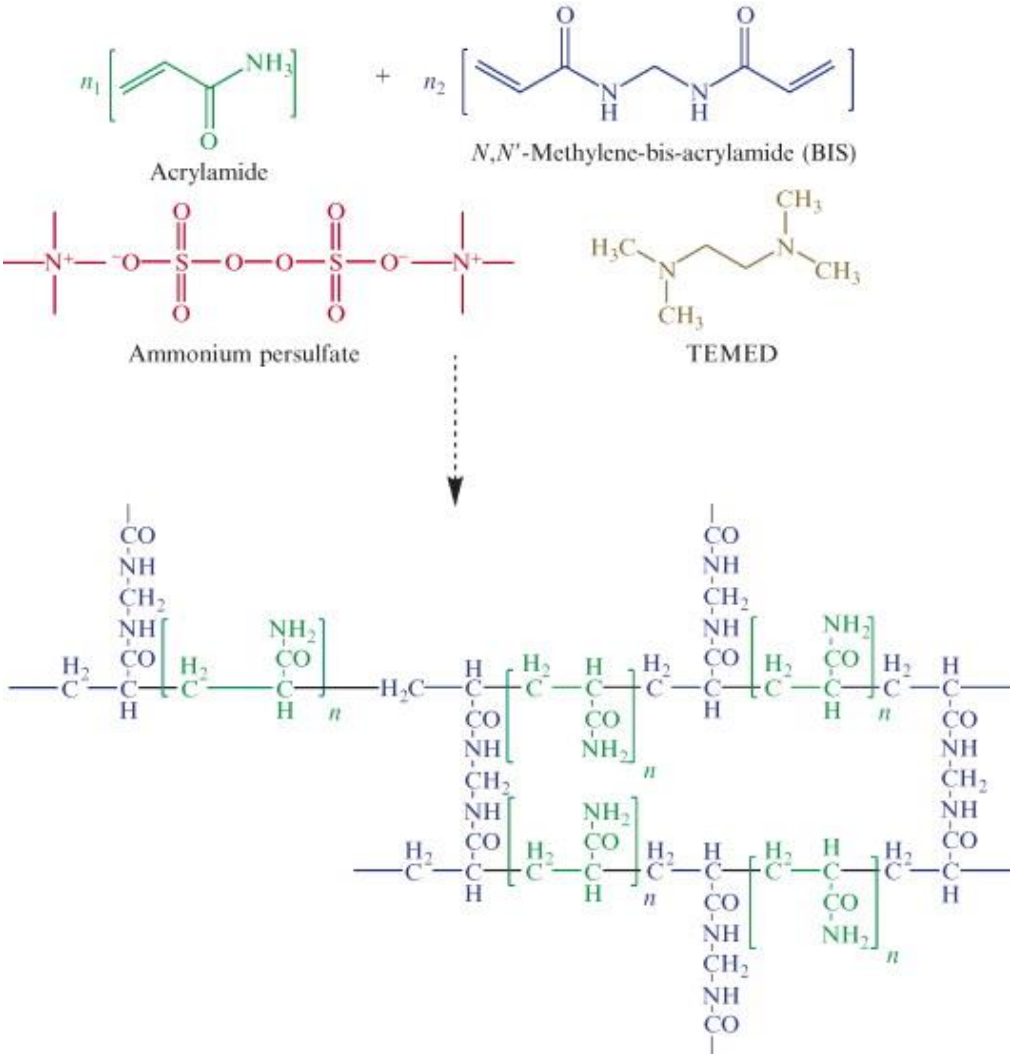


**Figure 3.11.** *Polymerization reaction of polyacrylamide* [26].

Polyacrylamide hydrogels are largely used because they have a homogeneous and reproductible structure that can be modified changing the concentration of acrylamide monomers and/or varying the percentage of bifunctional monomers [25]. Increasing the acrylamide concentration, the molecular weight of polyacrylamide chains can be raised. The monomer concentration must be kept lower than 10 wt%, otherwise a polymer insoluble in water is produced. In addition, the polymerization can be controlled also by the temperature. Low temperatures promote the synthesis of high molecular weight PAA. The rate of radical generation is increased by elevated temperatures and this decreases the molecular weight of the final product, favouring termination reactions. Temperature can't be raised above 70°C because it may favour intermolecular reactions that decreases the polymer solubility in water. In addition, also the concentration of initiators influences the reaction. An increase of their concentration raises the number of active sites that react, and this decreases the final molecular weight, promoting

termination reactions. The radical polymerization reaction of PAA is inhibited by oxygen because it acts as a scavenger of free radicals. For this reason, the gels can be produced only in absence of oxygen: degassing the solutions or working in a nitrogen atmosphere [27].

PAA has been long used for molecular biology, genetic and biochemistry applications. It is also suitable as a biomaterial for cell culture since it shows several advantageous characteristics [2]. Thanks to the strong crosslinking bonds between polymeric chains, the mechanical behaviour of PAA hydrogels can be considered elastic, showing a complete recovery after removal of a stress [28]. The elastic modulus can be varied by changing relative concentrations of acrylamide and bis-acrylamide, allowing the production of hydrogels with a wide range of stiffness. In addition, the adsorption of serum proteins or the nonspecific binding of cell surface receptors is typically negligible on PAA hydrogels. Therefore, in order to allow cell attachment on polyacrylamide hydrogels, adhesive molecules must be linked to its surface. Furthermore these gels are translucent and this allows their characterization with an immunofluorescence analysis [2].

However, the use of PAA as a substrate for cell culture has some limitations and disadvantages. PAA hydrogels need to be coated with adhesive proteins in order to provide a suitable surface for cells but the link between this polymer and adhesive proteins isn't easily achievable [28]. These proteins, then, will control the adhesion and spreading of cells in the two-dimensional space. Nowadays are available different coating strategies for this purpose. Two heterobifunctional crosslinkers that have been widely used are Sulfo SANPAH and NHS, both can covalently bind to PAA network and with the adhesive peptide[6]. Sulfosuccinimidyl-6-(40-azido-20-nitrophenylamino) hexanoate, known as sulfo-SANPAH binds to PAA after UV light-mediated photoactivation, and can react with primary amines of adhesive peptides and protein used for coating. This heterobifunctional crosslinker has been extensively used for PAA hydrogels coating but this technique has several limitations, it is not cost-effective, the reagents have a limited shelf life and it is not feasible for production scaling up [29]. Acrylic acid N-hydroxy succinimide ester (NHSac) co-polymerizes with acrylamide and bis acrylamide during PAA hydrogels polymerization step. Then, NHS can covalently bind to any amine containing ligand. Unfortunately, NHS is not water soluble, and can be solubilized in toluene or other organic compounds. Mixing NHS solution in toluene with Acrylamide and bis-acrylamide solution in water can induce formation of an irregular matrix, with locally altered mechanical propriety and cracks or breaks in the gel[29]. In all of these protocols a protein is required and the most largely used in literature are collagen I, collagen IV, laminin and fibronectin. In this study,

polyacrylamide hydrogels have been modified to enhance the fibronectin coating that can provide adhesion sites for integrin binding. In addition, it must be considered that the amount of fibronectin immobilized on the substrate influences cell behaviour by modulating the type, density and stability of integrin-based focal adhesions [2].

### *3.1.2 Polyethylene glycol (PEG) hydrogels*

Polyethylene glycol (PEG) hydrogels are synthetic hydrogels extensively used in biomedicine and biomedical applications. They are also called poly (oxyethylene) or poly (ethylene oxide) hydrogels. These hydrogels are hydrophilic polymers, characterized by high biocompatibility, flexibility and solubility in water. They are also bioinert materials because proteins and cells can't adhere on their surface [30]. This prevents the interaction with non-specific proteins, reducing immune and inflammatory responses of the body. In addition, the chemistry of PEG molecules is versatile and this provide the ability to fine tuning cells adhesiveness, incorporating chemical and physical cues for stem cells [25]. In fact, biochemical modifications can be made for eliciting desired cell responses such as adhesion, differentiation, proliferation and motility of cells. For example these polymers can be functionalized with adhesive peptide ligands or larger extracellular matrix proteins, such as laminin and collagen [30]. In this study PEG hydrogels have been covalently conjugated with the cell-adhesive ligand CRGDS (cysteine–arginine–glycine–aspartic acid–serine). The RGD sequence can be recognized by some integrins in cell membranes, allowing cell adhesion on the hydrogel. The functionalization with RGD peptides allows to fine-tune both concentration and presentation of integrin ligands.

Polyethylene glycol hydrogels can be obtained through either physically or chemically crosslinking[25]. First ones are formed by molecular entanglement and/or weak secondary forces such as van der Waals interactions, ionic interactions, hydrogen bonding and hydrophobic interaction. Chemically crosslinked gels are more robust and are often catalysed by physical conditions, such as high temperatures and UV irradiation, and/or by initiators and catalysts. These polymerization conditions have to be chosen in order to ensure biocompatibility to the material [25].

Chemically crosslinked PEG hydrogels can be obtained with different types of reactions. For example: photo-polymerization, click chemistry and enzyme-catalysed reactions[25]. The polymerization reaction on which we focused are click chemistry reactions because they are reproducible and controllable. In fact, the nature of crosslinker molecules and hydrogel

properties can be designed precisely according to experimental aims. The crosslinkers that can be chosen are peptides or chemical entities. PEG molecules and crosslinking reactions by click chemistry are bio-compatible and this makes PEG well suited materials to be employed for 3D cell culture and ultimately organoid formation.

Click chemistry consists in a class of reactions that are fast and high yielding, requiring mild reaction conditions. This type of reaction doesn't produce by-products or side reactions [25]. Therefore, a single product can be obtained with high yield, due to a high thermodynamic driving force that drives the reaction quickly and irreversibly. This class of reactions are commonly used to covalently link two molecules, at least one of which is a biocompatible small molecule. Click chemistry doesn't refer to a simple specific reaction but describes a way of generating products that follow examples in nature. In addition, this class of reactions is stereoselective and insensible to solvent parameters, oxygen and water. The click chemistry reaction used to obtain PEG hydrogels is a thiolene conjugate addition, represented in figure 3.12 [25].

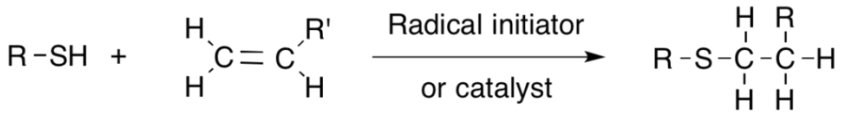


**Figure 3.12.** *Representation of the thiolene reaction.*

The thiolene rection is an organic reaction between a thiol and an alkene, that produce a thioether. PEG hydrogels obtained using the click reaction have higher swelling capacities and significantly improved mechanical properties than photochemically crosslinked hydrogels. However, the gelation time is longer but it can be reduced modifying the temperature and the catalyst concentration[25].

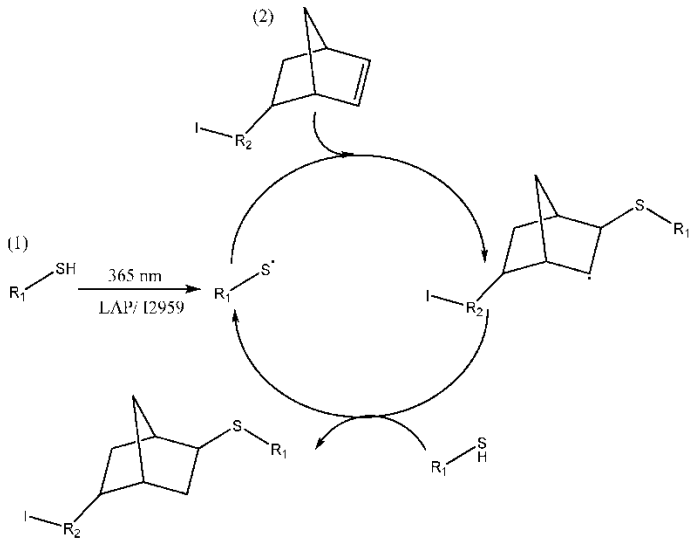


**Figure 3.13.** *Scheme of photoinitiated thiolene click reaction on PEG-Norbornene.*

This click chemistry reaction has been used to functionalize polyethylene glycol hydrogels with peptides. The rection occurs by a photopolymerization that links thiol groups of CRGDS peptides with alkene groups of norbornene polyethylene glycol (PEG-NB) monomers. Thiol groups are present in the cysteine amino acid. The hydrogels have been obtained using four arms PEG-NB and eight arm PEG-NB monomers. The molecular formulas of this PEG monomers are displayed in figures 3.14 and 3.17. The hydrogel obtained has a homogeneous network thanks to the step-growth mechanism of polymerization. In addition, the hydrogel is obtained by the reaction of the functionalized PEG-NB with a cross-linking peptide containing cysteine. The cross-link peptide links the free PEG-arms remained, creating the gel. The reaction proceeds through a radical mediated step growth polymerization under the exposure to 365 nm light in the presence of the photoinitiator LAP (lithium phenyl-2,4,6-trimethylbenzoylphosphinate)[31]. The free-radical thiolene addition reaction is represented in figure 3.13.

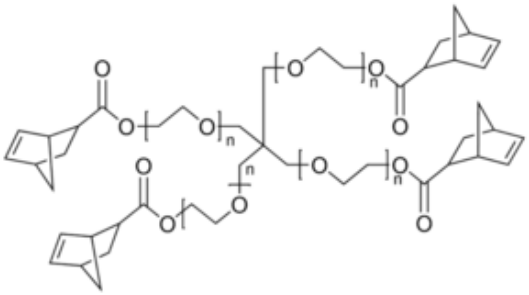

**Figure 3.14.** *Molecular formula of PEG norbornene 4 arm monomer.*

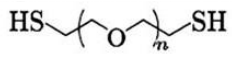


**Figure 3.15.** *Non-degradable crosslinker molecule* [32].

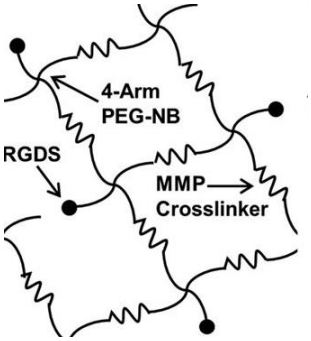


**Figure 3.16.** *Hydrogel networks formed by 4-arm PEG-NB molecules with MMP degradable peptide crosslinker* [33].

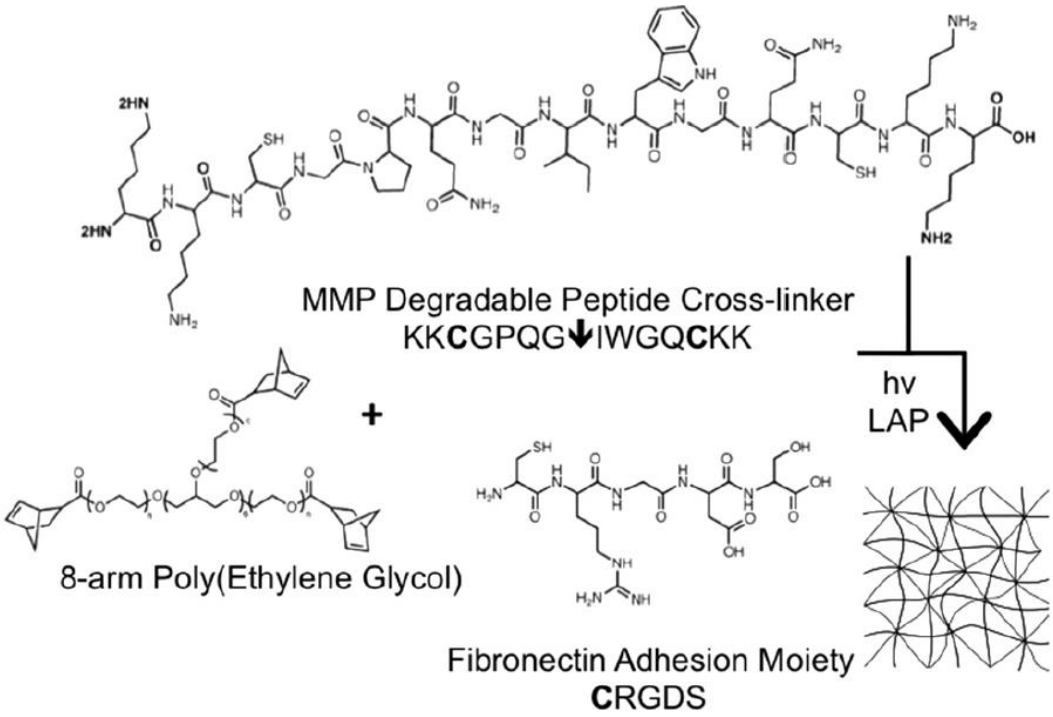


**Figure 3.17.** *Schematic illustration of the formation of peptide functionalized degradable PEG hydrogels* [31].

The crosslinker that can be used in order to produce the hydrogel can be degradable or non-degradable. An example of non-degradable crosslinker is represented in figure 3.15., On the other hand, a degradable crosslinker can be a peptide with a specific sequence sensitive to metalloproteinase degradation and two cysteines amino acids on the sides. which consist in a matrix metalloproteinase (MMP)-degradable cross-linking peptide, that contain cysteines amino acids. A schematic representation of the gel that can be obtain is presented in figure 3.16.

This case is particularly advantageous in applications such as cell 3D embedding since Cells can degrade this crosslinker throw the proteolysis. Figure 3.17 represents the reaction that allows to synthetize degradable PEG hydrogels, using the MMP-degradable peptide cross-linker.

Mechanical properties of these hydrogels can be controlled by the cross-linking density between PEG molecules. In particular, the storage modulus G' is increased by a directly increase of the cross-linking density, that can be raised with the PEG backbone molecule concentration. In this way, hydrogels with a wide range of stiffness can be obtained, without modifying the amount of RGD pendant biomolecules [31]. These hydrogels allow the study of the influence of the substrate stiffness on the cells, keeping constant the number of adhesive sites. Similarly, the importance of the number of adhesion sites on cell behaviour can be studied varying the amount of the pendant RGD peptide in the material. Different hydrogels can be produced with a wide range of adhesion properties by altering the concentration of CRGDS but keeping constant the matrix elastic modulus. A non-bioactive peptide is incorporated in order to maintain a constant total pendant peptide concentration (CRGDS + CRDGS) [31].

## 3.3 Cryogels

Cryogels are hydrogels with large interconnected pores produced by cryogelation[17]. Cryogenic processes have been largely used to create these unique polymeric materials. Nowadays they are mainly applied in the biomedical, environmental science and food technology fields. Cryogelation consists in a process in which gelation occurs under semi-frozen conditions, obtaining a polymer network cross-linked around ice crystals. After the melting of ice crystals, a polymeric material with an interconnected and microporous network, called cryogel, is produced. This microstructure is surrounded by a highly dense polymeric wall [34]. If a solution, in which a polymerization is occurring, is frozen, ice crystals nucleates from the aqueous phase and they concentrate reagents in the unfrozen or semifrozen phase. This process allows the formation of a cross-linked network [17]. The schematic representation of a cryogelation process of methacrylated alginate is displayed in figure 3.18. In the biomedical field, these materials are advantageous because cryogels allow an immediate diffusion of solutes of practically any size and promote infiltration and survival of mammalian cells, despite the conventional nanoporous hydrogels. Furthermore, the microstructure of cryogels confers them exceptional elasticity and shape-memory properties, allowing them to be syringe injected through hypodermic needles. Thanks to these unique properties, cryogels have been used for cell

delivery, drug delivery, cancer immunotherapy, tissue engineering, bio separations, biosensors and cell cultures in three dimensions [34]. In this work, cryogels have been used for cancer immunotherapies studies and they have been synthetized in order to be injected into a body. The cancer therapy is an important application of cryogels because the injection of molecules or cells in a body is a successful method to control the immune system. Different types of cells and biomolecules can be injected with cryogels. However, an effective cancer vaccine has to stimulate some specific immune responses, avoiding the ability of tumours to protect themselves, as previously described in chapter 2. A promising approach in cancer immunotherapy is the use of inactive tumor cells, because they offer the possibility to provide a cancer vaccine for a specific type of tumor. Tumor cells are taken from a patient and then irradiated, in order to inactivate them. In addition, cancer vaccines often include adjuvants, that improve the efficacy of the tumor vaccine[35].

Cancer vaccines have been produced synthetizing injectable cryogels which includes adjuvants and inactive tumor cells. The adjuvants used are: ODN and cytokines[35].

A cryogel, in order to be injected into a body, has to satisfy the following requirements[35]:

- the material must be compressible and flow under moderate pressure,
- it should maintain enough integrity and strength during injection,
- after the injection, the cryogel should rapidly regain its original shape and size from the collapsed state,
- the cryogel should retain inside biomolecules and/or cells during the injection process and allow their subsequent release.

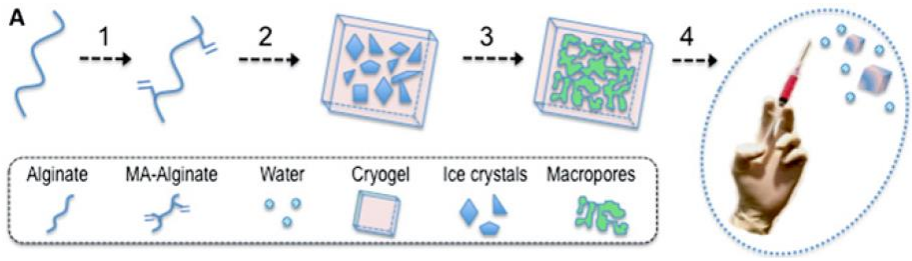


**Figure 3.18.** *Overview of the cryogelation process of MA-alginates* [17].

Cryogels can be produced by many different polymers, such as methacrylated alginates, polyethylene glycol diacrylates (PEGDA) and four arm polyethylene glycol acrylates (PEG). These cryogels can be functionalized by different adhesive proteins, such as CRGDS or

GelMA, that provides cells adhesion and spreading. Four arm PEG acrylate is a multi-arm polyethylene glycol with acrylate groups at each terminal of the four arms. Its chemical formula is displayed in figure 3.19. The cryogel can be synthetized by radical polymerization of monomers using redox initiators APS and TEMED.

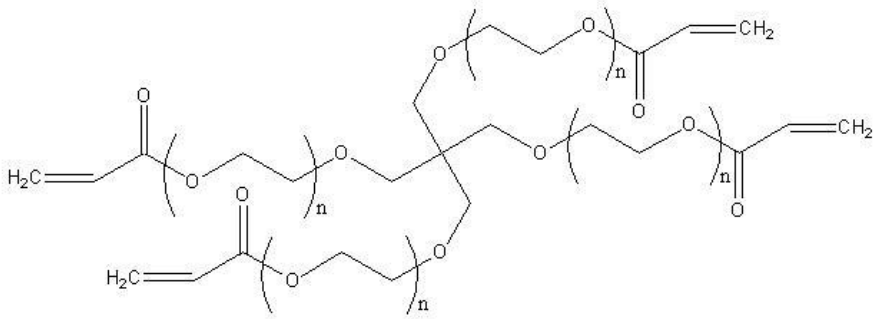

**Figure 3.19.** *Polyethylene Glycol Acrylate 4 arms.*

Polyethylene glycol diacrylate, or PEGDA, is a linear polymer obtained from polyethylene glycol, which has acrylate groups at the ends. The cryogel can be synthetized by radical polymerization of monomers using redox initiators APS and TEMED. This polymer is displayed in figure 3.20.

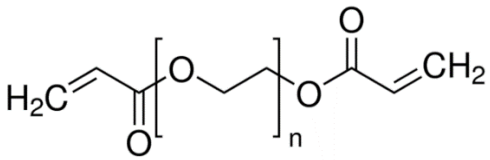

**Figure 3.20.** *Polyethylene glycol diacrylate* [36].

Methacrylated alginates have been largely used to produce injectable cancer vaccines. They are produced throw the methacrylation reaction of sodium alginate. The reaction occurs between 2-aminoethyl methacrylate (AEMA) and sodium alginate at room temperatures. Reagents are dissolved in a buffer solution of 2-morpholinoethanesulfonic acid (MES). N-hydroxy succinimide (NHS) and 1-ethyl-3-(3-dimethylaminopropyl)-carbodiimide hydrochloride (EDC) are added to the solution in order to activate the carboxylic acid groups of alginates. The reaction is represented in figure 3.21. After the methacrylation of sodium alginate, cryogels can be obtained throw a redox-induced free-radical polymerization of MA-alginate. The initiators and catalyst used are TEMED and APS[17].

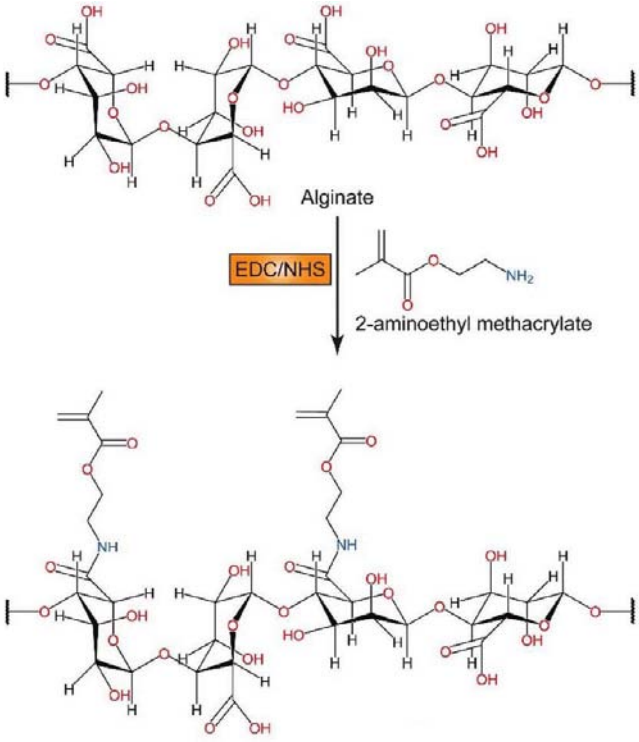


**Figure 3.21.** *Methacrylation of sodium alginate.*

# Chapter 4

# Mechanical properties of hydrogels

This chapter describes the mechanical properties of hydrogels, and the three main techniques that are normally used to characterize them, and the two methods designed and realized in this thesis work. Hydrogels can have elastic or viscoelastic behaviours, depending on their specific composition.

## 4.1 Mechanical properties

The determination of the mechanical properties of polymeric gels is particularly important for various biomedical applications. In fact, as explained in chapter 1, the variation of mechanical properties of hydrogel substrate modifies and controls the behaviour of the cells that adhere to them. However, while tremendous advances have been made in the comprehension of molecular mechanisms by which cells mechanically perceive a hydrogel stiffness and affect their behaviour, controlling and determining mechanical properties of hydrogels is still a challenge, but fundamental in order to understand their effects on adherent cells[37].

The properties of hydrogels are greatly influenced by the characteristics of their structure. In particular, they are mainly influenced by the type and the density of bonds between polymeric chains. In general, if the density of the crosslinking network increases, hydrogels become stiffer. The other structural key parameter is the type of cross-links between polymeric chains, that can be of different nature. Bonds between chains can range between strong covalent ones to weak noncovalent bonds, such as hydrogen or dipole–dipole bonds, that in some cases can be both present, forming a supramolecular structure. The behaviour of the hydrogel is noticeably influenced by the strength of these bonds. If the structure has covalent bonds, the material shows an elastic behaviour because bonds persist also when external force is applied and holds the polymeric chains tightly. In addition, this confers a rubber-like behaviour to the hydrogel. In fact, once a stress is applied, the material deforms almost instantaneously and, when the stress is released, the deformation is completely recovered. In the case of hydrogels

where polymeric chains are bounded by noncovalent interactions, the material has a viscoelastic behaviour (or at most, viscoplastic) in response to an external force. The strength of these bonds is lower than the one of covalent bonds, and they break and reform during the application of an external force. Therefore, the cross-linking network is modified, and the polymeric chains are reorganized. In general, if the binding energy of intrachain bonds is higher, the possibility to reorganize the polymeric network is lower, and if there is more elastic deformation of the material, then there is less viscoelastic one. Figure 4.1 shows the bonding energy of different type of bonds [38].

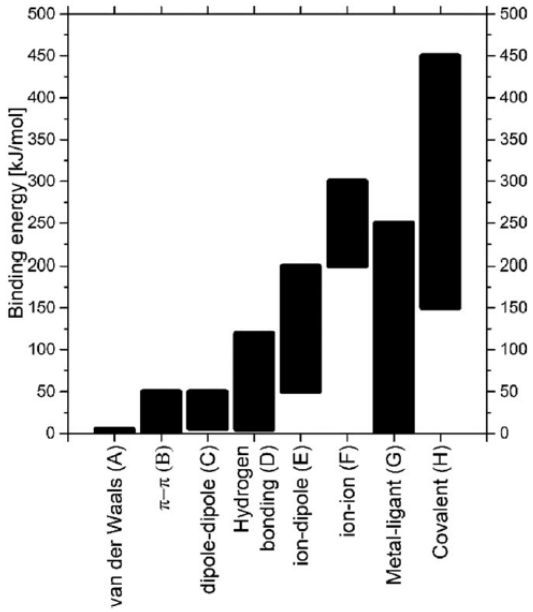


**Figure 4.1.** *Bonding energy of each type of bond* [38].

Elasticity (often called stiffness) and it is the measure of the resistance of a substance to being deformed elastically when a stress is applied. The parameters that are considered are the Young's modulus (E, [kPa]) and the shear modulus (G, [kPa]). The Young's modulus is also called elastic modulus and it is a measure of the tensile elasticity or the tendency of an object to deform along an axis when opposing forces are applied along that axis; it is defined as the ratio of tensile stress to tensile strain [39]. The shear modulus is also known as modulus of rigidity and it is the ratio of shear stress to the shear strain. If the considered material has different values of these moduli depending on different axis considered, the material has an anisotropic behaviour. Instead, in the case of hydrogels a perfectly incompressible isotropic behaviour can be assumed, where these moduli aren't a function of the axis of measure, and so the elastic and shear moduli can be related with the relation $E = 3G$ [38].

The assumption of incompressibility can be justified by the fact that, thanks to their microstructure, hydrogels can absorb and retain a large amount of water and swell after the synthesis. Swelling increases their biocompatibility, because they became softer and more rubbery, simulating better living tissues [39]. The water content of hydrogels is higher than 90%, and this makes difficult their characterization by many techniques normally used to analyse nonhydrated materials, such as mid-IR spectroscopy and differential scanning calorimetry [39]. Some dynamic mechanical analysis, for example Rheometry, are easy methods for characterizing the bulk mechanical properties and the density of crosslinking network of hydrogels [39].

One of the best theories that can describe the bulk properties of elastic hydrogels using characteristics of the microscopic structure of a material is the rubber elasticity theory (Eq. 1). It states that elastic modulus is directly proportional to the crosslinking density of the microstructure υ [mol/m$^3$] and to the temperature T [K] [39].

$$E = 3 \cdot G = 3 \cdot G_{dry} \cdot \phi^{\frac{1}{3}} = 3 \cdot \upsilon \cdot R \cdot T \cdot \phi^{\frac{1}{3}} = 3 \cdot \frac{\rho}{M_c} \cdot R \cdot T \cdot \phi^{\frac{1}{3}} \quad (1)$$

Where the $G_{dry}$ is the shear modulus of the dry hydrogel in [kPa], ϕ the polymer volume fraction and R is the gas constant [8,314 J/ (mol K)]. The crosslinking density of the structure υ can be expressed as the mass concentration of the dry polymer ρ [g / m$^3$] divided by the average molecular number weight of the chain between two cross-links $M_c$ [g/m]. The theory is based on the assumption that crosslinked polymer strands are connected throw points and that the chain distribution is represented by a Gaussian distribution. This equation can be extended considering the influence of other factors: material's anisotropy (Poisson's ratio), defects of the network and inclusion of entanglements. The elastic modulus is influenced a lot by the swelling of the network [39]. It is found from the Eq. 1 that the shear modulus of the swollen hydrogel can be scaled with the polymer volume fraction to the power of 1/3 [38]. In fact, samples have to be analysed at least after 24 hours from their synthesis, in order to complete the absorption of water inside the network [39]. In addition, can be observed from Eq. 1 that an increase of the average molecular number of chains between two cross-links, lowers the elastic modulus of the material, because the density of crosslinks is lowered, increasing the distance between cross-links. In this way a softer hydrogel is obtained. These considerations lead to the possibility to properly control the mechanical properties of the hydrogel by the variation of the polymer concentration or of the $M_c$. Stiffer hydrogels can be obtained increasing the polymer concentration in the

solution or increasing the quantity of the cross-linker in the polymerization solution, obtaining a decrease of the average molecular number weight of the chain between two cross-links [38].

Rubber elasticity can be described also from another point of view. A concept that is particularly important is entropy. Entropy may be defined as a measure of the thermal energy that is stored in a molecule. Rubber elastic theory considers a polymer chain in a cross-linked network as an entropic spring. When the chain is stretched, some of the network chains are forced to become straight. Individual backbone units are forced into rotational conformations in order to increase their end-to-end distances and this led to a reduction of the number of conformations (states) that are still thermally accessible, therefore a lower amount of thermal energy that can be stored and the entropy is reduced. This entropy decrease rises the elastic force in the network chains, also called restoring force, which causes the polymer chain to return to its equilibrium or unstretched state, characterised by a higher value of entropy. This is the reason why rubber bands return to their original state.

Hydrogels with weak crosslinking bonds don't have an elastic behaviour characteristic of a pure elastic solid, because during the deformation under an applied force, some conformational changes take place inside the structure. The rupture and formation of crosslinks dissipate energy and generate a viscoelastic behaviour, a behaviour that exhibit both viscous and elastic characteristics when a deformation is applied. The relationship between stress and strain in viscoelastic materials is time-depend. The material response to an applied stress depends on the application time of the load. Furthermore, the deformation is recovered in long times. In viscoelastic materials there are two regions with different responses once an external stress is applied: the linear and non-linear viscoelastic region. In the linear viscoelastic region (LVE) materials show a linear relationship between stress and strain at any given time. The theory that describes this behaviour is linear viscoelasticity. LVE is observed in the case of small deformations applied to the material. As can be seen in equation 3, the stress is directly proportional to the deformation.

$$\sigma = \varepsilon \cdot f(time) \tag{3}$$

In LVE, elastic moduli are independent from amplitude of the deformation and they show constant values (a plateau), as can be seen in the figure 4.2. The parts on the left of the diagrams are characterised by lower values of strain applied to the material. The diagram on the left has a higher value of G' than G'' in the LVE region. In this case the sample has a gel-like or solid structure. The other one has a higher value of G'' in the LVE region, thus the sample is fluid.

The second region that can be identified in the viscoelastic behaviour is the non-linear one. This is identified from the other region thanks to the linearity limit. A non-linear viscoelastic behaviour is usually observed in the case of large deformations applied to the polymer. There is a generic dependence of the stress from deformation and time.

$$\sigma = f(\varepsilon, time) \tag{4}$$

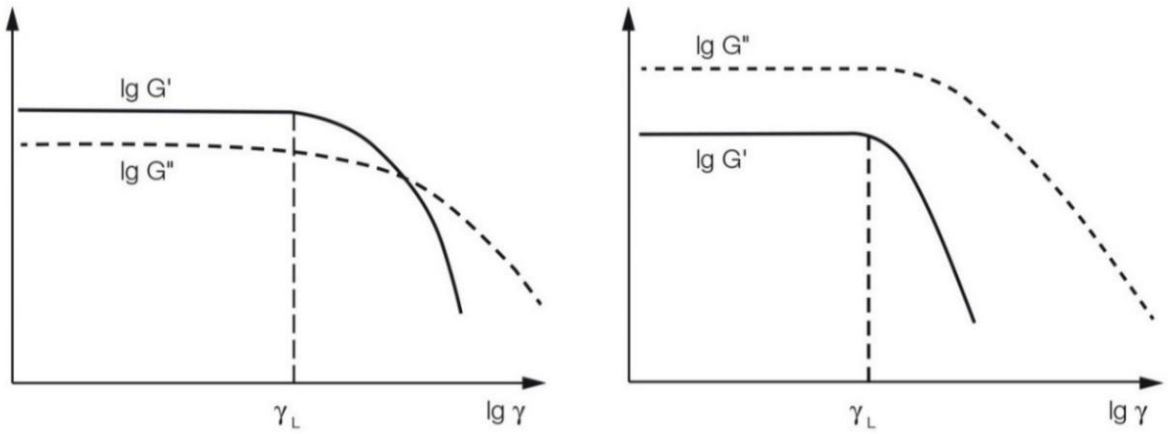


**Figure 4.2.** *Results of two amplitude sweeps, the functions of G' and G'' show constant plateau values within the LVE region.*

Viscoelasticity can be studied using dynamic mechanical analysis. It is applied a small oscillatory stress to a sample with an angular frequency ω and is measured the resulting strain. The strain response has as well oscillatory values. Between the two cyclic trends there is a phase shift $\delta$. In order to represent the relations between the oscillatory stress and strain, can be used a complex dynamic modulus G.

$$G = G' + i\,G'' \tag{5}$$

$$G' = \frac{\sigma_0}{\varepsilon_0} cos\delta \tag{6}$$

$$G'' = \frac{\sigma_0}{\varepsilon_0} sin\delta \tag{7}$$

Where $i^2 = -1$, and $\sigma_0$ and $\varepsilon_0$ are the amplitudes of stress and strain.

The viscoelasticity can be described with several rheological models that combine springs and dashpots elements in order to calculate the relaxation modulus G(t). The most general viscoelastic model that describes linear viscoelasticity is the ‘‘generalized Maxwell’’ model

which combine parallelly a spring and ‘‘η’’ Maxwell elements. Each of them is characterized by an elastic modulus and a relaxation time. The ensemble of the relaxation times of the ‘‘η’’ Maxwell elements defines the relaxation spectra of the material. The simplest model that describes properly both the creep and stress relaxation behaviours of a viscoelastic material is the Standard Linear Solid (SLS) rheological model. This is a generalized Maxwell model where only one Maxwell element is put in parallel with a spring. On the left of figure 4.3 is represented the schematic representation of the normal Maxwell model, on the right the standard linear solid rheological model.

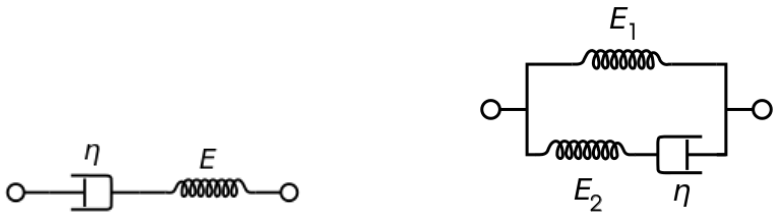


**Figure 3.** *(Left) Maxwell model, (right) the standard linear solid rheological model.*

Springs elements model the elastic deformation of the material and are characterized by the elastic constant E, that is the elastic modulus of the material. $\varepsilon$ is the deformation that occurs under the given stress $\sigma$.

$$\sigma = E\,\varepsilon \tag{8}$$

Dashpots elements represent the viscous deformation of the material and are characterized by the viscosity η of the material. $\frac{d\varepsilon}{dt}$ represents the variation of strain in the time.

$$\sigma = \eta\frac{d\varepsilon}{dt} \tag{9}$$

The standard linear solid model is also known as the Zener model and it can be represented by the Maxwell representation or by the Kelvin representation. The first one is displayed in the right part of figure 3. The stress-strain equation related to this model is the following one.

$$\sigma(t) + \frac{\eta}{E_2}\frac{d\sigma(t)}{dt} = E_1\,\varepsilon(t) + \frac{\eta(E_1+E_2)}{E_2}\,\frac{d\varepsilon(t)}{dt} \tag{10}$$

In addition, it can be defined the relaxation time τ, that indicates the time needed to the system to return to its equilibrium state, after undergoing a perturbation.

$$\tau = \frac{\eta}{E_2} \quad (11)$$

The relaxation time tends to zero for very stiff materials, characterized by high values of G' and low values $M_c$. The hydrogel elasticity became predominant over the viscous dissipations. For systems that present very few cross-links and high values of $M_c$, the value of G' is very low and their mechanical behaviour tends to be more viscous than elastic. In this case as well, the relaxation time tends to zero because chains can instantaneously rearrange in the space after a perturbation. Hydrogels with intermediate values of crosslinks and $M_c$, presents an enhanced viscoelastic behaviour and the relaxation time is higher [38].

## 4.2 Mechanical characterization techniques

The mechanical properties of hydrogels can be determined by means of standardized and expensive techniques. Rheometry is not the only technique that can be used to measure the elastic modulus of hydrogel materials. Other ones that can be used are atomic force microscopy and compression. Compression tests have been widely used to test biological soft tissues. In addition, indentation and micropipette aspiration techniques are described. These two mechanical characterization techniques were used and optimized in this study to determine the elastic modulus of synthetized hydrogels.

### *4.2.1 Atomic force microscopy AFM*

Atomic force microscopy is a technique that is able to determine the local wet samples mechanical properties, including hydrogels in their swelling solution and cells in their culture medium. It can determine the surface modulus in a local point, thanks to the contact between the probe and the surface [39] . A microprobe flexible cantilever is indented on the surface of the sample. Its position and displacement can be controlled with nanometric precision. In response to the indentations on the material, the probe deflects elastically according to the mechanical properties of the sample. The measure of the displacement is allowed by a light from a laser diode that hits the probe and, after the reflection on it, reach a photodiode detector that register its position. This type of detection allows the measurement of small tip deflections because it magnify the signal into a detectable one. The cantilever tip can have a pyramidal or spherical shape.

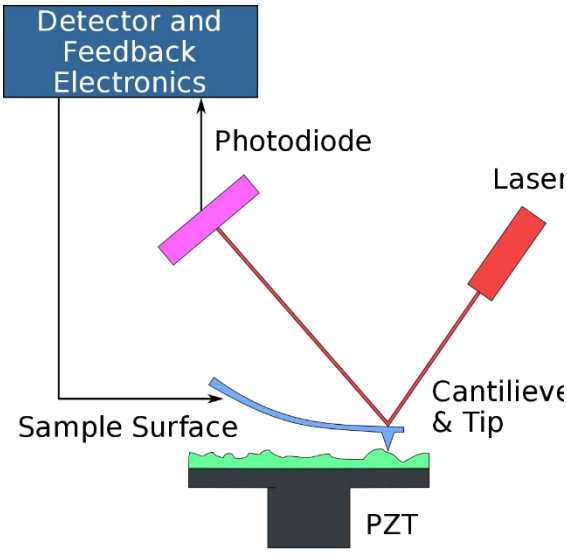


**Figure 4.4.** *Schematic representation of AFM.*

At a specific point on the gel surface, the tip indentation can be plotted ad a function of the applied force as can be observed in figure 4.5. These data are then converted into surface modulus using the spring constant for the probe and a proper model for elasticity and Poisson's ratio for the material analysed [39]. The equation that can be used for the calculation of elastic modulus of hydrogels is the following one.

$$E = \frac{\pi \cdot k \cdot (1 - \nu^2)}{2 \cdot tan\alpha} \frac{d}{\delta^2} \tag{12}$$

Surface and bulk hydrogel's mechanical properties are often described by Hertz model. Instead the value of Poisson's ratio is different from the surface (0,2) to the bulk where its value is 0,45-0,5 [39].

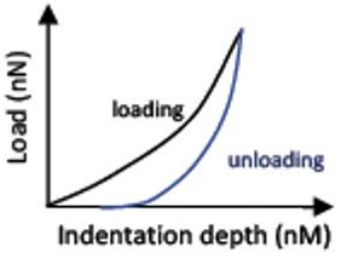


**Figure 4.5.** *Atomic Force Microscopy output.*

### 4.2.2 Rheology

Rheometry is a convenient method for hydrogels characterization, because it is quick, sensitive and requires small sample sizes [39]. This method allows the study of characteristic of the microstructure of the sample, such as crosslinking density, proximity of the glass transition, molecular weight and structural homogeneity or heterogeneity [40]. Rheology can be defined as the science that study the deformation and flow of matter, and it has been used in order to characterize hydrogels, viscoelastic materials. The mechanical behaviour of hydrogel, such as rigidity modulus and viscosity, is usually function of time, degree of deformation and geometry of the applied deforming force. Hydrogels can be classified as thixotropic materials. Their response to an applied force is nonlinear, they undergo a decrease in the viscosity with an increase of shear rate. For this reason, there are two different methods available to describe its rheological parameters: static and dynamic method. The static method observes the development in time of the strain due to the progressive change of the stress applied, or vice versa. Instead, the dynamic method involves the application of a harmonically varying strain. Small amplitude oscillatory shear (SAOS) is the main dynamic rheological technique that allows the characterization of small amount of sample, with a mass below 1 g. The hydrogel tested was cylindrical with a diameter of 24 mm and a height of 1 mm. Sample is placed between two parallel disks and torsional oscillations with small amplitude are exerted in order to generate shear flow stresses in the specimen. The configuration of rheological experiments is showed in figure 4.6. Testing the material in its linear viscoelastic regime (LVE) can be used the dynamic moduli (G'(ω) and G''(ω)) to study gel structure and mechanical behaviour. As can be seen in figure 4.7, in LVE moduli are independent from amplitude of the deformation Rheometry allows to obtain two mechanical moduli G' and G'' in the frequency domain. G' is the storage modulus that is a measure of the energy stored by the sample, and therefore it is directly related to the elasticity. G'' is the loss modulus that is a measure of the amount of energy loss by the sample through viscous dissipations, and therefore it is related to the viscosity of the sample. The data obtained from oscillatory rheometry method belongs to the frequency domain. These dynamic mechanical data can be converted to the time domain thanks to the Eq. 2, obtaining the relaxation modulus G(t), where t is $1/\omega$[38].

$$G(t) = G'(\omega) - 0{,}4\, G''(0{,}4\,\omega) + 0{,}014\, G''\,(10\,\omega) \qquad (2)$$

If G' is measured at low frequency of oscillations, it's identified as the shear modulus [40]. G'' is the viscous modulus or loss modulus. If G'' is much higher than G', the viscous property of the

hydrogel is higher than the elastic property in the period of deformation. This behaviour is characteristic of uncross-linked hydrogels. Instead, when G' is much higher than G'' an increase of slope of the elastic modulus curve is observed, indicating an increase of the elastic behaviour of gel. In this case the material is partially cross-linked. If the hydrogel network is highly cross-lined, G' and G'' are both very hight and almost parallel to each other. If an uncross-lined hydrogel is measured in the LVE the point where G' and G'' intersects each other is known as the yield point. However, analysing fragile sample with this technique can be challenging, since mechanical perturbation induced in the sample can damage its structure, altering the final shear or elastic modulus measurement [40].

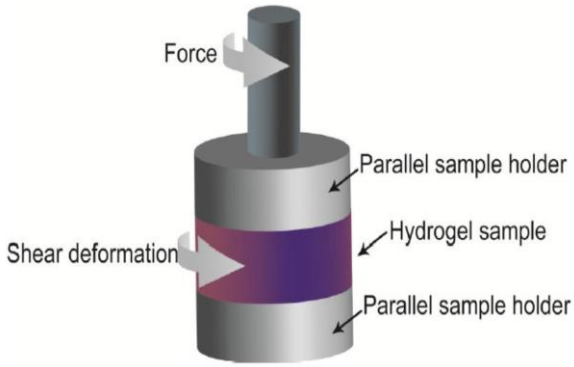


**Figure 4.6.** *Parallel plate-plate configuration for the rheological measurement* [41].

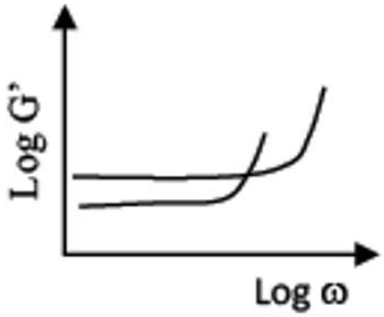


**Figure 4.7.** *Rheometry analysis output.*

In a dynamic mechanical analysis, the applied shear strain in the sinusoidal oscillation can be described by Eq. 13 and the resulting shear stress in output by Eq. 14.

$$\gamma(t) = \gamma_0 \cdot \sin(\omega t) \tag{13}$$

$$\tau(t) = \tau_0 \cdot \sin(\omega t + \delta) \tag{14}$$

where $\omega$ is the angular frequency of oscillation and $\delta$ the phase difference between the two waves. If the material has a pure elastic behaviour, the two waves are in phase and $\delta = 0°$, in

the other case, if it has a pure viscous response, there is a difference between the waves of 90°. For hydrogel materials that are viscoelastic, the value of $\delta$ is in between the two responses. In addition, Eq. 14 can be rearranged in order to express the moduli G'(ω) and G''(ω), previously defined in Eq.s 6 and 7.

$$\tau(t) = \gamma_0[G'(\omega) \cdot sin(\omega t) + G''(\omega) \cdot \cos(\omega t)] \quad (15)$$

$$tan\delta = \frac{G''(\omega)}{G'(\omega)} \quad (16)$$

Figure 4.8 shows the graphical representation of the amplitude oscillatory shear measurement. It can be observed the delayed response of the material when it is subjected to a shear deformation.

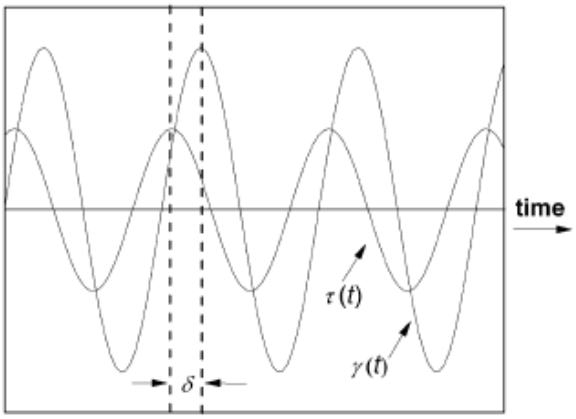


**Figure 4.8.** *Graphical representation of the amplitude oscillatory shear measurement* [42].

### 4.2.3 Uniaxial compression

Uniaxial compression test is another technique that can be used to examine the mechanical properties of hydrogels. The specimen is placed between two parallel plates and it is then compressed, by applying a uniform force (F) on the surface.

The mechanical properties can be evaluated by means of theoretical models, that considers the pressure applied and the amount of compression of the hydrogel. Stress ($\sigma_{true}$ [kPa]) and strain ($\varepsilon_{true}$) can be calculated knowing F and the uniaxial displacement of the gel, using the equation 17. Where $h_0$ is the initial height of the sample and Δh is the stroke of the upper plate.

$$\sigma_{true} = \frac{F}{A} \; ; \; \varepsilon_{true} = \frac{\Delta h}{h_0} \tag{17}$$

The elastic modulus can be calculated, using equation 18, knowing the stress and strain data, obtained applying a wide range of forces.

$$E = \frac{\sigma_{true}}{\varepsilon_{true}} \tag{18}$$

Figure 4.9 represents the configuration for the uniaxial compression measurement.

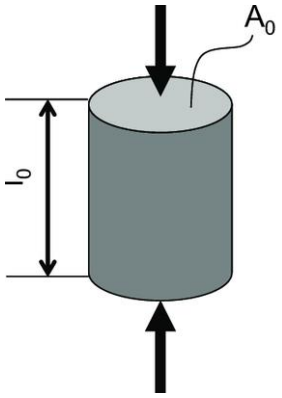


**Figure 4.9.** *Configuration for the uniaxial compression measurement.*

This is a simple method to measure the elastic modulus of hydrogels that doesn't limit the geometry of the sample. The hydrogel that have been tested was cylindrical and had the diameter of 24 mm and an initial height of 5 mm [43]. The measurement of elastic modulus of hydrogels by this technique may encounter some problems. For example, the sample must have a perfectly flat surface, and sometimes the swelling process modifies the geometry of the material obtaining non regular forms. In addition, hydrogels are very fragile and large stresses can break the sample, and traction measurements can't be performed because they can't be caught by the instrument.

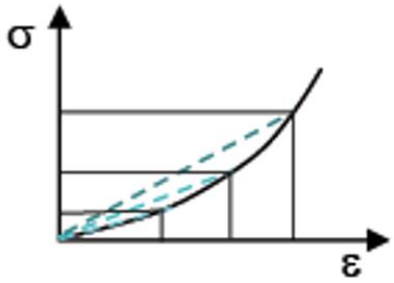


**Figure 4.9.** *Uniaxial compression output.*

### 4.2.4 Indentation

Indentation is a technique for the characterization of the mechanical properties of materials. Several methods have been developed as Brinell, Vickers, Rockwell and other ones[44].

In the field of biomaterials, indentation is particularly interesting in the characterisation of hydrogels since it is affordable and quick technique compared to other traditional ones as rheometry and atomic force microscopy (AFM), that are expensive and cannot be carried out in situ under cell culture conditions. In short, the hydrogel is indented by a microsphere, that causes a displacement in the material. Its measurement can deliver the Young's modulus by means of Hertz theory. This technique is particularly suitable in biological applications since it enables a straightforward measurement, it does not require expensive instrumentation that normally are not available in bio-labs, and it achieves high productivity[45].

In this work, this simple technique was implemented at constant force according to the method explained by Frey *et al.* and Long *et al.*[45,46], as represented in figure 4.10. The material was indented by means of different spheres with diameter in the range of 4-5.5 mm. Spheres made of different materials were employed to exploit different densities (i.e. plastic, glass or steel), thus applying difference applied forces.

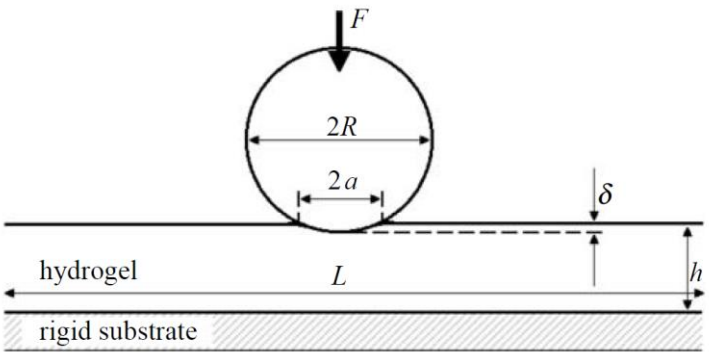


**Figure 4.10.** *Representation of the indentation technique of a hydrogel, in which δ is the depth of the displacement, a the contact radius, F the applied force*[47].

The elastic modulus is normally calculated exploiting the Hertzian contact theory. The Hertzian formula gives the relation between the load and displacement for a semi-infinite in-compressible elastic half-space that was indented by a rigid sphere. This relation is expressed by equation 19, where R is the radius of the sphere, δ is the depth of indentation, E is the elastic modulus and F is the load.

$$E = \frac{3\,F\,(1-v^2)}{4\,\delta^{\frac{3}{2}}\,R^{\frac{1}{2}}} \tag{19}$$

The Hertzian theory is based on the following assumptions:

- The substrate is a linear elastic semi-infinite half-space
- The substrate is in-compressible, then the Poisson ratio is equal to 0.5.
- The contact between the indenter and the surface is assumed to be without friction and adhesion.
- The sample strain is assumed to be smaller than 10%. In other worlds the ratio δ/h is equal to 0.1, where h is the height of the hydrogel.
- The indentation is low. This assumption is satisfied when $a^2 = R \cdot \delta$, where $a$ is the contact radius.

Since these assumptions are strictly limiting and cannot be easily satisfied, in some cases some corrections can be undertaken.

Moreover, there are more complex indentation methods, especially implemented to evaluate the viscoelastic behaviour of biomaterials. In fact, some cases, tests are performed at fixed penetration depth, measuring the time evolution of the required force[48]. This is the case of indentation load relaxation method, in which the hydrogel is immersed in a solvent and indented by means of a tip indenter. The mechanical force is applied by means of stepper motor, and a load cell is placed between the motor and the indenter

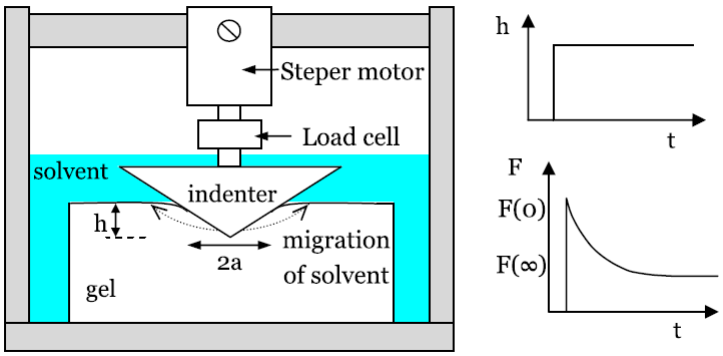


**Figure 4.11.** *Experimental set-up of for indentation load relaxation method* [48] *and displacement and load time profiles.*

In these case indentation tests allow also to determine transport properties without performing additional measurements. Other more complex methods were set-up in the literature, as long-focal-microscopy-based spherical microindentation in which a hydrogel disk is suspended and loaded by means of a microsphere, and central displacement is measured[43].

### 4.2.5 Micropipette aspiration

Micropipette aspiration technique is a simple and economical method that enables the measurement of biomaterials mechanical properties. It was invented in 1983 for measuring the bending rigidity of red blood cells membrane[49]. In later years, it was implemented also for other purposes as mechanical measurements of soft tissues[50], living cells[51] and multilayer biological soft materials[52]. This method is particularly effective since it overcomes costly loading instrumentations, applying a force in a simple way. Hence, the micropipette technique, is particularly suitable in biological laboratories thanks to its low cost, high throughput and versatility.

In short, the tip of a micropipette is placed in contact with the specimen and the internal pressure of the micropipette is reduced to cause the aspiration of the material. The maximum height of the displacement $L$ is optically measured, as well as the pressure drop inside the pipet.

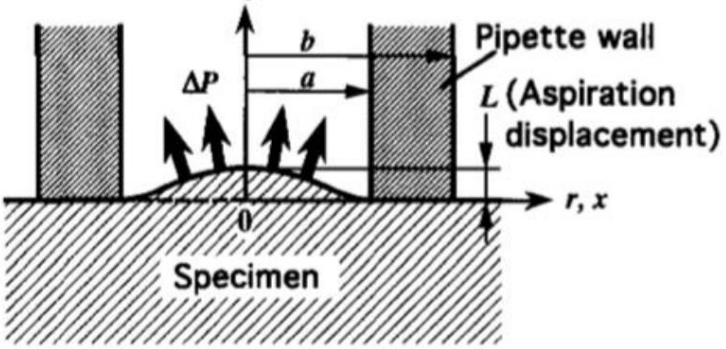


**Figure 4.12.** *Schematic representation of a micropipette aspiration test*[50].

Elastic modulus can be determined once the aspiration displacement $L$ and the pressure drop $\Delta P$ are collected. For this purpose, Aoki *et al.*[50] proposed equation 20:

$$E = C_I^A \frac{\Delta P \cdot a}{L} \tag{20}$$

where $E$ is the elastic modulus, $a$ is the internal radius of the micropipette and $C_I^A$ is coefficient that considers the wall thickness, since it is function of $b/a$ ratio ($b$ external radius of the micropipette). For infinite $b/a$ values, $C_I^A$ is equal to 0.97. This model assumes that the material is isotropic, incompressible, homogeneous and linearly elastic. As a matter of fact, in the literature other more complex models have been implemented, on the base also of Finite Element Method (FEM) simulations, that guarantee higher accuracy, as in the case of Zhang *et al*[52].

# Chapter 5

# Methods

The methods implemented and optimised in this study are illustrated. In particular, the methods used to synthetize polyacrylamide hydrogels, polyethylene oxide hydrogels and cryogels are described in this chapter. In addition, the realization of two methods, which allow to measure the elastic modulus of hydrogels, are illustrated. In conclusion, seeding procedure and analysis of the biological readout through immunofluorescence technique are described.

## 5.1 PAA synthesis

Two types of polyacrylamide hydrogels were synthetized. The first (PAA) composed only of AA and BAA as reported in literature[2] and a the second one (PAA-OH) including also N-Hydroxyethyl acrylamide (AA-OH)[6], which favours the following functionalization with cell-adhesive proteins. Polyacrylamide hydrogels with tuneable stiffness were obtained by changing relative concentrations of acrylamide and bis acrylamide in the solution. Polymerizing the solution inside a mould, PAA hydrogels with specific shapes can be obtained. In the synthesis, a glass coverslip functionalized with TMSPM (3 - (Trimethoxy silyl) propyl methacrylate) was used to provide a support to the gels.

### Mould preparation

Moulds allows to obtain polyacrylamide hydrogels with precise sized and smooth surfaces. The moulds were prepared using poly (dimethyl siloxane), or PDMS, and Kapton foils. PDMS layers were prepared by mixing Sylgard 184 elastomer and curing agent (1:10 ratio by weight). The solution was then degassed for fifteen minutes and poured in Pyrex glass petri dishes. In order to remove bubbles from the mixture, it was degassed a second time for fifteen minutes. PDMS was obtained after baking it at 70° for 2 hours. The layer was detached from the petri dish and the gaskets can be obtained cutting the PDMS with punchers of differ sizes and shapes. Cylindrical PAA hydrogels used for 2D cell culture are 0.3 mm high, with diameters of 22 mm or 30 mm. PAA hydrogels used for mechanical testing have higher volumes in order to reduce the

edge effects perceived in measurements and mostly to avoid the influence of the glass-gel interface adhesion during the mechanical characterization. Rectangular PAA hydrogels were used for micropipette measurements and they were 2 mm high with a surface 4 mm large and 10 mm long. When PDMS gaskets with the required dimensions were obtained, they were washed with pure ethanol and placed on polystyrene or Kapton foils. In fact, clean PDMS exhibit a good adhesion to polystyrene and Kapton. After complete ethanol evaporation, gaskets are firmly attached to the substrate forming a watertight interface but, at the same time, they can be removed any time using forceps. In order to reduce the inhibition of thermal polymerization of PAA hydrogels, PDMS gaskets are internally covered with Kapton tape.

Instead, PAA hydrogels for macro indentation measurements has a cylindrical shape and they were obtained by casting the solution in plastic moulds. These were obtained by lapping a 48-well tissue culture plate to match the desired height of the sample. PDMS weren't used in this case because it incorporates a high amount of oxygen, which inhibits the polymerization.

### Glass cover functionalization

In order to create a support for PAA and PEG hydrogels, glass coverslips were functionalized with a solution of TMSPM. The functionalization solution was prepared under the chemical hood and its composition is reported in table 5.1.

**Table 5.1.** *Composition of TMSPM functionalization solution.*

| | **%V/V** |
|---|---|
| Pure ethanol | 93 |
| Acetic acid | 5 |
| TMSPM | 2 |

Cover glasses were activated through flame treatment to clean the surface and expose hydroxyl reactive groups. Cover glasses were placed into a glass petri dish with the activated surface on the top. A volume of 200 μL of functionalization solution was dropped on the glass coverslips and they were kept covered for fifteen minutes with an aluminium foil which protects them from the light, allowing the functionalization reaction to take place. The cover glasses were then washed three times with acetone 99%.

### Polyacrylamide hydrogel synthesis

Diluted solutions of acrylamide, bis-acrylamide and hydroxyethyl-acrylamide were prepared using milli Q water. The concentrations of the diluted solutions are reported in table 5.2.

**Table 5.2.** *Concentration of stock water solutions.*

| | **Concentration (wt/V)** |
|---|---|
| Acrylamide (AA) | 40 % |
| N, N'-Methylene-bis-acrylamide (BAA) | 2 % |
| Hydroxyethyl-acrylamide (AA-OH) | 48,5% |

In order to obtain PAA hydrogels, solutions of Milli Q water, acrylamide (AA) and Bis-acrylamide (BAA) were prepared in defined concentrations according to table 5.3. PAA-OH hydrogels were obtained preparing solution of Milli Q water, acrylamide (AA), Bis-acrylamide (BAA) and N-Hydroxyethyl acrylamide (AA-OH) according to table 5.4. The compositions of these gels were calculated to have 0,1 mM of AA-OH in the final solutions substituting part of the AA and keeping this amount constant for all the stiffness. As described in equation 5.1, the number of moles of AA in PAA gels are equal to the sum of the moles of AA and AA-OH in PAA-OH hydrogels.

$$(n_{AA})_{PAA} = (n_{AA} + n_{AAOH})_{PAAOH} \tag{5.1}$$

After mixing, the solutions were warmed at 37°C for 5 minutes inside a water bath and then they were degassed for 15 minutes at -0,9 bar, since oxygen can inhibit polymerization reaction and can induce an alteration in mechanical properties of the final product. Polymerization set-up was then prepared: micropipettes, functionalized glass coverslips, initiators and tweezers; In order to start the radical polymerization reaction, initiators were added to achieve a final concentration of 1%V/V for APS and 0,1% V/V for TEMED. APS powder was weighted and solubilized in milli Q water. The first seven PAA and PAAOH require a 10% APS solution, the other ones a 20% solution. Thermal polymerization and radical formation start instantly, the solution was thus poured rapidly into the mould and covered with a functionalized cover glass, in order to isolate them from oxygen. During this operation, air bubbles doesn't have to be incorporated inside the gasket. If the gel was prepared for mechanical tests, 300 µL of solution were needed. If the gel was prepared for cell culture, the volume needed was 140 µL. The polymerization time was a function of the composition of gels and they are reported in table 5.5. Less concentrated gels require more time to polymerize than the other. The first seven polyacrylamides in table 5.3 and 5.4 have a polymerization time of seventeen minutes. The hydrogels number eight has an intermediate concentration of reagents and they were polymerized for twelve minutes. Hydrogels number nine and ten have a higher concentration of reagents and they were polymerized for ten minutes. Hydrogels were then removed shortly

after polymerization, to avoid PAA dehydration and the consequent attachment to the mould. Otherwise cracks and dis-homogeneities form on the surface leading to altered cells behaviour. Polymerized hydrogels are then placed in a petri dish and covered with milli-q water to incorporate it into the polymer network and reach an equilibrium state. Swelling occurs overnight at RT in milli Q water. Swelling is also important since unreacted monomers are toxic for cells and can diffuse outside the gel. Hydrogels washed once with milli Q water to remove unreacted AA, then they are ready for the following functionalization step.

**Table 5.3.** *Polyacrylamide solutions composition for each mL.*

| | wt% AA/BAA | WATER [µL] | AA (40%) [µL] | BAA (2%) [µL] |
|---|---|---|---|---|
| PAA 1 (0.15KPA) | 3.5/0.03 | 897.5 | 87.5 | 15.0 |
| PAA 2 (0.7 KPA) | 4/0.03 | 885.0 | 100.0 | 15.0 |
| PAA 3 (1KPA) | 5/0.03 | 860.0 | 125.0 | 15.0 |
| PAA 4 (1.37KPA) | 3/0.15 | 850.0 | 75.0 | 75.0 |
| PAA 5 (1.67KPA) | 3/0.225 | 812.5 | 75.0 | 112.5 |
| PAA 6 (2 KPA) | 4/0.1 | 850.0 | 100.0 | 50.0 |
| PAA 7 (2.5 KPA) | 4/0.15 | 825.0 | 100.0 | 75.0 |
| PAA 8 (4 KPA) | 5/0.15 | 800.0 | 125.0 | 75.0 |
| PAA 9 (8 KPA) | 5/0.225 | 762.5 | 125.0 | 112.5 |
| PAA 10 (40KPA) | 8/0.48 | 560.0 | 200.0 | 240.0 |

**Table 5.4.** *Hydroxy-polyacrylamide solutions composition for each mL.*

| | wt% (AA+AAOH)/BAA | WATER [µL] | AA (40%) [µL] | BAA (2%) [µL] | AAOH (48,5%) [µL] |
|---|---|---|---|---|---|
| PAAOH 1 | 4.0/0.03 | 891.2 | 68.8 | 15.0 | 25.0 |
| PAAOH 2 | 4.5/0.03 | 878.7 | 81.3 | 15.0 | 25.0 |
| PAAOH 3 | 5.5/0.03 | 853.7 | 106.3 | 15.0 | 25.0 |
| PAAOH 4 | 3.5/0.15 | 843.7 | 56.3 | 75.0 | 25.0 |
| PAAOH 5 | 3.5/0.225 | 806.2 | 56.3 | 112.5 | 25.0 |
| PAAOH 6 | 4.5/0.1 | 843.7 | 81.3 | 50.0 | 25.0 |
| PAAOH 7 | 4.5/0.15 | 818.7 | 81.5 | 75.0 | 25.0 |
| PAAOH 8 | 5.5/0.15 | 793.7 | 106.3 | 75.0 | 25.0 |
| PAAOH 9 | 5.5/0.225 | 756.2 | 106.3 | 112.5 | 25.0 |
| PAAOH 10 | 8.5/0.48 | 553.7 | 181.3 | 240.0 | 25.0 |

## Fibronectin functionalization

The fibronectin coating was optimised in order to have a simple and cost and time effective method. The functionalization of PAA-OH hydrogels with fibronectin must be performed under a sterile hood. First, a diluted Fibronectin solution was prepared in sterile PBS, with a final concentration of 25 µg/mL. PBS used must be cold and the diluted solution was then stored at 4°C. In order to sterilize PAA hydrogels prepared, the bottom of each coverslip was cleaned

with ethanol 70% and then moved into a sterile multi-well (flat bottomed, 6-multiwell tissue culture plate). Hydrogels were sterilized in dry condition for fifteen minutes under the UV light (λ=254 nm) inside the hood. After the sterilization, gels were functionalized filling each well with 1,5 mL of fibronectin solution and multiwells were putted inside an incubator overnight.

## 5.2 PEG synthesis

Polyethylene glycol hydrogels were synthetized crosslinking norbornene units with a custom cysteine terminated peptide (CRDGPQGIWGQDRC), with an UV assisted reaction and LAP (Lithium phenyl-2,4,6-trimethylbenzoylphosphinate) as photoinitiator. These hydrogels allow to uncouple the effects of matrix's mechanical and biological cues on cell behaviour, taking advantage of the lego-like approach by which, we can completely tailor the mechanical properties and the density of the cell-adhesive moieties independently. Moreover, they offer the possibility to embed cells, thanks to the mild synthesis conditions and the use of non-toxic precursors and compounds. Both 4-arm and 8-arm PEG-norbornene macromers were used, varying their concentration in the initial solution. Since this material is like a blank slate for cells due to the lack of cell-adhesive moieties, different concentrations of a custom RGD peptide with a reactive cysteine on one side (GRGDSPC), are linked to the PEG macromers in order to allow cell adhesion. To assure a high yield reaction between PEG-NB and RGD peptide and therefore to precisely control the density of cell-adhesive sites, it has also been developed a method in which a pre-reaction step is made between PEG-NB and RGD peptide and a small amount of photoinitiator[31].

PEG-NB hydrogels for cells cultures are synthetized on glass bottom petri dishes (Cellvis) functionalized with TMSPM. A drop of the prepolymer solution is placed in the centre of the petri dish. Since detaching of the PEG hydrogels is challenging from Kapton, polystyrene or clean glass, non-adhesive glass coverslips were placed over the solution drop, in order to give a homogeneous flat surface to hydrogels. PEG-NB hydrogels for mechanical measurements were casted in PDMS gaskets closed by a TMSPM substrate on one side and a non-adhesive glass coverslip on the other.

### Preparation of hydrophobic non-adhesive glass coverslips

Glass coverslips were functionalized with Trichloro(1H,1H,2H,2H-perfluorooctyl) silane, which makes the surface hydrophobic. Coverslips with a diameter of 15 mm were washed in acetone, air dried and dehydrate for 5 minutes at 150 °C on a hot plate. Glass surfaces of slides were activated in a plasma cleaner. The chamber was evacuated for one minute and then the

plasma treatment was applied for another minute. Slides were then positioned inside a vacuum chamber, in a sample holder, to keep them detached and in a vertical position. Under a chemical hood, 200 µL of silane were pipetted on the bottom of the chamber, inside a glass petri dish and then the jar was evacuated up to -0.9 bar. After this, the sealed jar was heated at 180°C for 3 hours in a hoven. After the heat treatment, the system was slowly cooled down to room temperature. The coverslips were recovered under the chemical hood and heated at 180 °C for 10 minutes on a hot plate. The detaching slides were then collected in a PS Petri dish enveloped in aluminium foil to protect them from light. The functionalized coverslips must be used within a day.

### Preparation of functionalized petri

Glass bottom petri dish with an external diameter of 35 mm were functionalized with TMSPM. Glass surface of the petri was activated in a plasma cleaner. The chamber was evacuated for two minutes and the plasma treatment was applied for one minute. Petri were then functionalized with TMSPM solution. A new solution must be prepared each time according to table 5.1. The solution was pipetted inside the petri which was closed with its cover for 15 minutes. The unreacted solution was removed washing three times the petri dishes with ethanol 70%. Three more washes were performed with milli Q water. Petri dishes were then dried in air.

### Synthesis with PEG four arms and eight arms without pre-reaction step

To independently study how adhesion and hydrogel mechanic instruct cell behaviour, different PEG-NB hydrogels were prepared varying the concentrations of PEG macromer and crosslinker (keeping the same amount of RGD peptide) as described in tables 5.6 and 5.8 or fixing the macromer concentration and varying the RGD concentration (tables 5.7, 5.9). Stock solutions of PEG-NB, crosslinker, RGD peptide and LAP were prepared, according to table 5.5 and following a specific order. LAP and PEG-NB were dissolved in PBS and mixed carefully to ensure the complete resuspension. Crosslinker and RGD peptides were dissolved in milli Q water right before the use to minimize the oxidation of reactive thiols presented by the cysteine. Diluted solutions were prepared, adding the correct amounts of reagents in the following order: PEG-NB, crosslinker, RGD and LAP and add the right amount of 1X PBS to achieve the final volume. Solutions were mixed using a pipette and, in order to create a 150 µm height hydrogel with a diameter of 15 mm, 26.5 µL of solution was placed at the centre of a functionalized glass bottom petri dish. The drop was then spread with a detaching slide, taking care to keep it away

from the edges of the petri dish to avoid the solution flow out of the glass sandwich. The polymerization of the solutions was then carried out by means of a 400 nm UV led lamp. The intensity of the lamp was set at 5% in the case of solutions with a PEG concentration equal or greater than 6% and at 8% for those with a lower concentration. Concentrated solutions were irradiated for two minutes, the others for six minutes. Once the polymerization was completed, the detaching slides were removed very slowly from the hydrogel to avoid breaking it. The hydrogels obtained were then let to swell in PBS overnight.

**Table 5.5.** *Properties of stock solutions used.*

| | **PEG-NB 4A** | **PEG-NB 8A** | **Crosslinker** | **RGD** | **RDG** | **LAP** | **PBS** |
|---|---|---|---|---|---|---|---|
| Concentration (%w/w) | 25 | 25 | 5 | 5 | 5 | 2 | 1 |
| Purity (%w/w) | 100.00 | 100.00 | 95.22 | 96.98 | 96.98 | 95.00 | 100 |
| Molecular Mass [Da] | 20000 | 40000 | 1540 | 690.7 | 690.7 | 264.2 | - |

**Table 5.6.** *Composition of PEG-NB 4 arms solution with different PEG concentration, final volume 100 µL.*

| **%w/w Final PEG concentration** | **Final RGD concentration [mM]** | **Molar ratio PEG/CrossL** | **PEG-NB 4 arms [µL]** | **Crosslinker [µL]** | **RGD [µL]** | **LAP [µL]** | **PBS [µL]** |
|---|---|---|---|---|---|---|---|
| 3.5% | 3 | 1/1.3 | 14.0 | 17.8 | 4.3 | 1.8 | 62.1 |
| 4% | 3 | 1/1.2 | 16.0 | 21.0 | 4.3 | 2.1 | 56.6 |
| 5% | 3 | 1/1.2 | 20.0 | 27.5 | 4.3 | 2.6 | 45.6 |
| 7% | 3 | 1/1.1 | 28.0 | 40.4 | 4.3 | 3.7 | 23.6 |
| 9% | 3 | 1/1.1 | 36.0 | 53.4 | 4.3 | 4.7 | 1.6 |

**Table 5.7.** *Composition of PEG-NB 4 arms solution with different RGD concentration, final volume 100 µL.*

| **%w/w Final PEG concentration** | **Final RGD concentration [mM]** | **Molar ratio PEG/CrossL** | **PEG-NB 4 arms [µL]** | **Crosslinker [µL]** | **RGD [µL]** | **RDG [µL]** | **LAP [µL]** | **PBS [µL]** |
|---|---|---|---|---|---|---|---|---|
| 9% | 0.5 | 1/1.1 | 36.0 | 53.4 | 0.7 | 3.6 | 4.7 | 4.1 |
| 9% | 1 | 1/1.1 | 36.0 | 53.4 | 1.4 | 2.9 | 4.7 | 3.6 |
| 9% | 2 | 1/1.1 | 36.0 | 53.4 | 2.8 | 1.5 | 4.7 | 2.6 |
| 9% | 3 | 1/1.1 | 36.0 | 53.4 | 4.3 | 0.0 | 4.7 | 1.6 |

**Table 5.8.** *Composition of PEG-NB 8 arms solutions with different PEG concentration, final volume 100 µL.*

| %w/w Final PEG concentration | Final RGD concentration [mM] | Molar ratio PEG/CrossL | PEG-NB 8 arms [µL] | Crosslinker [µL] | RGD [µL] | LAP [µL] | PBS [µL] |
|---|---|---|---|---|---|---|---|
| 4.7% | 3 | 1/2.3 | 18.8 | 6.6 | 4.3 | 2.5 | 66.8 |
| 5.0% | 3 | 1/1.6 | 20.0 | 10.1 | 4.3 | 2.6 | 62.7 |
| 5.2% | 3 | 1/1.7 | 20.8 | 9.9 | 4.3 | 2.7 | 61.7 |
| 5.5% | 3 | 1/1.4 | 22.0 | 12.7 | 4.3 | 2.9 | 58.1 |
| 7% | 3 | 1/1.8 | 28.0 | 12.6 | 4.3 | 3.7 | 50.1 |
| 9.0% | 3 | 1/1.2 | 36.0 | 24.3 | 4.3 | 4.7 | 30.7 |
| 9.0% | 3 | 1/1.9 | 36.0 | 32.0 | 4.3 | 4.7 | 20.6 |
| 12.5% | 3 | 1/1.3 | 50.0 | 31.1 | 4.3 | 6.6 | 6.8 |

**Table 5.9.** *Composition of PEG-NB 8 arms solutions with different RGD concentration, final volume 100 µL.*

| %w/w Final PEG concentration | Final RGD concentration [mM] | Molar ratio PEG/CrossL | PEG-NB 8 arms [µL] | Crosslinker [µL] | RGD [µL] | RDG [µL] | LAP [µL] | PBS [µL] |
|---|---|---|---|---|---|---|---|---|
| 9% | 0.2 | 1/1.2 | 36.0 | 24.3 | 0.3 | 4.0 | 4.7 | 33.5 |
| 9% | 1 | 1/1.2 | 36.0 | 24.3 | 1.4 | 2.9 | 4.7 | 32.7 |
| 9% | 3 | 1/1.2 | 36.0 | 24.3 | 4.3 | 0.0 | 4.7 | 30.7 |

## Synthesis of PEG eight arm with premix

In order to favour the reaction between 8-arm PEG-NB and RGD peptides, the previous method was modified by dividing the polymerization in two steps. The first reaction was the functionalization reaction of PEG-NB with the monofunctional peptides. This reaction occurs by exposing the pre-solution of PEG-NB, RGD, RDG (when needed) and LAP to a UV ray of 15% intensity for ten minutes. The amount of LAP added consists of a fifth of moles of RGD and RDG. Then PBS, crosslinker and LAP were added. The amount of LAP added for the crosslinking step consists of 0.5% by weight of the mass of PEG. The final solutions with a concentration of PEG lower than 10% were irradiated with a UV ray of 15% intensity for ten minutes. The most concentrated solutions were irradiated for two minutes with a UV ray intensity of 6%.

**Table 5.10.** *Composition of PEG-NB 8 arms solutions with different PEG concentration, final volume 100 µL.*

| Final hydrogels properties | | | PREMIX | | | Polymerization | | |
|---|---|---|---|---|---|---|---|---|
| %w/w PEG | RGD [mM] | Molar ratio PEG/Crosslinker | PEG-NB 8 arms [µL] | RGD [µL] | LAP [µL] | Crosslinker [µL] | LAP [µL] | PBS [µL] |
| 4.7% | 3 | 1/2.3 | 18.8 | 4.3 | 2.3 | 6.6 | 1.2 | 66.8 |
| 5.0% | 3 | 1/1.6 | 20.0 | 4.3 | 2.3 | 10.1 | 1.3 | 62.0 |
| 5.2% | 3 | 1/1.7 | 20.8 | 4.3 | 2.3 | 9.9 | 1.4 | 61.3 |
| 5.5% | 3 | 1/1.4 | 22.0 | 4.3 | 2.3 | 12.7 | 1.4 | 57.2 |
| 9.0% | 3 | 1/1.2 | 36.0 | 4.3 | 2.3 | 24.3 | 2.4 | 30.8 |
| 13.0% | 3 | 1/1.15 | 52.0 | 4.3 | 2.3 | 36.6 | 3.4 | 1.4 |

**Table 5.11.** *Composition of PEG-NB 8 arms solutions with different RGD concentration, final volume 100 µL.*

| Final hydrogels properties | | | PREMIX | | | | Polymerization | | |
|---|---|---|---|---|---|---|---|---|---|
| %w/w PEG | RGD [mM] | Molar ratio PEG/Crosslinker | PEG-NB 8 arms [µL] | RGD [µL] | RDG [µL] | LAP [µL] | Crosslinker [µL] | LAP [µL] | PBS [µL] |
| 9.0% | 0.2 | 1/1.2 | 36.0 | 0.3 | 4.0 | 2.3 | 24.3 | 2.4 | 34.8 |
| 9.0% | 1 | 1/1.2 | 36.0 | 1.4 | 2.9 | 2.3 | 24.3 | 2.4 | 33.6 |
| 9.0% | 3 | 1/1.2 | 36.0 | 4.3 | 0.0 | 2.3 | 24.3 | 2.4 | 30.8 |

## 5.3 Cryogel synthesis

Cryogels made of methacrylated alginate and PEG acrylate were developed, adapted from experiments reported in literature [17,53].

### Methacrylation of alginate

The methacrylation of sodium alginate has been performed in Prof Paolo Sgarbossa laboratory in order to produce methacrylate-alginate cryogels. In the reactions the reagents used were sodium alginate, AEMA (2 – amino ethyl methacrylate), NHS (N – hydroxy succinimide), EDC (1 – ethyl – 3 (3 dimethyl amino)) and MES (2 – morpholino ethane sulfuric acid).

First, MES buffer was prepared (0,6% wt/vol, pH 6,5). A 100 mM solution was prepared dissolving 1 g of sodium alginate in MES buffer. 1.3 g of NHS and 2.8 g of EDC were then added to the solution. After 5 minutes, 2.24 h of AEMA was dissolved. The solution was mixed vigorously for 24 hours. Methacrylated alginate was obtained by precipitation in acetone. The precipitate was filtered and then dried under vacuum at RT overnight. The product was analysed by NMR technique, in order to quantify the yield of the reaction.

## Synthesis PEG-Acrylate and PEGDA cryogels

Different cryogels were synthetized using 4-arm PEG Acrylate (PEG-AC) four arm (20 kDa) or PEGDA (575 kDa). These cryogels were functionalised with RGD (GRGDSPC) peptide and/or GELMA. PEG and PEGDA cryogels functionalised with RGD were produced with a molar ratio between cysteine and acrylate of 1:4 and 1:8. Cryogels were functionalised also with GELMA, varying its concentration from 0.1% to 2%. Cryogels functionalised with RGD peptide were produced in TEA buffer (0.3 M, pH 8).

PE cylindrical moulds, closed at one end with PDMS, were washed with ethanol and placed in a tube rack at -20°C. After that, 20% wt PEG-AC and PEGDA solutions and 4% wt RGD solution were prepared in TEA buffer, because it promotes the reaction between acrylate and thiol groups, increasing the yield of reaction. Instead, the solvent used in the production of cryogels functionalized with GELMA was milli Q water. In an eppendorf, the pre-solution was prepared adding PEG or PEGDA and RGD and/or GELMA, according to the following tables. After mixing, the solutions of PEG or PEGDA and RGD were put in a warm room of 37°C for 1 hour. The solution was then diluted adding TEA buffer or milli Q water and cooled to 4°C for 30 minutes. 10% APS solution was prepared with Milli Q wate. Pre-cooled solution was put in ice top to keep them cold while adding the radical initiators. The polymerization was activated by adding TEMED and APS, mixing the solution after each addition. As soon as possible, a volume of 200 µL of solution must be inserted into each mould and then cooled to -20°C for at least 15 hours. Cryogels were then obtained removing them from the mould with large and wide tweezers, to don't break the material. Cryogels were stored in a falcon filled with Milli Q water.

Table 5.12 reports the composition of cryogels with a final concentration of PEG of 7.5% and a ratio between cysteine and acrylate groups of 1:4 and 1:8. Table 5.13 describes the composition of cryogels with a final concentration of PEGDA of 5%, functionalized with the same amount of RGD peptide of table 5.12. PEG and PEGDA cryogels functionalized with GELMA are reported in tables 5.14 and 5.15. Finally, table 5.16. describes a PEG cryogel functionalized with both RGD and GELMA.

**Table 5.12.** *Composition of 7.5% PEG and RGD cryogels, final volume solution 500 mL.*

| PEG 7.5% | PEG 20% in TEA [µL] | RGD 4% in TEA [µL] | TEA [µL] | APS 10% in $H_2O$ | TEMED [µL] |
|---|---|---|---|---|---|
| 1:4 C:A | 188.0 | 32.5 | 269.0 | 10.0 | 0.7 |
| 1:8 C:A | 188.0 | 16.3 | 285.0 | 10.0 | 0.7 |

**Table 5.13.** *Composition of 5% PEGDA and RGD cryogels, final volume solution 500 mL.*

| PEGDA 5% | PEGDA 20% in TEA [µL] | RGD 4% in TEA [µL] | TEA [µL] | APS 10% in $H_2O$ | TEMED [µL] |
|---|---|---|---|---|---|
| 1:4 C:A | 125 | 32.5 | 332.0 | 10.0 | 0.7 |
| 1:8 C:A | 125 | 16.3 | 348.0 | 10.0 | 0.7 |

**Table 5.14.** *Composition of 7.5% PEG and GELMA cryogels, final volume solution 500 mL.*

| PEG 7.5% | PEG 20% in $H_2O$ [µL] | GELMA 8% in $H_2O$ [µL] | $H_2O$ [µL] | APS 10% in $H_2O$ | TEMED [µL] |
|---|---|---|---|---|---|
| 1% GELMA | 188.0 | 62.5 | 238.5 | 10.0 | 0.7 |
| 2% GELMA | 188.0 | 125.0 | 176.0 | 10.0 | 0.7 |

**Table 5.15.** *Composition of 5% PEGDA and GELMA cryogels, final volume solution 500 mL.*

| PEGDA 5% | PEGDA 20% in $H_2O$ [µL] | GELMA 8% in $H_2O$ [µL] | $H_2O$ [µL] | APS 10% in $H_2O$ | TEMED [µL] |
|---|---|---|---|---|---|
| 1:4 C:A | 125.0 | 62.5 | 301.8 | 10.0 | 0.7 |
| 1:8 C:A | 125.0 | 125.0 | 239.3 | 10.0 | 0.7 |

**Table 5.16.** *Composition of 7.5% PEG, RGD and GELMA cryogels, final volume solution 500 mL.*

| PEG 7.5% | PEG 20% in TEA [µL] | RGD 4% in TEA [µL] | GELMA 10% in $H_2O$ [µL] | TEA [µL] | APS 10% in $H_2O$ | TEMED [µL] |
|---|---|---|---|---|---|---|
| 1:8 C:A | 188.0 | 11.3 | 2.5 | 287.5 | 10.0 | 0.7 |

## Synthesis of cryogels with PEG-AC, RGD and adjuvants.

PE cylindrical moulds, closed at one end with PDMS, were washed with ethanol and placed in a tube rack. In order to identify the type of cryogel synthetized, a number was written on each mould. After that, 20% wt PEG-AC solution and 4% wt RGD solution were prepared with TEA buffer. In an eppendorf, the pre-solution was prepared adding PEG and RGD, according to the table 5.17. After mixing, the solution was put in a warm room of 37°C for 1 hour and then cooled to 4°C for 30 minutes. 10% APS solution, ODN (5 µg/µL) and cytokines (1 µg/µL) were

prepared in Milli Q water. After pre-cooling, the pre-solution, ODN, cytokines and the moulds were put into ice. A volume of 81,7 µL of PEG and RGD solution was pipetted inside the eppendorf which contains adjuvants. The polymerization was activated by adding TEMED and APS and mixing the solution after each addition. As soon as possible, a volume of 200 µL of solution must be inserted into each mould and then cooled to -20°C for at least 15 hours. The cylinder was cut into smaller parts in order to open the microstructure of the material and, after removing them from the mould, cryogels were obtained.

**Table 5.17.** *Composition of PEG-Acrylate and RGD solution to obtain a 200 µL cryogel.*

| PEG 7,5% | PEG 20% in TEA buffer [µL] | RGD 4% in TEA buffer [µL] | ODN in H2O 5 µg/µL [µL] | GM-CSF in H2O 1 µg/µL [µL] | APS 10% in H2O [µL] | TEMED [µL] |
|---|---|---|---|---|---|---|
| **1:8** | 75,2 | 6,5 | 100 | 15 | 4 | 0,26 |

## 5.4 Macroindentation measurements

Macro-indentation technique was implemented to measure the elastic modulus of synthetized hydrogels. The hydrogels synthetized have an initial diameter of 5 millimetres and a height of 4 millimetres. After the synthesis they were extracted by the mould and we let them swell in water overnight at RT. PEG hydrogels were analysed after one day and the PAA hydrogels after two days from the synthesis, to allow them to reach an equilibrium state of swelling. During the measurement, hydrogels were kept out of water for less than 1 minute, in order to reduce the dehydration that could vary their mechanical characteristics. A reflex camera with 18-55 mm lens was used. A sample was placed in the photography lightbox over a plastic support, built ad hoc, and the light behind the gel was switch on to reach a better contrast. The indenter was placed gently on the central part of the gel surface. Indenter must have suitable weight and dimension, depending on the sample in analysis. The indenters used are listed in table 5.18 and two examples of a measure with the macroindentation technique are reported in figure 5.1.

**Table 5.18.** *List of indenters used for macro-indentation, their diameters and weights.*

| Indenters | Diameter (mm) | Weight (mg) |
|---|---|---|
| Plastic sphere | 4 | 47 |
| Glass sphere | 5 | 165 |
| Metallic sphere | 5.5 | 700 |
| Glass sphere loaded on plastic support | 5 | 7585 |

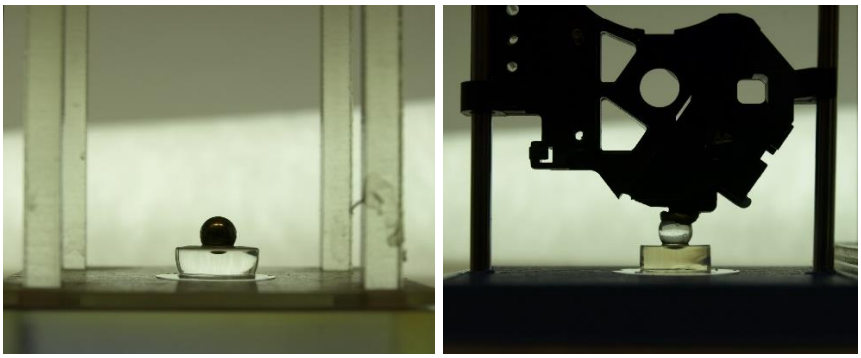

**Figure 5.1.** *Example of macroindentation on a soft (left) and a stiff (right) hydrogel with the steel sphere and the glass sphere with a plastic overweight which is supported by two metal tracks to avoid its overturning.*

The reflex camera was placed on a jack to set the right framing adjusting its height, since the camera has to seat on the same plane of the hydrogel surface. The zoom must be set in order to focus the spherical indenter. After zoom and focus setting, a picture is captured and analysed using a MATLAB script realized for these measurements to measure indenter diameter, indenter height outside the gel and gel height. The measurements (in pixel) were reported on an excel spreadsheet, in order to obtain elastic modulus. In the MATLAB script, the diameter of the sphere was measured in order to convert measurement in pixel into meter, knowing the diameter of the sphere in meter. The height of the spherical indenter outside the gel was measured to obtain indentation data. The elastic modulus can be calculated exploiting the Hertzian theory (§ 4.2.4).

Since the Hertz theory assumptions could not be easily satisfied, some correction were applied. In the case of large sample deformation and non-linear material, a corrected elastic modulus can be calculated using the model obtained by Long et al (2011), using a finite-element method [45]. The height of the gel is used to correct measured elastic modulus using the following equations.

$$\frac{E}{E_H} = \psi = \frac{1 + 2.3\,\omega}{1 + 1.15\,\omega^{\frac{1}{3}} + \alpha\left(\frac{R}{h}\right)\omega + \beta\left(\frac{R}{h}\right)\omega^2} \quad (1)$$

$$\omega \equiv \left(\delta\frac{R}{h^2}\right)^{\frac{3}{2}} \quad (2)$$

$$\alpha\left(\frac{R}{h}\right) = 10.05 - 0.63\sqrt{\frac{h}{R}}\left(3.1 + \left(\frac{h}{R}\right)^2\right) \quad (3)$$

$$\beta\left(\frac{R}{h}\right) = 4.8 - 4.23\left(\frac{h}{R}\right)^2 \quad (4)$$

In these equations, $E_H$ is the measured elastic modulus calculated by Hertzian theory, equation 1, and ω is an adimensional parameter that considers all the measured variables: indenter radius, indentation δ and sample height. α and β are correction parameters for frictionless or non-slip conditions. In fact, they consider the interaction between the indenter and the sample. This expression for the correction factor accurately matches the simulations results for the parameter range of $0.5 \leq \frac{R}{h} \leq 12.7$ and $\frac{\delta}{h} \leq \min\left(0.6, \frac{R}{h}\right)$[45].

## 5.5 Micropipette aspiration

The second simple and cost-effective technique we developed to measure the elastic modulus of hydrogels, is based on micropipette aspiration. This technique allows to correlate the aspirated length of a hydrogel inside the glass capillary when a certain negative pressure is applied with the elastic modulus of the hydrogel. The set-up used in this measurement technique is showed in figure 5.3 and consists on a digital camera, a computer, a microscope, a syringe pump, a pressure sensor, a sample holder, a glass capillary tube, with an external diameter of 1 mm and an internal diameter of 750 μm. The camera was connected to the microscope, allowing to photography the hydrogel aspired into the capillary tube. The hydrogel (high of 2 mm and a surface 4 mm large and 10 mm long) was supported in a vertical position by a sample holder, which was inserted into a glass bottom petri dish. This petri allows to observe the sample throw the microscope. The capillary tube was inserted through a hole in the vertical side of the petri assuring the alignment with the surface of the sample. An example of a sample analysed by the micropipette aspiration technique is reported in figure 5.2. In addition, figure 5.2 shows a sample set for a measure with the micropipette aspiration technique.

**Figure 5.2.** *Sample of PEG hydrogel (left) and set-up (right) for the micropipette aspiration.*

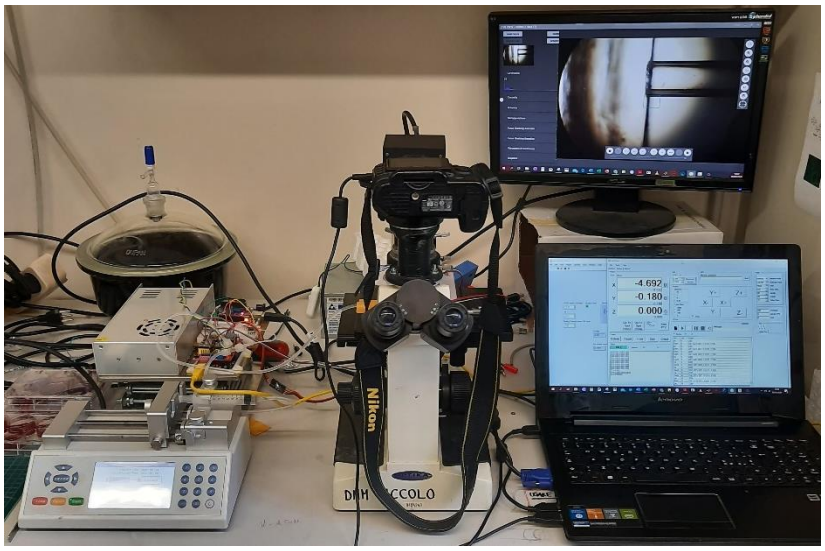


**Figure 5.3.** *Micropipette aspiration equipment: syringe pump, microscope, camera, computer.*

Little PTFE tubes connect the capillary tube to pressure sensors and to a syringe. The tubes were filled with water, if the sample was a PAA hydrogel, or with PBS 1x if the sample was a PEG hydrogel. The gel is moved toward the open end of the glass capillary with a custom-made positioning system until a full contact between the two surfaces is achieved, then, the syringe pump was used to exert a defined pressure on the hydrogel. Two different sensors were used to characterize the totality of the gels prepared: an more precise sensor capable of measuring a range between -160 mbar and 160 mbar (Honeywell HSCDRRN160MDAA5) was used for softer gels, a second sensor with a wider pressure range for the stiffer (Honeywell HSCDRRN600MDAA3). A computer allows to control the camera, the pressure sensors and the system used to move the petri dish and the sample close to the capillary tube. The software which allows to control them are LabVIEW, digicam controller and GRBL panel. Digicam controller shows the evolution of the aspiration in live and allow to take the picture of the aspiration to be analysed. GRBL panel controls the position and the speed of the petri dish movement. A LabVIEW program turns on the sensors and stores the value of the measured

pressure when the capillary is photographed. This equipment allows to measure the elastic modulus of hydrogels, according to the following protocol. Samples were inserted into the sample holder; Due to the higher swelling of the softer hydrogels, it may be necessary to cut the hydrogel and/or the glass slide. After inserting the sample holder, the petri dish was filled with water or PBS, in order to allow a correct observation of the hydrogel aspiration. The syringe and the plastic tubes were then filled with the same fluid. The capillary was moved close to the surface of the gel and the pressure sensor was set on zero. Turning on the syringe pump, a negative pressure was exerted on the surface of the gel by drawing the fluid into the syringe. The meniscus that forms inside the capillary can be photographed and, at the same time, the measured pressure value can be stored. The image was then analysed through a MATLAB script which determines the aspirated length of the gel in the centre of the meniscus. The elastic modulus was calculated in an excel file using the following equation, adapted from Ding et al. (2018) and obtained throught FEM simulations[54].

$$E = \frac{p_a}{0.872\left(\frac{l}{a}\right) + 0.748\left(\frac{l}{a}\right)^2} \tag{6}$$

Where $E$ was the elastic modulus, $p_a$ was the applied pressure, $l$ was the aspiration length and $a$ was the internal radius of capillary tube. This equation allows to calculate the elastic modulus in the case of large deformation of the hydrogel $\frac{l}{a} > 0.3$.

## 5.6 Cell seeding

PAA hydrogels synthesized with the previously described method were seeded with an immortalized cell line: MCF10A. Under a biological hood, the hydrogels were washed from the fibronectin solution with PBS and then placed in an incubator for ten minutes at 37 ° C in an atmosphere with 5% $CO_2$. Subsequently MCF10A cells from ATCC were prepared. The culture medium, in which cells were immersed, was removed from the flask and substituted with 2 mL of a trypsin solution was then added to break the focal adhesions and detach the cells from the plastic bottom. The flask was placed in an incubator for ten minutes. Once completely detached, the base culture medium was added to the flask, in order to stop the trypsin action. The solution obtained was then divided into falcons according to the calculated cells' total number and the desired cell's density on the hydrogel surface and centrifugated. Once the supernatant was eliminated, the cells were dispersed in the complete culture medium, which was a DMED/F-12 medium, enriched with horse serum, glutamine and pen/strep (5% V/V, 1%

V/V and 1% V/V), and freshly supplemented with cholera toxin, insulin, hEGF, hydrocortisone (10 µL, 10 µL, 5 µL and 4 µL for each 10 mL of final solution). Cells suspension was seeded as a drop of complete culture medium on top of fibronectin-coated hydrogels. The adherence between cells and the substrate takes eight to fifteen hours to occur. After attachment, the hydrogel containing wells were filled with 1.5 mL of complete culture medium. Cells were fixed with paraformaldehyde 4% for downstream analyses after 24 h.

## 5.7 Immunofluorescence

Immunofluorescence (IF) is a technique used to target fluorescent dyes specifically bound to molecules within the cell. Here it is used to analyse the localization of YAP / TAZ transcription factors inside the seeded cells and other cell parts such as nuclei and cytoskeleton. IF technique is based both on an indirect and direct staining method to analyse the structure of the cell and the localization of the proteins of interest. In indirect approach, primary and secondary antibodies conjugated to fluorescent dyes bind to the protein of interest (YAP/TAZ in this work). Direct staining, here, is used to bind fluorescent probed phalloidin to the F-actin filaments of the cells and 4′,6-diamidino-2-phenylindole (DAPI) to the DNA inside the nucleus to reveal the structure of the cells. The fluorescence can then be quantified using a confocal laser scanning microscope.

Cells seeded on hydrogels were fixed in PFA 4% for 10 minutes and, after washing with PBS, cells were permeabilized 10 min at RT with PBS 0.3% Triton X-100. Samples were then blocked in 10% Goat Serum in PBS 0.1% Triton X-100 (PBS-t) for 1 hour. Hydrogels were then incubated with primary antibody mouse anti YAP-TAZ (diluted in 2% GS in PBS-t) overnight at 4°C. After this, cells were washed four times in PBS-t and incubated with secondary antibody 568 Goat Anti-rabbit IgG and Alexa Fluor 488 Phalloidin (1:200 V/V and 1:100 V/V in 2% GS in PBST) for 2 hours at room temperature inside a dark box. Samples were mounted with ProLong-DAPI (Molecular Probes, Life Technologies) that allows to label cell nuclei. Once ready, samples were imaged using a confocal microscope (Leica TCS SP5 equipped with a 40x oil objective) and analysed with Volocity software. Samples can be stored at 4°C for several days, in order to maintain the fluorescence.

# Chapter 6

# Young modulus calculation: results

This chapter describes the theoretical models implemented to calculate the elastic modulus of hydrogels basing on the experimental data of the macro-indentation measurements. Since the models available in the literature have some limitations, FEM simulations (Abacus by Simulia$^{TM}$) were performed to calculate a correction factor that takes into account boundary effects and non-linearities of hydrogel samples. FEM simulations were performed with the collaboration of Prof. Lucia Nicola (DII).

## 6.1 Limitations on Macroindentation models

The elastic modulus of hydrogels is normally calculated exploiting the Hertzian contact theory. However, the assumptions on which this theory is based are strictly limiting and can't be easily satisfied. In fact, it assumes a semi-infinite material and it does not consider the edge effects deriving from having a hydrogel with finite height and diameter supported on a rigid substrate. In addition, Hertzian theory assumes that the material has a linear elastic behaviour. Figure 6.1 shows the experimental results of a uniform compression test done on a hydrogel with a diameter of 30 mm and 5 mm height. In this figure, the assumption is satisfied if the indentation is lower than about 10% of the sample height, because the hydrogel has a non-linear elastic response for higher deformations. From the experimental point of view, measurements done on hydrogels with low indentations are less accurate since the relative error in determining small indentations is greater.

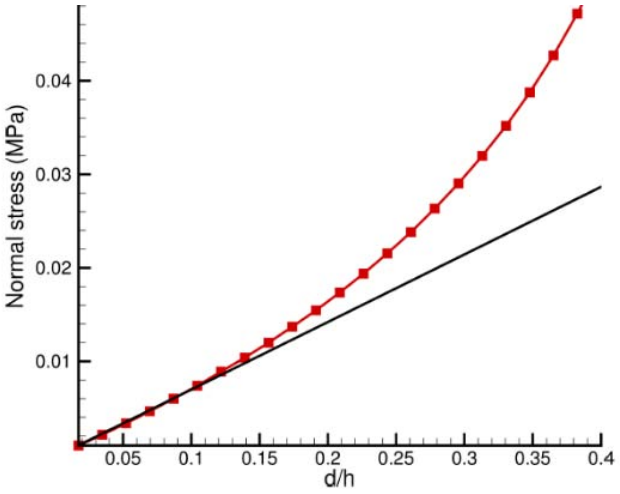


**Figure 6.1.** *Uniform compression test on a hydrogel with 30 mm of diameter and 5 mm height.*

Hertzian theory also assumes that the contact radius $a$ between the sphere and the surface must be low. This assumption is satisfied when $a^2 = R \cdot \delta$. Hence, FEM simulations have been performed to determine which is the maximum allowed depth of indentation ($\delta_{max}$) that satisfies this assumption for a given radius of the indenter (R) and substrate geometry. The maximum allowed depth of indentation is found to be dependent on the sample diameter D and the sample height h. The area bounded by the R vs $\delta_{max}$ curves of figure 6.2 is the region in which the assumption is valid. The simulations were performed on substrates with a diameter of 30 mm and a height of 5, 18 and 30 mm. This Hertzian assumption is satisfied only if the sample has large diameter and height, and only very low values of indentations are allowed if the measurement is done with radius of the sphered between 2 and 2.5 mm.

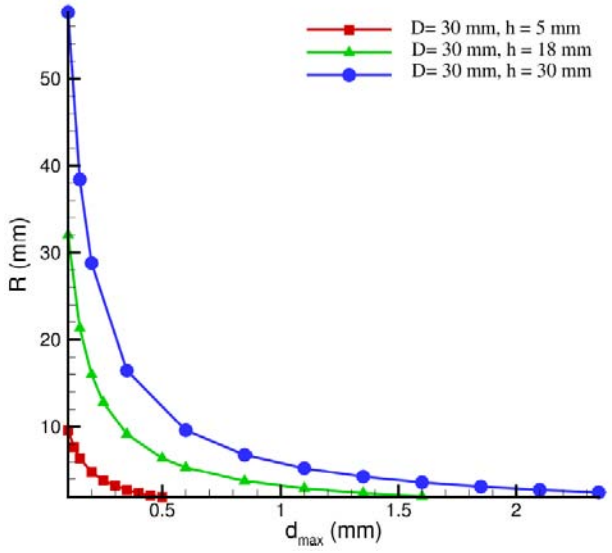


**Figure 6.2.** *Sphere radius R vs maximum indentation $\delta_{max}$ obtained from FEM simulations on substrates with 30 mm of diameter and different heights h.*

Since the Hertz theory assumptions could not be easily satisfied, some corrections were undertaken. In the case of large sample deformation and non-linear material, a corrected elastic modulus can be calculated using the model obtained by Long *et al*., using a finite-element method[45]. The height of the gel is used to correct the measured elastic modulus using the following equations.

$$\frac{E}{E_H} = \psi = \frac{1 + 2.3\,\omega}{1 + 1.15\,\omega^{\frac{1}{3}} + \alpha\left(\frac{R}{h}\right)\omega + \beta\left(\frac{R}{h}\right)\omega^2} \quad (1)$$

$$\omega \equiv \left(\delta\frac{R}{h^2}\right)^{\frac{3}{2}} \quad (2)$$

$$\alpha\left(\frac{R}{h}\right) = 10.05 - 0.63\sqrt{\frac{h}{R}}\left(3.1 + \left(\frac{h}{R}\right)^2\right) \quad (3)$$

$$\beta\left(\frac{R}{h}\right) = 4.8 - 4.23\left(\frac{h}{R}\right)^2 \quad (4)$$

In these equations, $E_H$ is the measured elastic modulus calculated by Hertzian theory, equation (§ 4.2.4), and ω is an adimensional parameter that considers all the measured variables: indenter radius, indentation δ and sample height. α and β are correction parameters for frictionless or non-slip conditions. In fact, they consider the interaction between the indenter and the sample. This expression for the correction factor accurately matches the simulations results for the parameter range of $0.5 \leq \frac{R}{h} \leq 12.7$ and $\frac{\delta}{h} \leq \min\left(0.6, \frac{R}{h}\right)$[45].

This corrected equation of Hertzian theory (equation 5) for finite height can be also written in a short form, equation 6, from Dimitrias *et al.* [55]. This equation is valid if the indentation is lower than 10% of the hydrogel height. In addition, the influence of the finite diameter of the material is not considered.

$$F = \frac{4\,E\,\delta^{\frac{3}{2}}R^{\frac{1}{2}}}{3\,(1-\upsilon^2)}\,f\left(\frac{a}{h}\right) \quad (5)$$

$$f\left(\frac{a}{h}\right) = 1 + 1.133\left(\frac{a}{h}\right) + 1.283\left(\frac{a}{h}\right)^2 + 0.769\left(\frac{a}{h}\right)^4 + 0.0975\left(\frac{a}{h}\right)^6 \quad (6)$$

In order to experimentally estimate the validity of this corrected equation, six polyacrylamides with different elastic modulus were synthesized and tested with macro-indentation. Then, the

values of elastic modulus obtained were compared with the elastic modulus determined by means of FEM simulations.

Macroindentation analysis have been made on PAA hydrogels using spheres with different diameters and weight. The measurements have been repeated 8 times in order to increase the accuracy of the measure. Mean values of elastic modulus have been calculated using the Hertzian formula and the one with the correction for the finite height.

PAA 2 have been measured using the black plastic sphere and the glass sphere, as can be seen in figure 6.3. Mean values of indentations and elastic modulus by Hertzian formula and the one corrected for finite height are reported in table 6.1. The errors calculated are the standard deviations.

**Figure 6.3.** *PAA 2 indented with plastic sphere (left) and glass sphere (right).*

**Table 6.1.** *Mean values of PAA 2 of E Hertzian and E Corrected on height.*

| | **Indentation %** | | **MEAN** | **SD** | **Error %** |
|---|---|---|---|---|---|
| Plastic | 19.5 ÷ 22.7 | E Hertzian | 0,167 | 0,011 | 6,3 |
| | | E Corrected | 0,129 | 0,009 | 7,0 |
| Glass | 32.0 ÷ 38.0 | E Hertzian | 0,237 | 0,024 | 10,3 |
| | | E Corrected | 0,158 | 0,019 | 12,1 |

PAA 3 was measured using the black plastic sphere, glass sphere and steel sphere as can be seen in figure 6.3. Mean values of indentations and elastic modulus by Hertzian formula and the one corrected for finite height are reported in table 6.2.

**Figure 6.3.** *PAA 3 indented with plastic (left), glass (centre) and steel sphere (right).*

**Table 6.2.** *Mean values of PAA 3 of E Hertzian and E Corrected on height with plastic sphere.*

| | Indentation % | | MEAN | SD | Error % |
|---|---|---|---|---|---|
| Plastic | 5.9 ÷ 8.9 | E Hertzian | 2,476 | 0,476 | 19,2 |
| | | E Corrected | 2,130 | 0,434 | 20,4 |
| Glass | 8.5 ÷ 15.7 | E Hertzian | 1,289 | 0,453 | 35,2 |
| | | E Corrected | 0,980 | 0,384 | 39,2 |
| Steel | 24.0 ÷ 27.4 | E Hertzian | 1,954 | 0,127 | 6,5 |
| | | E Corrected | 1,260 | 0,093 | 7,4 |

PAA 6 have been measured using the black plastic sphere, glass sphere and steel sphere, as can be seen in figure 6.4. Mean values of indentations and elastic modulus by Hertzian formula and the one corrected for finite height are reported in table 6.3.

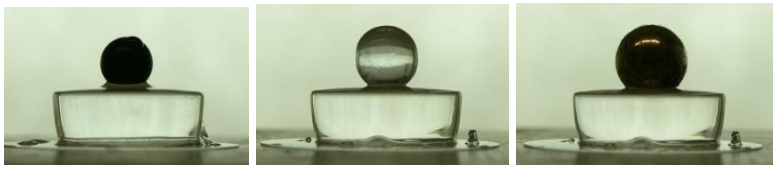

**Figure 6.4.** *PAA 6 indented with plastic (left), glass (centre) and steel sphere (right).*

**Table 6.3.** *Mean values of PAA 6 of E Hertzian and E Corrected on height with plastic sphere.*

| | Indentation % | | MEDIA | SD | Error % |
|---|---|---|---|---|---|
| Plastic | 3.3 ÷ 5.1 | E Hertzian | 2,476 | 0,476 | 19,2 |
| | | E Corrected | 2,130 | 0,434 | 20,4 |
| Glass | 8.4 ÷ 11.0 | E Hertzian | 2,999 | 1,299 | 43,3 |
| | | E Corrected | 1,820 | 0,269 | 14,8 |
| Steel | 16.4 ÷ 19.4 | E Hertzian | 3,965 | 0,310 | 7,8 |
| | | E Corrected | 2,603 | 0,211 | 8,1 |

PAA 8 have been measured using the steel sphere and the indenter, as can be seen in figure 6.5. Mean values of indentations and elastic modulus by Hertzian formula and the one corrected for finite height are reported in table 6.4.

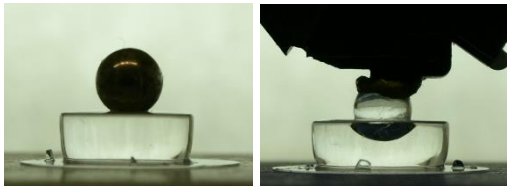

**Figure 6.5.** *PAA 8 indented with steel sphere (left) and indenter (right).*

**Table 6.4.** *Mean values of PAA 8 of E Hertzian and E Corrected on height with steel sphere.*

| | Indentation % | | MEDIA | SD | Error % |
|---|---|---|---|---|---|
| Steel | 7.3 ÷ 8.9 | E Hertzian | 12,368 | 1,007 | 8,1 |
| | | E Corrected | 9,477 | 0,869 | 9,2 |
| Indenter | 33.7 ÷ 39.7 | E Hertzian | 14,863 | 1,303 | 8,8 |
| | | E Corrected | 9,049 | 0,798 | 8,8 |

PAA 9 have been measured using the steel sphere and the indenter, as can be seen in figure 6.6. Mean values of indentations and elastic modulus by Hertzian formula and the one corrected for finite height are reported in table 6.5.

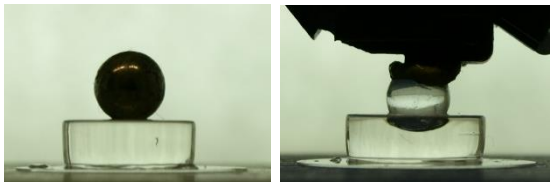

**Figure 6.6.** *PAA 9 indented with steel sphere (left) and indenter (right).*

**Table 6.5.** *Mean values PAA 9 of E Hertzian and E Corrected on height.*

| | Indentation % | | MEDIA | SD | Error % |
|---|---|---|---|---|---|
| Steel | 6.4 ÷ 8.8 | E Hertzian | 16.80 | 2.92 | 17.4 |
| | | E Corrected | 12.81 | 2.42 | 18.9 |
| Indenter | 31.4 ÷ 36.4 | E Hertzian | 19.92 | 1.66 | 8.3 |
| | | E Corrected | 11.65 | 0.97 | 8.4 |

PAA 10 have been measured using the steel sphere and the indenter, as can be seen in figure 6.7. Mean values of indentations and elastic modulus by Hertzian formula and the one corrected for finite height are reported in table 6.6.

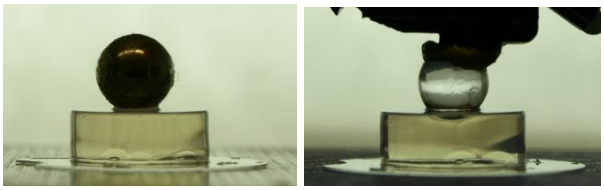

**Figure 6.7.** *PAA 10 indented with steel sphere (left) and indenter (right).*

**Table 6.6.** *Mean values PAA 10 of E Hertzian and E Corrected on height with steel sphere.*

| | Indentation % | | MEDIA | SD | Error % |
|---|---|---|---|---|---|
| Steel | 3.8 ÷ 6.2 | E Hertzian | 47.41 | 36.03 | 76.0 |
| | | E Corrected | 41.40 | 34.75 | 83.9 |
| Indenter | 11.5 ÷ 15.0 | E Hertzian | 79.46 | 10.20 | 12.8 |
| | | E Corrected | 56.04 | 8.12 | 14.5 |

From the previous tables, the values of the elastic modulus obtained by different measurements of the same hydrogel is not constant and it strongly depends on the indentation percentage. This can be explained as follows. First, some results are obtained with indentation higher than 10%, hence it falls within the region of nonlinearity. Second, results obtained with indentation lower than 10% should be discarded since the relative error on δ is high. As can be seen in table 6.6, the error on the mean value of the calculated elastic modulus is remarkable, up to 84%. the mean value of elastic modulus calculated has an elevated percentage error, up to 84%. Therefore, spheres which indents the material more than 10% must be chosen but the Long's correction is not valid anymore and must be adjusted.

To evaluate how much the Long's correction deviates at high indentation percentage, FEM simulations were performed. Six case studies were considered, one for each PAA sample. Each one was indented by the most suitable indenting conditions that guarantees the best compromise between low measurement error and low indentation percentage. In the case of PAA 2, plastic sphere was chosen because the percentage of indentation and of error are lower than the one obtained with the glass sphere. In the case of PAA 3 and PAA 6, the steel sphere was chosen because, even though the percentage of indentation is higher than for glass sphere, the values of elastic modulus have a lower standard deviation. The indentation using the plastic sphere, in these two hydrogels, is very low and the measures are not reproducible. The measures that can be considered more reliable for PAA 8 are those obtained with the steel sphere, because the percentage of indentation and of error are lower than 10%. For PAA 9 and PAA 10, the indenter was chosen because the measures are more accurate, due to the low indentation in the case of steel sphere. The following tables report eight experimental measurements of the elastic modulus of the six hydrogels done with the chosen spheres.

**Table 6.7.** *Macroindentation of PAA 2 with black plastic sphere.*

| h gel [m] | Indentation [m] | Indentation % | E Hertzian [KPa] | E Corrected [KPa] |
|---|---|---|---|---|
| 0.0047 | 0.0009 | 19.5 | 0.187 | 0.145 |
| 0.0046 | 0.0010 | 22.2 | 0.155 | 0.118 |
| 0.0046 | 0.0010 | 21.8 | 0.160 | 0.123 |
| 0.0047 | 0.0010 | 21.1 | 0.162 | 0.125 |
| 0.0045 | 0.0010 | 22.7 | 0.155 | 0.117 |
| 0.0047 | 0.0010 | 20.5 | 0.173 | 0.134 |
| 0.0048 | 0.0009 | 19.8 | 0.179 | 0.140 |
| 0.0048 | 0.0010 | 20.5 | 0.167 | 0.130 |

**Table 6.8.** *Macroindentation of PAA 3 with steel sphere.*

| h gel [m] | Indentation [m] | Indentation % | E Hertzian [KPa] | E Corrected [KPa] |
|---|---|---|---|---|
| 0.0044 | 0.0012 | 27.0 | 1.771 | 1.126 |
| 0.0043 | 0.0011 | 25.9 | 1.938 | 1.231 |
| 0.0043 | 0.0010 | 24.1 | 2.182 | 1.403 |
| 0.0044 | 0.0011 | 24.8 | 1.993 | 1.292 |
| 0.0045 | 0.0011 | 24.5 | 1.991 | 1.301 |
| 0.0045 | 0.0011 | 24.9 | 1.958 | 1.270 |
| 0.0043 | 0.0012 | 27.4 | 1.781 | 1.118 |
| 0.0045 | 0.0011 | 24.0 | 2.048 | 1.345 |

**Table 6.9.** *Macroindentation of PAA 6 with steel sphere.*

| h gel [m] | Indentation [m] | Indentation % | E Hertzian [KPa] | E Corrected [KPa] |
|---|---|---|---|---|
| 0.0040 | 0.0007 | 18.0 | 3.780 | 2.508 |
| 0.0040 | 0.0007 | 16.9 | 4.113 | 2.772 |
| 0.0042 | 0.0007 | 16.4 | 4.076 | 2.794 |
| 0.0040 | 0.0007 | 17.5 | 3.920 | 2.613 |
| 0.0038 | 0.0007 | 17.2 | 4.309 | 2.838 |
| 0.0039 | 0.0007 | 16.8 | 4.349 | 2.897 |
| 0.0039 | 0.0007 | 18.5 | 3.810 | 2.484 |
| 0.0040 | 0.0007 | 18.4 | 3.700 | 2.430 |

**Table 6.10.** *Macroindentation of PAA 8 with steel sphere.*

| h gel [m] | Indentation [m] | Indentation % | E Hertzian [KPa] | E Corrected [KPa] |
|---|---|---|---|---|
| 0.0042 | 0.0003 | 7.3 | 13.939 | 10.874 |
| 0.0041 | 0.0003 | 7.9 | 12.537 | 9.659 |
| 0.0042 | 0.0003 | 8.3 | 11.303 | 8.672 |
| 0.0041 | 0.0003 | 8.0 | 12.417 | 9.522 |
| 0.0041 | 0.0003 | 8.5 | 11.318 | 8.628 |
| 0.0040 | 0.0003 | 7.9 | 13.033 | 9.979 |
| 0.0041 | 0.0003 | 7.5 | 13.601 | 10.534 |
| 0.0040 | 0.0003 | 8.5 | 11.891 | 8.984 |

**Table 6. .** *Macroindentation of PAA 9 with glass sphere loaded with a plastic support.*

| h gel [m] | Indentation [m] | Indentation % | E Hertzian [KPa] | E Corrected [KPa] |
|---|---|---|---|---|
| 0,0037 | 0,0012 | 33,5 | 19,36 | 11,51 |
| 0,0036 | 0,0013 | 36,4 | 17,76 | 10,23 |
| 0,0036 | 0,0012 | 33,7 | 19,74 | 11,59 |
| 0,0037 | 0,0013 | 35,0 | 18,45 | 10,80 |
| 0,0036 | 0,0012 | 33,3 | 20,52 | 11,98 |
| 0,0035 | 0,0011 | 32,5 | 21,96 | 12,74 |
| 0,0036 | 0,0011 | 31,4 | 22,78 | 13,40 |
| 0,0035 | 0,0011 | 32,5 | 21,96 | 12,74 |

**Table 6.12.** *Macroindentation of PAA 10 with glass sphere loaded with a plastic support.*

| h gel [m] | Indentation [m] | Indentation % | E Hertzian [KPa] | E Corrected [KPa] |
|---|---|---|---|---|
| 0.0035 | 0.0005 | 14.1 | 76.34 | 53.17 |
| 0.0036 | 0.0004 | 12.4 | 89.19 | 64.00 |
| 0.0036 | 0.0005 | 14.4 | 72.20 | 50.35 |
| 0.0036 | 0.0005 | 15.0 | 67.54 | 46.70 |
| 0.0036 | 0.0005 | 13.4 | 81.33 | 57.24 |
| 0.0036 | 0.0005 | 14.8 | 70.26 | 48.55 |
| 0.0035 | 0.0005 | 13.8 | 79.61 | 55.45 |
| 0.0037 | 0.0005 | 14.0 | 72.36 | 51.13 |

For each hydrogel, the measurement of elastic modulus obtained with the higher indentation, have chosen to be used in the FEM simulation (Abaqus by Simulia$^{TM}$). The finite element mesh that was generated is represented in figure 6.8. and the normal displacement calculated for PAA 10 in figure 6.9. Quad-mesh was chosen with 64000 elements.

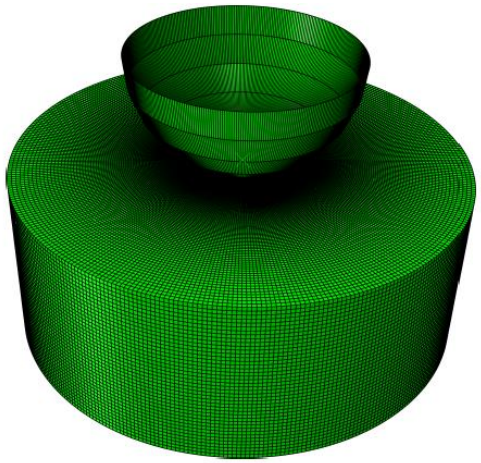

**Figure 6.8.** *Finite element mesh consisting of 64000 elements.*

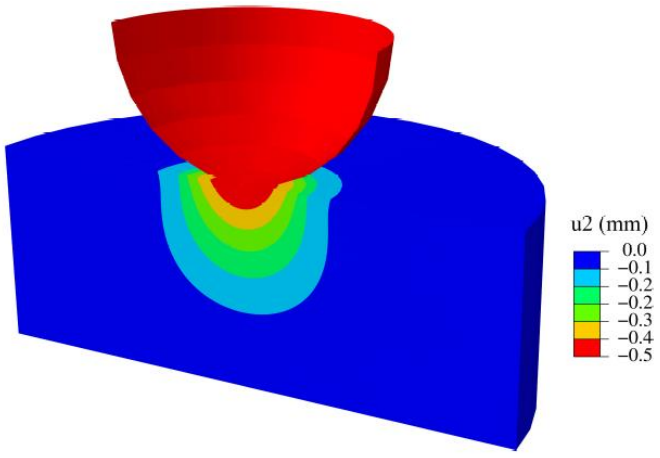


**Figure 6.9.** *Normal displacement shown for PAA 10.*

The elastic modulus obtained by the FEM simulations on the six hydrogels are reported in table 6.13. R is the radius of the sphere, δ is the indentation in the gel, h is the height of the gel, F is the weight of the indenter, D is the diameter of the gel, $E_{ft}$ is the elastic modulus calculated from the equation corrected for finite height, $E_{FEM}$ is the elastic modulus obtained from the FEM simulations.

Therefore, it was possible to compare the values of the elastic modulus obtained by both methods, i.e. the equation by Long *et al.*[45] and the FEM simulations. In conclusion, if the most suitable experimental conditions are chosen, the Long's method error on the value obtained by the FEM simulation ranges from 8% to 15%. This deviation could be related on the influence of the finite diameter of the material, which is not considered in the equation 6, and also on the non-linearity response of the material.

**Table 6.13.** *FEM simulations and comparison with corrected for a finite height.*

| Gel | R | δ | h | F | D | $E_{fh}$ | $E_{FEM}$ | % ($E_{FEM}$-$E_{fh}$)/$E_{FEM}$ |
|---|---|---|---|---|---|---|---|---|
| PAA 2 | 0,00199 | 0,001 | 0,0045 | 0,00046 | 0,0137 | 0,12 | 0.15 | 14,49 |
| PAA 3 | 0,0027 | 0,0011 | 0,0045 | 0,0069 | 0,0125 | 1,30 | 1.45 | 10,35 |
| PAA 6 | 0,0027 | 0,0007 | 0,0042 | 0,0069 | 0,0115 | 2,79 | 3.15 | 11,31 |
| PAA 8 | 0,0027 | 0,0003 | 0,0041 | 0,0069 | 0,0109 | 9,66 | 11.0 | 12,19 |
| PAA 9 | 0,0024 | 0,0011 | 0,0036 | 0,0744 | 0,0106 | 13,3 | 14.6 | 8,72 |
| PAA 10 | 0,0024 | 0,0005 | 0,0036 | 0,0744 | 0,0098 | 46,7 | 53.5 | 12,71 |

## 6.2 FEM symulation of mechanical behaviour of hydrogels

Other FEM simulations were performed to study the influence of the finite diameter of the sample on the calculation of the elastic modulus, not yet studied in literature. The simulations were carried out considering a hypothetical hydrogel with the characteristics reported in table 6.14. The values of the hydrogel diameters that were investigated are 0.25, 0.50, 0.75, 1.0, 2.5, 5.0, 7.5, 10, 15 and 25 m. FEM simulations allowed to obtain the value of the elastic modulus for the ten different hydrogels.

**Table 6.14.** *Fixed hydrogel characteristics, used in the FEM symulation.*

| h [m] | R [m] | δ [m] | a [m] | E [KPa] | υ |
|---|---|---|---|---|---|
| 1 | 1 | 0.005 | 0.07 | 10 | 0.5 |

A correction factor $g(x)$ is then defined, in order to identify an equation which relates the FEM solutions determined and the solutions obtained from the equation of Hertz with the correction for the finite height by London. The correction factor, equation 7, is defined as the load

calculated from the FEM solution, $F^{FEM}$, normalised on the load calculated by the Long's equation, $F^{ft}$. $F^{ft}$ was determined by the equations 5 and 6, using the values reported in table 6.14.

$$g(x) = \frac{F^{FEM}}{Fft} \tag{7}$$

The equation $g(x)$ is a function of the independent and adimensional variable $x$. Two different cases where postulated for the definition of the x value. In case 1, the variable $x$ was defined as the contact radius $a$, normalised on the diameter $D$ of the hydrogel, equation 8. In this way, the influence of the indented area on the deviation between the two loads is investigated. In case 2, the variable $x$ was defined as the height $h$ of the hydrogel, normalised on its diameter $D$, equation 9. Case 2 allows to determine the influence of the dimensions of the hydrogel on the deviation between the force determined by the FEM simulation and the force calculated considering the finite height correction.

$$\text{Case 1: } x \rightarrow \frac{a}{D} \tag{8}$$

$$\text{Case 2: } x \rightarrow \frac{h}{D} \tag{9}$$

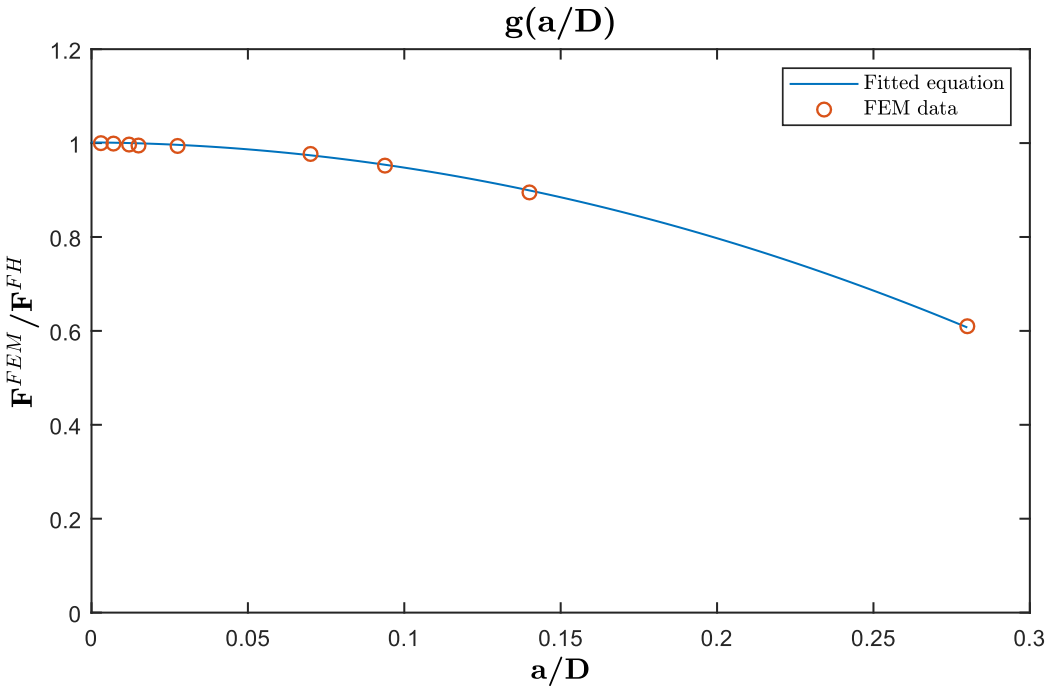


**Figure 6.10.** *Influence of a/D on normalised FEM data (circles) and fitted data (line).*

Figure 6.10 shows the deviation between the simulated force and the Long's equation calculated force as function of the normalised indented radius. High indenting conditions leads to a

remarkable error of the Long's approach. Equation 10 is a polynomial correlation obtained by fitting the normalised FEM data obtained in figure 6.10.

$$g_1\left(\frac{a}{D}\right) = -4.8378\left(\frac{a}{D}\right)^2 - 0.0529\,\frac{a}{D} + 1.0014 \tag{10}$$

Figure 6.10 shows an increase influence of the ratio between the height and the diameter of the hydrogel on the deviation from the FEM solution and Long's solution. Equation 11 is obtained by fitting the normalised FEM data obtained in figure 6.10.

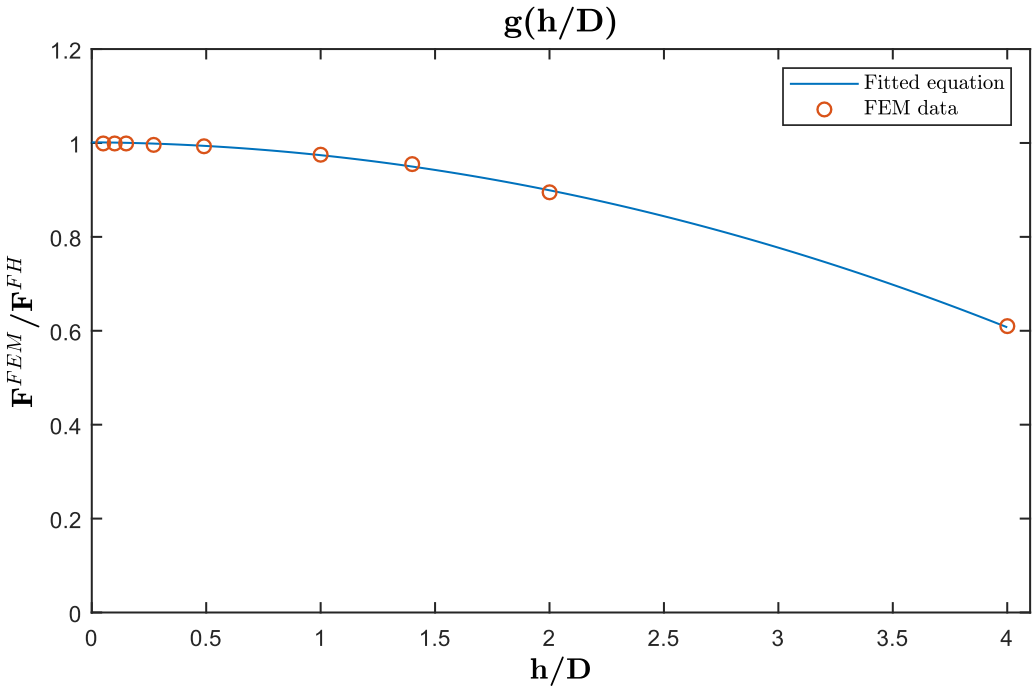


**Figure 6.10.** *Influence of h/D on normalised FEM data (circles) and fitted data (line).*

$$g_2\left(\frac{h}{D}\right) = -0.0237\left(\frac{h}{D}\right)^2 - 0.0037\,\frac{h}{D} + 1.0014 \tag{11}$$

These polinomial correlations (equations 10 and 11) are corrective factors that can be incorporated into equation 12 and allow the calculation of the elastic modulus, considering the influence of the finite diameter of the gel. In order to estimate the deviation of the values obtained from these corrections from the value obtained by FEM simulations in table 6.13, the elastic modulus is calculated by equation 12 for the two cases. The results are displayed in table 6.15.

$$E = \frac{3\,F\,(1-\upsilon^2)}{4\,\delta^{\frac{3}{2}}\,R^{\frac{1}{2}}}\,\frac{1}{f\left(\frac{a}{h}\right)}\,\frac{1}{g(x)} \tag{12}$$

**Table 6.15.** *Comparison between elastic modulus obtained by FEM simulations and the one calculated using the equations considering the finite diameter.*

| Gel | $E_{FEM}$ [kPa] | E: $g_1$ [kPa] | E: $g_2$ [kPa] | $\%\frac{E_{FEM} - E:g_1}{E_{FEM}}$ | $\%\frac{E_{FEM} - E:g_2}{E_{FEM}}$ |
|---|---|---|---|---|---|
| PAA 2 | 0.15 | 0.1244 | 0.1176 | 9.40 | 14.32 |
| PAA 3 | 1.45 | 1.446 | 1.305 | 0.36 | 10.07 |
| PAA 6 | 3.15 | 3.016 | 2.802 | 4.26 | 11.04 |
| PAA 8 | 11.0 | 10.057 | 9.692 | 8.57 | 11.89 |
| PAA 9 | 14.6 | 15.28 | 13.43 | -4.89 | 7.82 |
| PAA 10 | 53.5 | 50.28 | 46.85 | 6.02 | 12.43 |

From the table 6.15 can be observed that the values of elastic modulus obtained from the equation determined in the case 1 are at maximum 10% lower than the one obtained by the FEM simulation. The elastic modulus obtained with the equation in the case 2 are at maximum 14% lower than the FEM one.

These equations show that both the ratios $\frac{a}{D}$ and $\frac{h}{D}$ affects the value of the elastic modulus calculated by the equation with the correction on the finite height. For this reason, another corrective coefficient must be investigated, which is a function of the two dimensionless variables. The finite width correction term $g\left(\frac{a}{D},\frac{h}{D}\right)$ was numerically evaluated through FEM simulation by varying the height $h$ and width $D$, so that $\frac{h}{D}$ falls within the range 0.2 - 0.75. In the simulations, the radius of the indenter $R$ and the depth of indentation $\delta$ are also varied. The values of $\frac{a}{D}$ falls within the range 0.01 – 0.15.

Figure 6.11 shows the finite width correction for the elastic modulus for various values of $\frac{a}{D}$ and figure 6.12 for varies values of $\frac{h}{D}$.

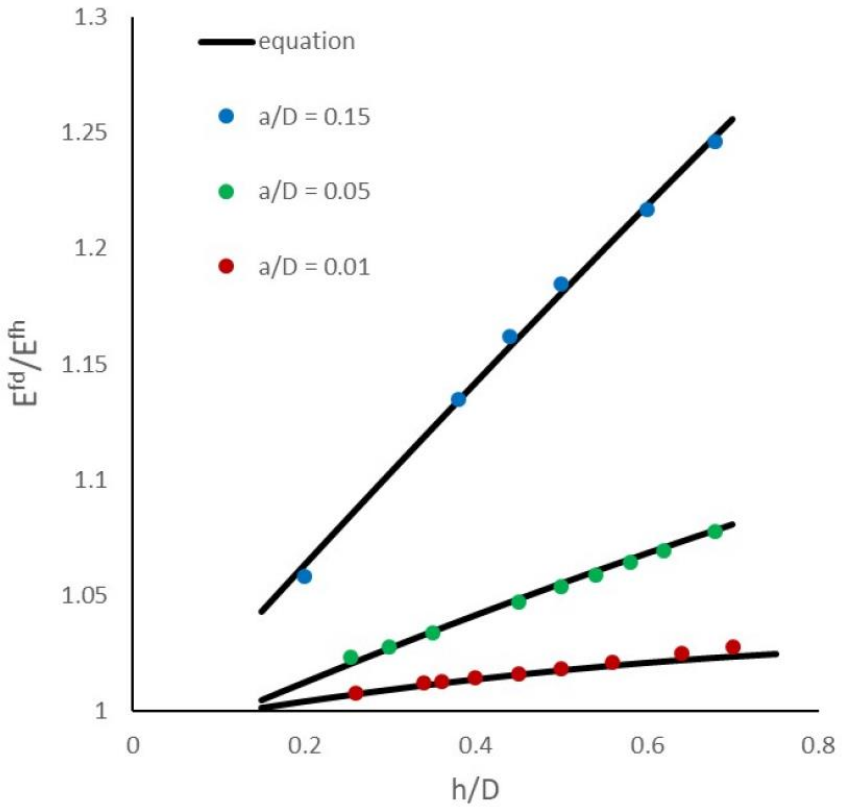


**Figure 6.11.** *Correction factor for finite width for various values of a/D.*

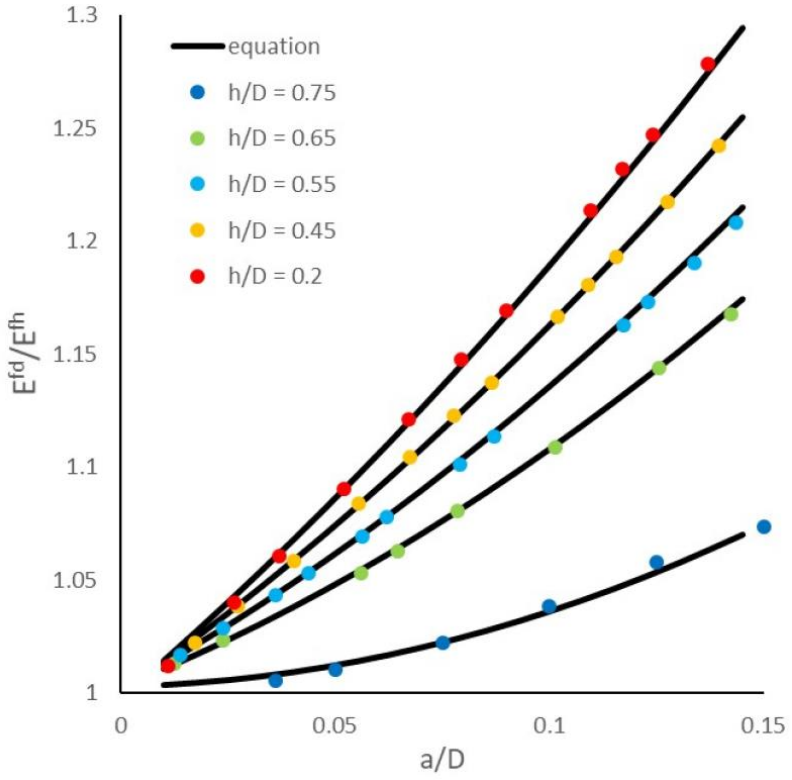


**Figure 6.12.** *Correction factor for finite width for various values of h/D.*

The equation 13 is the correction factor for the height of the substrate and it is obtained by regression analysis of the curves in figures 6.11 and 6.12. The solid black lines in figures 6.11 and 6.12 displays the polynomial expression, which has been stopped to the second power.

$$g\left(\frac{a}{D},\frac{h}{D}\right) = 1 + 1.26\left(\frac{a}{D}\right) + 0.07\left(\frac{h}{D}\right) - 4.52\left(\frac{ah}{D^2}\right) - 2.03\left(\frac{a^2}{D^2}\right) - 0.06\left(\frac{h^2}{D^2}\right) \quad (13)$$

The elastic modulus with the finite diameter correction can be calculated by the equation 14.

$$E^{fd} = E^{fh} \cdot \left(1 - 0.3\,\frac{a}{D} + 0.02\frac{h}{D} + 2.87\frac{ah}{D^2} + 2.89\frac{a^2}{D^2} - 0.01\frac{h^2}{D^2}\right) \quad (14)$$

**Table 6.15.** *Comparison between elastic modulus obtained by FEM simulations and the one calculated using the equations considering the finite height and the finite diameter.*

| Gel | % indentation | $E_{FEM}$ [kPa] | $E^{fd}$ [kPa] | $\%\frac{E_{FEM} - E^{fd}}{E_{FEM}}$ |
|---|---|---|---|---|
| PAA 2 | 22.7 | 0.15 | 0.13 | 5.6 |
| PAA 3 | 24.5 | 1.45 | 1.52 | -4.5 |
| PAA 6 | 16.4 | 3.15 | 3.17 | 2.1 |
| PAA 8 | 7.9 | 11.0 | 10.59 | 3.8 |
| PAA 9 | 31.4 | 14.6 | 15.78 | -8.33 |
| PAA 10 | 15.0 | 53.5 | 52.98 | 0.97 |

Equation 14 allows the calculation of elastic modulus considering the correction for finite height and finite diameter of the hydrogel. $E^{fh}$ is the elastic modulus corrected for a finite height of the gel, calculated by the equation 5 and 6.

Using the indentation, height and diameter values of the gels measured experimentally, reported in table 6.13, and equation 14 for the calculation of the elastic modulus, the results reported in table 6.15 were obtained.

The values of elastic moduli obtained by the equation 14 are compared with the one obtained by the FEM simulations, which are recalled in table 6.15 from table 6.13.

Observing the values reported in table 6.15 it can be concluded that, using equation 14, an elastic modulus value is obtained that deviates at most ± 10% from the value that would be obtained from FEM simulations. In addition, if the indentation of the samples is kept below

25%, the value differs by a maximum of ± 6% from the value that is obtained from the finite element analysis.

In conclusion, using this approach based on both FEM simulations and mathematical correlations, it was possible to implement an accurate model for the determination of the elastic modulus starting from experimental data obtained with the macroindentation method.

# Chapter 7

# Synthesis and characterization of hydrogels and cryogels: results

Protocols that allow the synthesis of substrates for cell cultures were developed and optimized in order to make them standardized and easy to reproduce in other laboratories. In fact, the methods developed does not require special equipment. These methods allowed to synthetize polyacrylamide and polyethylene glycol hydrogels with different mechanical properties and different types of adhesion sites for cells, in the case of polyethylene hydrogels. In addition, cryogels with different compositions have been synthetized in order to obtain a three-dimensional material with cells adhesion sites and a microstructure with open and connected micro porosities, which is able to be used as a cancer vaccine support.

## 7.1 Polyacrylamide hydrogels

Polyacrylamide (PAA) hydrogels have been used for many years as a biomaterial for cell culture, because they have a homogeneous and reproducible structure that can be modified by changing the concentration of its acrylamide and/or varying the percentage of bisacrylamide. However, the use of PAA as a substrate for cell culture has some limitations and disadvantages. These hydrogels can't incorporate adhesive sites for cells, because the covalent link between this polymer and adhesive proteins isn't easily allowed. Therefore, PAA hydrogels need to be coated with adhesive proteins in order to provide a suitable surface for cells.

### 7.1.1 Synthesis of PAA and PAA-OH

The method for the synthesis of polyacrylamide, PAA, hydrogels are well known and they have been largely used and optimised in the literature [2,27,45]. All the values of composition of PAA hydrogel investigated allowed to obtain a homogeneous gel with reproducible characteristics. The composition of these hydrogels was optimized in order to improve and simplify their bio-functionalization. In particular, two different types of polyacrylamide hydrogels were

synthetized. The first was obtained by polymerising acrylamide and bis acrylamide, PAA hydrogels. In the second case, the amount of acrylamide was reduced, replacing it with the monomer N-Hydroxyethyl acrylamide (AA-OH, PAA-OH hydrogels), in order to increase the hydrophilicity of the synthesized polymer. In addition, the influence of the amount of acrylamide and bis acrylamide monomers was investigated. In PAA hydrogel, the range of percentage by weight of acrylamide studied was from 3.5 to 8 wt% and that of bisacrylamide from 0.03 to 0.48 wt%. In the case of PAA-OH, the range of percentages by weight is from 4.0 to 8.5, because the molar mass of N-Hydroxyethyl acrylamide is higher than the one of acrylamide. Different hydrogels with different mechanical characteristics were obtained. The compositions and the percentage by weight are reported in the following tables already shown in chapter 5, for the sake of clarity.

**Table 7.1.** *Polyacrylamide solutions composition for each mL.*

| | **wt% AA/BAA** | **WATER [µL]** | **AA (40%) [µL]** | **BAA (2%) [µL]** |
|---|---|---|---|---|
| PAA 1 | 3.5/0.03 | 897.5 | 87.5 | 15.0 |
| PAA 2 | 4/0.03 | 885.0 | 100.0 | 15.0 |
| PAA 3 | 5/0.03 | 860.0 | 125.0 | 15.0 |
| PAA 4 | 3/0.15 | 850.0 | 75.0 | 75.0 |
| PAA 5 | 3/0.225 | 812.5 | 75.0 | 112.5 |
| PAA 6 | 4/0.1 | 850.0 | 100.0 | 50.0 |
| PAA 7 | 4/0.15 | 825.0 | 100.0 | 75.0 |
| PAA 8 | 5/0.15 | 800.0 | 125.0 | 75.0 |
| PAA 9 | 5/0.225 | 762.5 | 125.0 | 112.5 |
| PAA 10 | 8/0.48 | 560.0 | 200.0 | 240.0 |

**Table 7.2.** *Hydroxy-polyacrylamide solutions composition for each mL.*

| | **wt% (AA+AAOH)/BAA** | **WATER [µL]** | **AA (40%) [µL]** | **BAA (2%) [µL]** | **AAOH (48,5%) [µL]** |
|---|---|---|---|---|---|
| PAAOH 1 | 4.0/0.03 | 891.2 | 68.8 | 15.0 | 25.0 |
| PAAOH 2 | 4.5/0.03 | 878.7 | 81.3 | 15.0 | 25.0 |
| PAAOH 3 | 5.5/0.03 | 853.7 | 106.3 | 15.0 | 25.0 |
| PAAOH 4 | 3.5/0.15 | 843.7 | 56.3 | 75.0 | 25.0 |
| PAAOH 5 | 3.5/0.225 | 806.2 | 56.3 | 112.5 | 25.0 |
| PAAOH 6 | 4.5/0.1 | 843.7 | 81.3 | 50.0 | 25.0 |
| PAAOH 7 | 4.5/0.15 | 818.7 | 81.5 | 75.0 | 25.0 |
| PAAOH 8 | 5.5/0.15 | 793.7 | 106.3 | 75.0 | 25.0 |
| PAAOH 9 | 5.5/0.225 | 756.2 | 106.3 | 112.5 | 25.0 |
| PAAOH 10 | 8.5/0.48 | 553.7 | 181.3 | 240.0 | 25.0 |

## 7.1.2 Mechanical characterization of PAA and PAA-OH

The hydrogels successfully synthetized were tested by the macroindentation and the micropipette methods. The aim is studying the influence of the composition of the material on the mechanical properties, and find a complete range of stiffness biologically significant. Through macroindentation and micropipette methods, it was possible to experimentally measure the elastic modulus of these hydrogels.

In addition, PAA hydrogels were also measured by two standardized mechanical characterization techniques: rheometry and compression. Table 7.3 reports the mean elastic modulus values obtained by macroindentation, micropipette, rheometry and compression techniques.

In the case of macroindentation, the elastic modulus was calculated by means of equation 14 of chapter 6 which consists in the Hertzian equation corrected both for finite height and finite diameter of the gel. Figures 7.1 and 7.2 shows the measured hydrogels. PAA 2 was indented with the plastic sphere. PAA 3, PAA 6 and PAA 8 were indented with the steel sphere. PAA 9 and PAA 10 was measured with the glass sphere loaded with a plastic support. These spheres were chosen in order to minimize the indentation on the material, i.e. to minimize the non-linear response by the material.

**Figure 7.1.** *PAA 2 indented with plastic sphere (left), PAA 3 (centre) and PAA 6 (right)were indented with steel sphere.*

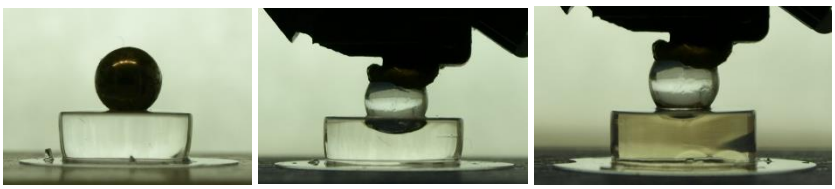

**Figure 7.2.** *PAA 8 indented with steel sphere (left) and PAA 9 (centre) and PAA 10indented with glass sphere loaded by a plastic support.*

However, for low sphere penetration, the method didn't allow a reliable measurement because the estimation of the indentation's depth was affected by a large error. Figure 7.3 shows a PAA hydrogel indented with the steel sphere and analysed by the MATLAB script.

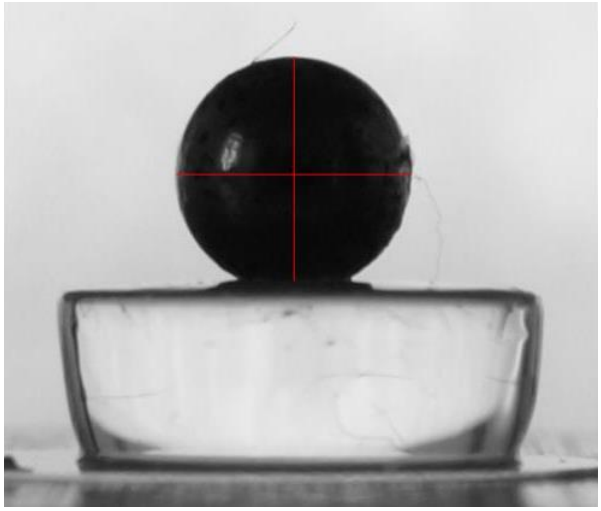

**Figure 7.3.** *PAA 8 hydrogel measured by the macroindentation method and indented with steel sphere.*

The measurement of the height of the hydrogel was easier in the case of PAA 8, 9 and 10, because of the more regular shape and the flat surface of the gels. In other cases, as PAA 2, the hydrogel was difficult to measure because of the irregular surface. The PAA hydrogels with lower amount of weight fraction percentages of monomers incorporate more water and increases more their volume after the synthesis. The swelling often leads to a modification of the initial shape of the material: as example, with curved surface (concave or convex) the identification of the top surface is hard and the measure error can be large.

Micropipette aspiration method also allowed to determine the elastic modulus of PAA hydrogels. Figure 7.4 shows a PAA hydrogel aspired by a capillary tube and the identification of the aspirated length, L, and the internal radius, a, of the capillary tube. During the measurements with the micropipette aspiration, the length aspired L was tried to be kept as lower as possible to reduce the non-linear response of the hydrogel and to avoid breakage of the material surface. The voltage signal of the pressure transducer, the internal capillary radius and aspired length calculated by the MATLAB script were used to determine the elastic modulus of the material by the equation 6 of chapter 5. This equation considers a correction for large deformation of the hydrogel. Measurements were repeated several times on the same sample in order to achieve a more accurate value.

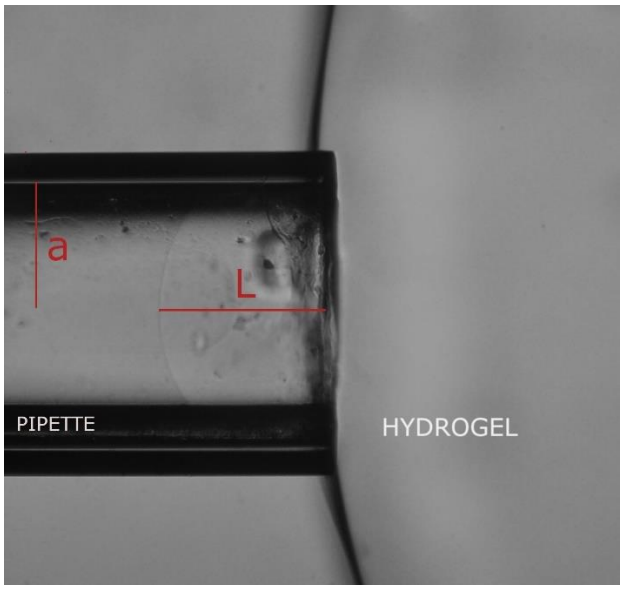


**Figure 7.4.** *Polyacrylamide hydrogel measured by the micropipette aspiration method.*

To test the reliability of our two methods, PAA hydrogels were also tested by rheometry and compression techniques, with the collaboration of Prof. Maurizio Ventre (IIT laboratory of Napoli). The mean elastic modulus obtained by macroindentation measurements are close to the one measured by uniaxial compression and rheometry test, as can be observed in table 7.3. This confirms that the macroindentation technique allows to determine reliable values of elastic modulus. Therefore, this cheaper and rapid method can be used instead of standardized methods that use expensive instruments, such as uniaxial compression and rheology. In general, the elastic modulus values obtained from repeated measurements on the same sample was very close to each other allowing to have a low dispersion of values compared to the average one. Therefore, we can say that the developed macroindentation test is a reproducible method to measure elastic modulus of hydrogels. All the mechanical measurements allowed to determine that the elastic modulus of PAA hydrogels is strongly influenced by the concentration of the monomers in the solutions from which they are synthesized. It was therefore possible to synthesize six hydrogels with a significantly different elastic modulus by means of a reproducible and simple method.

**Table 7.3.** *Elastic modulus of PAA hydrogels measured by different techniques.*

| | Macroindentation [kPa] | Micro pipette [kPa] | Rheometry [kPa] | Compression [kPa] |
|---|---|---|---|---|
| PAA 2 | 0.14 ± 0.01 | 0.17 ± 0.02 | 0.91 ± 0.02 | 0.40 ± 0.14 |
| PAA 3 | 1.47 ± 0.10 | 0.81 ± 0.19 | | 1.85 ± 0.64 |
| PAA 6 | 2.99 ± 0.27 | 1.67 ± 0.28 | 4.14 ± 0.04 | 3.15 ± 0.35 |
| PAA 8 | 10.38 ± 0.93 | 5.77 ± 0.54 | 10.14 ± 1.13 | 8.45 ± 1.77 |
| PAA 9 | 13.89 ± 1.05 | 10.37 ± 0.67 | 12.87 ± 1.46 | 11.10 ± 0.99 |
| PAA 10 | 53.05 ± 8.77 | 46.95 ± 3.90 | | 59.05 ± 5.59 |

To investigate the influence of the addition of N-Hydroxyethyl acrylamide on the mechanical properties of the PAA hydrogels, PAA-OH hydrogels were measured by the macroindentation and the micropipette aspiration methods. The results obtained by the macroindentation method are represented in table 7.4. The hydrogels were indented with sphere with different weight, in order to obtain indentations values lower than 25%. Figures 7.5 and 7.6 shows the PAA-OH hydrogels synthetized and indented with the spheres. After determining the depth of indentation, the height and the diameter of the hydrogel, through the MATLAB script, elastic modulus were calculated by the equation 14 of chapter 6 which considers the correction for finite diameter and finite height of the material.

**Figure 7.5.** *PAA-OH 1 indented with plastic sphere (left), PAA-OH 2 indented with glass sphere (centre) and PAA-OH 3 indented with steel sphere (right).*

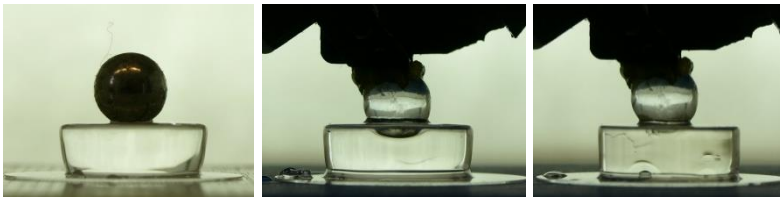

**Figure 7.6.** *PAA-OH 8 indented with steel sphere (left) and PAA-OH 9 (centre) and PAA-OH 10indented with glass sphere loaded by a plastic support.*

**Table 7.4**. *Macroindentation measurements of elastic modulus of polyacrylamide hydrogels with N-Hydroxyethyl acrylamide.*

| | Indentation | Sphere | Mean elastic modulus [kPa] |
|---|---|---|---|
| PAA OH 1 | 18 % | Plastic | 0.19 ± 0.02 |
| PAA OH 2 | 23 % | Glass | 0.42 ± 0.03 |
| PAA OH 3 | 23 % | Steel | 1.57 ± 0.08 |
| PAA OH 8 | 8 % | Steel | 10.60 ± 1.04 |
| PAA OH 9 | 23 % | Glass loaded with plastic | 22.5 ± 1.7 |
| PAA OH 10 | 11 % | Glass loaded with plastic | 78.3 ± 10.2 |

PAA-OH hydrogels were also measured by the micropipette aspiration method. Each hydrogel has been measured many times in order to obtain a more reliable result. The mean values of elastic modulus obtained are reported in table 7.5. Reliable measurements on these materials with the micropipette aspiration were carried out successfully, thanks to the fact that the polyacrylamide hydrogels have a regular surface and they are not too fragile during aspiration and have an elastic behaviour, recovering completely the deformation after the measure. The material deforms homogeneously and forms a symmetrical meniscus inside the capillary tube with the maximum aspiration length positioned in the centre of the tube.

**Table 7.5.** *Micropipette aspiration measurements of elastic modulus of polyacrylamide hydrogels with N-Hydroxyethyl acrylamide.*

| | Mean Elastic modulus [kPa] |
|---|---|
| PAA OH 1 | 0.33 ± 0.03 |
| PAA OH 2 | 0.40 ± 0.03 |
| PAA OH 3 | 0.53 ± 0.04 |
| PAA OH 4 | 2.73 ± 0.29 |
| PAA OH 6 | 4.60 ± 0.38 |
| PAA OH 8 | 8.95 ± 1.05 |
| PAA OH 9 | 18.7 ± 1.46 |
| PAA OH 10 | 47.1 ± 2.03 |

Micropipette aspiration measurements confirmed that the polyacrylamide hydrogels synthetized had a different elastic modulus, due to the different concentration of acrylamide and bisacrylamide in the solution. The synthetized hydrogels have very broad values of elastic modulus. The stiff polyacrylamide hydrogels synthetized can be used as a cell culture substrate which stimulate carcinogenesis. Instead, soft hydrogels synthetized can stimulate adipogenesis when it is used as a cell culture substrate.

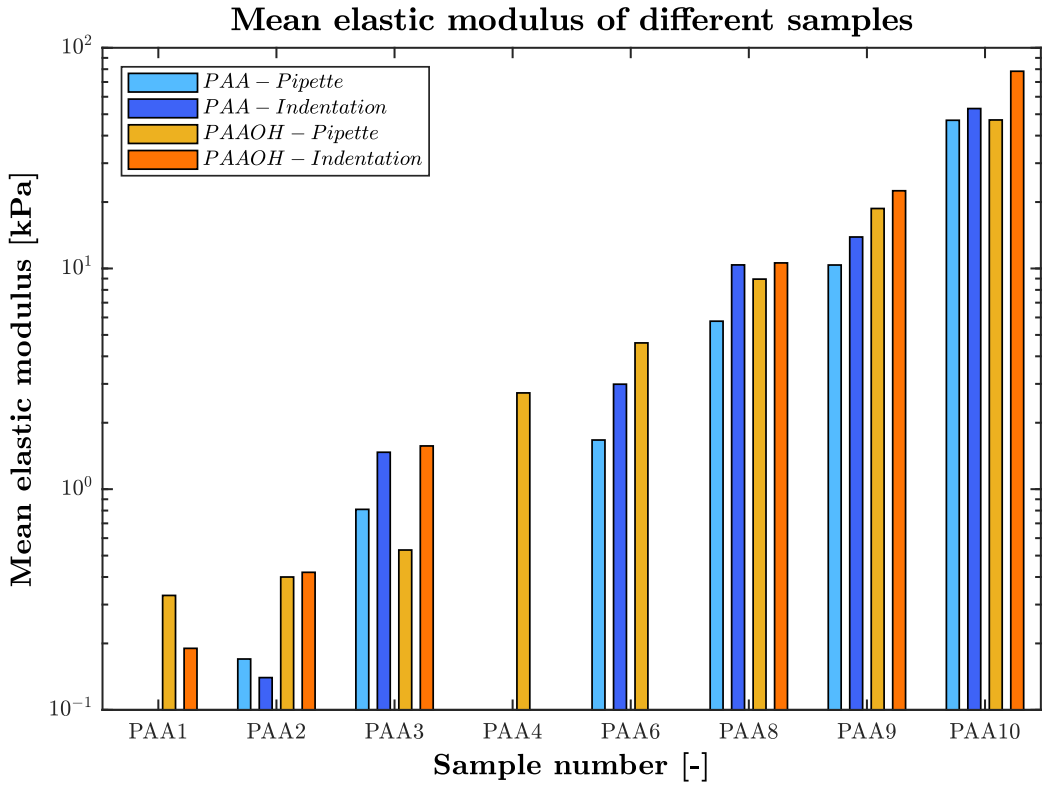


**Figure 7.7.** *Elastic modulus values of PAA and PAA-OH by macroindentation and micropipette aspiration methods.*

Figure 7.7 reports the comparison between elastic moduli determined by macroindentation and micropipette aspiration of PAA and PAA-OH hydrogels. The y-axis is reported in logarithmic scale for graphical purposes. From the comparison between the values of elastic modulus obtained by the PAA-OH hydrogels and the PAA hydrogel, can be observed that the addition of N-Hydroxyethyl acrylamide to these materials leads to an increase of their stiffness. This increase can be related to the increase of secondary bonds between the polyacrylamide chains. Figure 7.7 shows that there is a logarithmic increase of the elastic modulus from hydrogel 1 to 10, due to the variation of the composition of the gels, since the diagram is in logarithmic scale.

## 7.2 Polyethylene oxide hydrogels

Polyethylene glycol (PEG) hydrogels are synthetic biocompatible hydrogels which can be used as substrate for cell cultures. A method which allows to synthetize these hydrogels was developed and optimised. These materials are advantageous compared to PAA hydrogels because they allow to incorporate cell-adhesive ligands which provide adhesion sites for cells[39]. Therefore, polyethylene oxide hydrogels can be used as cell culture substrates without requiring the functionalization of their surface. Another advantage of PEG hydrogels is that the amount of the cell-adhesive ligands can be stoichiometrically varied, allowing the study of the relevance

of density of the adhesive ligands, a fundamental aspect in regulating the mechano-response of cells. If cell adhesive sites are more distant, cells are no more able to build stable focal adhesion also on stiff substrates and assume a more rounded shape as they were in a soft substrate. The ligand used in this study is a RGD peptide. In particular, stiff hydrogels with variable concentration of cell-adhesive ligands (RGD peptide) were synthetized to study this behaviour.

### 7.2.1 Synthesis of PEG-Norbornene

Two different multi-arm-PEG norbornene macromers were exploited and the synthesis procedure was modified, in order to develop a method which allows reproducible synthesis of PEG hydrogels with different elastic modulus and controlled concentration of adhesive sites. For the sake of clarity, the experimental matrixes of each type of PEG hydrogels investigated are recalled from chapter 5.

The first type of macromer used was a 4-arm-PEG norbornene terminated. The PEG concentration was varied in order to synthetize hydrogels with different mechanical properties. The molar ratio between PEG and crosslinker was kept constant, in order to not modify the degree of crosslinking in the material. In addition, concentrated PEG solutions were synthetized with decreasing concentration of RGD peptide and incorporating a non-bioactive peptide in order to keep constant the total pendant peptide concentration. Table 7.6 and 7.7 describe the composition of the PEG hydrogel investigated.

**Table 7.6.** *Composition of PEG-NB 4 arms solution with different PEG concentration, final volume 100 µL.*

| %w/w Final PEG concentration | Final RGD concentration [mM] | Molar ratio PEG/CrossL | PEG-NB 4 arms [µL] | Crosslinker [µL] | RGD [µL] | LAP [µL] | PBS [µL] |
|---|---|---|---|---|---|---|---|
| 3.5% | 3 | 1/1.3 | 14.0 | 17.8 | 4.3 | 1.8 | 62.1 |
| 4% | 3 | 1/1.2 | 16.0 | 21.0 | 4.3 | 2.1 | 56.6 |
| 5% | 3 | 1/1.2 | 20.0 | 27.5 | 4.3 | 2.6 | 45.6 |
| 7% | 3 | 1/1.1 | 28.0 | 40.4 | 4.3 | 3.7 | 23.6 |
| 9% | 3 | 1/1.1 | 36.0 | 53.4 | 4.3 | 4.7 | 1.6 |

**Table 7.7.** *Composition of PEG-NB 4 arms solution with different RGD concentration, final volume 100 µL.*

| %w/w Final PEG concentration | Final RGD concentration [mM] | Molar ratio PEG/CrossL | PEG-NB 4 arms [µL] | Crosslinker [µL] | RGD [µL] | RDG [µL] | LAP [µL] | PBS [µL] |
|---|---|---|---|---|---|---|---|---|
| 9% | 0.5 | 1/1.1 | 36.0 | 53.4 | 0.7 | 3.6 | 4.7 | 4.1 |
| 9% | 1 | 1/1.1 | 36.0 | 53.4 | 1.4 | 2.9 | 4.7 | 3.6 |
| 9% | 2 | 1/1.1 | 36.0 | 53.4 | 2.8 | 1.5 | 4.7 | 2.6 |
| 9% | 3 | 1/1.1 | 36.0 | 53.4 | 4.3 | 0.0 | 4.7 | 1.6 |

This method allowed to obtain the PEG-norbornene four arm hydrogels with the PEG concentration higher than 5%. In fact, the solutions with the PEG concentration of 3.5% and 4% didn't polymerize. Otherwise in the other compositions stable gels were obtained and used as cell culture substrates, but the results were not consistent.

In order to expand the range of stiffness and RGD concentration achievable, PEG-norbornene eight arm were used, 8-arm-PEG Norbornene. The increased number of arms, in fact, allows the formulation of solutions with a wider degree of crosslinking, also at lower concentrations of PEG, and RGD concentration. In the solution a non-adhesive peptide was incorporated (mono-cysteine terminated peptide containing RDG scramble sequence) in order to keep the total pendant peptide concentration constant. The compositions of the PEG hydrogels that were synthetized are reported in table 7.8 and 7.9.

**Table 7.8.** *Composition of PEG-NB 8 arms solutions with different PEG concentration, final volume 100 µL.*

| %w/w Final PEG concentration | Final RGD concentration [mM] | Molar ratio PEG/Crosslinker | PEG-NB 8 arms [µL] | Crosslinker [µL] | RGD [µL] | LAP [µL] | PBS [µL] |
|---|---|---|---|---|---|---|---|
| 4.7% | 3 | 1/2.3 | 18.8 | 6.6 | 4.3 | 2.5 | 66.8 |
| 5.0% | 3 | 1/1.6 | 20.0 | 10.1 | 4.3 | 2.6 | 62.7 |
| 5.2% | 3 | 1/1.7 | 20.8 | 9.9 | 4.3 | 2.7 | 61.7 |
| 5.5% | 3 | 1/1.4 | 22.0 | 12.7 | 4.3 | 2.9 | 58.1 |
| 7% | 3 | 1/1.8 | 28.0 | 12.6 | 4.3 | 3.7 | 50.1 |
| 9.0% | 3 | 1/1.2 | 36.0 | 24.3 | 4.3 | 4.7 | 30.7 |
| 9.0% | 3 | 1/1.9 | 36.0 | 32.0 | 4.3 | 4.7 | 20.6 |
| 12.5% | 3 | 1/1.3 | 50.0 | 31.1 | 4.3 | 6.6 | 6.8 |

**Table 7.9.** *Composition of PEG-NB 8 arms solutions with different RGD concentration, final volume 100 µL.*

| %w/w Final PEG concentration | Final RGD concentration [mM] | Molar ratio PEG/CrossL | PEG-NB 8 arms [µL] | Crosslinker [µL] | RGD [µL] | RDG [µL] | LAP [µL] | PBS [µL] |
|---|---|---|---|---|---|---|---|---|
| 9% | 0.2 | 1/1.2 | 36.0 | 24.3 | 0.3 | 4.0 | 4.7 | 33.5 |
| 9% | 1 | 1/1.2 | 36.0 | 24.3 | 1.4 | 2.9 | 4.7 | 32.7 |
| 9% | 3 | 1/1.2 | 36.0 | 24.3 | 4.3 | 0.0 | 4.7 | 30.7 |

The hydrogels with the compositions reported in tables 7.8 and 7.9 were successfully synthetized and the reproducibility of the synthesis were verified, since many of these hydrogels were synthetized with consistent properties. These hydrogels were also tested mechanically and biologically.

In order to improve the reproducibility of hydrogel synthesis and cells adhesion results, the polymerization method was optimized with 8-arm-PEG norbornene. In particular, the reaction between PEG and the RGD peptide was made during a pre-reaction step between these two molecules, with a lower concentration of photoinitiator LAP to avoid an early formation of a gel (1:5 respect to the total pendant peptides RGD and RDG 0,5% w/w). 8-arm-PEG norbornene hydrogels synthetized according to this method are reported in tables 7.10 and 7.11.

**Table 7.10.** *Composition of PEG-NB 8 arms solutions with different PEG concentration, final volume 100 µL.*

| Final hydrogels properties | | | PREMIX | | | Polymerization | | |
|---|---|---|---|---|---|---|---|---|
| %w/w PEG | RGD [mM] | Molar ratio PEG/Crosslinker | PEG-NB 8 arms [µL] | RGD [µL] | LAP [µL] | Crosslinker [µL] | LAP [µL] | PBS [µL] |
| 4.7% | 3 | 1/2.3 | 18.8 | 4.3 | 2.3 | 6.6 | 1.2 | 66.8 |
| 5.0% | 3 | 1/1.6 | 20.0 | 4.3 | 2.3 | 10.1 | 1.3 | 62.0 |
| 5.2% | 3 | 1/1.7 | 20.8 | 4.3 | 2.3 | 9.9 | 1.4 | 61.3 |
| 5.5% | 3 | 1/1.4 | 22.0 | 4.3 | 2.3 | 12.7 | 1.4 | 57.2 |
| 9.0% | 3 | 1/1.2 | 36.0 | 4.3 | 2.3 | 24.3 | 2.4 | 30.8 |
| 13.0% | 3 | 1/1.15 | 52.0 | 4.3 | 2.3 | 36.6 | 3.4 | 1.4 |

**Table 7.11.** *Composition of PEG-NB 8 arms solutions with different RGD concentration, final volume 100 µL.*

| Final hydrogels properties | | | PREMIX | | | | Polymerization | | |
|---|---|---|---|---|---|---|---|---|---|
| %w/w PEG | RGD [mM] | Molar ratio PEG/Crosslinker | PEG-NB 8 arms [µL] | RGD [µL] | RDG [µL] | LAP [µL] | Crosslinker [µL] | LAP [µL] | PBS [µL] |
| 9.0% | 0.2 | 1/1.2 | 36.0 | 0.3 | 4.0 | 2.3 | 24.3 | 2.4 | 34.8 |
| 9.0% | 1 | 1/1.2 | 36.0 | 1.4 | 2.9 | 2.3 | 24.3 | 2.4 | 33.6 |
| 9.0% | 3 | 1/1.2 | 36.0 | 4.3 | 0.0 | 2.3 | 24.3 | 2.4 | 30.8 |

Then, hydrogels with a 8-arm-PEG norbornene concentration from 4.7% to 13.0% and with a 3 mM RGD concentration were prepared. 9% PEG concentrated hydrogels were polymerised with a different RGD concentration. The materials synthetized with the method which includes a pre-polymerization were tested by the macroindentation and the micropipette aspiration method and they were used as cell culture substrates.

## 7.2.2 Mechanical characterization of PEG-Norbornene

Previously described 4-arm-PEG norbornene and 8-arm-PEG norbornene were tested by the macroindentation and the micropipette aspiration technique, in order to determine if the variation of the concentration of PEG-norbornene modifies the elastic modulus of hydrogels.

4-arm-PEG norbornene were measured by the macroindentation technique. After swelling, the shape of the material has become very irregular. The lateral zones of the hydrogel increased their volume more than the other zones and the surface of the gel has become concave. This made the measurement by macro-indentation more difficult because the area where the sphere indents the material was almost completely hidden by the lateral walls of the gel, as can be seen in figure 7.8 which reports the PEG four arm hydrogels indented with the plastic sphere. However, the PEG hydrogels were analysed, and the indicative results obtained are reported in table 7.12.

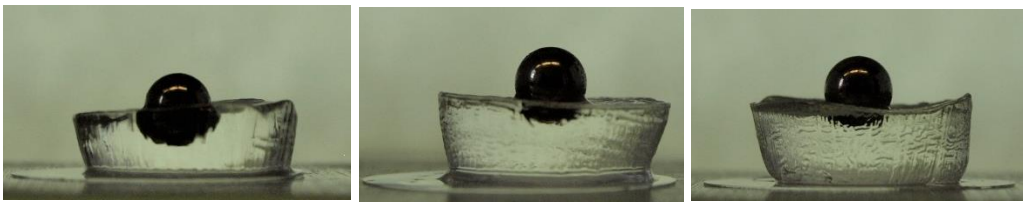

**Figure 7.8.** *PEG-NB 5% (left), PEG-NB 7% (centre) and PEG-NB 9% (right) indented with the plastic sphere.*

**Table 7.12.** *Mean elastic modulus of PEG-NB 4 arms obtained by the macroindentation method.*

| % w/w PEG | E [kPa] |
|---|---|
| 5 % | 0.6 ± 0.5 |
| 7 % | 1.8 ± 0.5 |
| 9 % | 9.0 ± 1.4 |

Table 7.12 shows that the different concentrations of PEG allows to synthetize hydrogels with different elastic modulus, even if the values obtained are not as reliable as the results of PAA hydrogels. This result was exploited in the synthesis of 8-arm-PEG norbornene hydrogels because the final 8-arm-PEG norbornene concentrations were kept equal to the one obtained by 4-arm-PEG norbornene hydrogels. 8-arm-PEG norbornene hydrogels were tested only by the micropipette aspiration method, because of the problem of irregular surfaces of gels previously encountered. Figures 7.9, 7.10 and 7.11 show micropipette analysis on PEG-NB 8 arm 4.7% without premix, PEG-NB 8 arm 5.5% without premix and PEG-NB 8 arm 13% with premix. The aspiration length is a function of both the pressure applied to the surface and the elastic modulus of the material. The length of aspiration of soft hydrogels is high even if the pressure applied is low. Stiff hydrogel, instead, requires a high depression to reach appreciable length of aspiration. PEG norbornene hydrogels measured were more fragile and more difficult to analyse than the PAA hydrogels measured because these materials sticks to the capillary tube and, when it is detached from their surface, some fragments of hydrogel can break off and remain attached to the capillary.

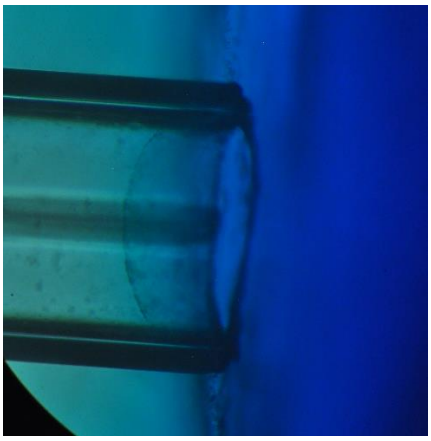

**Figure 7. 9** *Pipette aspiration measurement of a 4.7% PEG-NB 8 arm without premix, 3.84 mbar are exerted, and the gel is aspirated for 0.40 mm.*

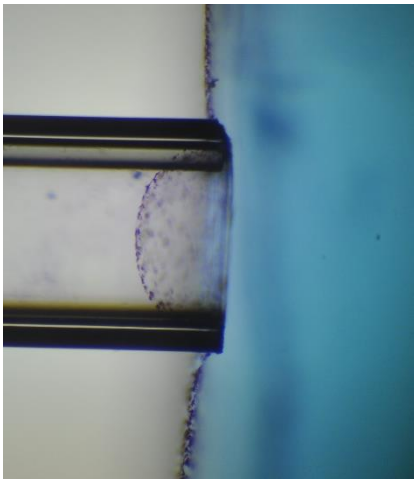

**Figure 7.10.** *Pipette aspiration measurement of a 5.5% PEG-NB 8 arm without premix, 21.3 mbar are exerted, and the gel is aspirated for 0,39 mm.*

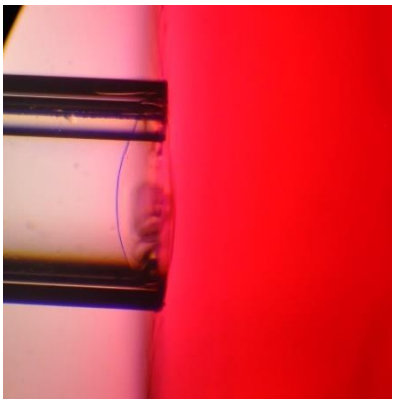

**Figure 7.11.** *Pipette aspiration measurement of a 13% PEG-NB 8 arm with premix, 68.9 mbar are exerted, and the gel is aspirated for 0.22 mm.*

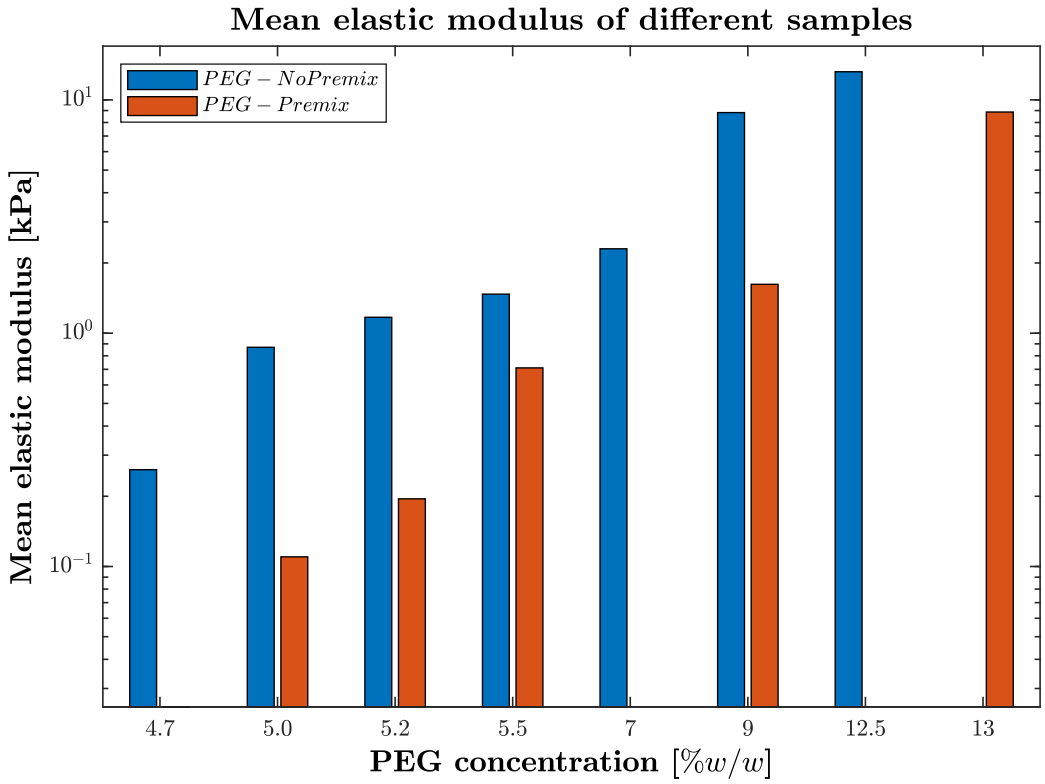


**Figure 7.12.** *Elastic modulus of PEG-NB 8 arm samples.*

**Table 7.13.** *Mean values of elastic modulus of PEG-NB 8 arm obtained by the method without (left) or with (right) premix.*

| % w/w PEG | E [kPa] (no premix) | E [kPa] (premix) |
|---|---|---|
| 4.7 % | 0.26 ± 0.023 | 0.025 ±0.08 |
| 5.0 % | 0.87 ± 0.13 | 0.11 ± 0.004 |
| 5.2 % | 1.17 ± 0.31 | 0.195 ± 0.03 |
| 5.5 % | 1.47 ± 0.19 | 0.71 ± 0.08 |
| 7 % | 2.30 ± 0.10 | |
| 9 % | 8.82 ± 0.32 | 1.62 ± 0.31 |
| 12.5 % | 13.2 ± 0.43 | |
| 13 % | | 8.87 ± 0.65 |

Table 7.13 and figure 7.12 report the mean elastic modulus obtained from the measures with the micropipette aspiration on the polyethylene eight arm hydrogels. The y-axis of figure 7.12 is reported in logarithmic scale for graphical purposes. For both hydrogels, synthetized with and without premix, it can be observed that the variation of PEG concentration significantly modifies the elastic modulus. It was therefore possible to synthesize PEG eight arm hydrogels cell adhesive on a wider range of elastic moduli. The range of elastic modulus obtained from the synthesis of these PEG norbornene eight arm hydrogels is not comparable to that obtained

with PAA-OH hydrogels. However, and most important, the relevance of biological results is comparable for the two hydrogel compositions, as it offers the same cell behaviour. Therefore, these hydrogels can be used as cell culture, by varying the elastic modulus and/or the RGD concentration to control cell behaviour.

## 7.3 Cryogels preparation

PEG cryogels were used in this study as a material for the development of a cancer vaccine. The main advantage of cryogels is that their microstructure has open and interconnected pores, and this allows the interaction of molecules in the cryogels with the external environment. In particular, one type of cell-based cancer immunotherapy is based on stimulation of dendritic cells (DCs) that activate anti-tumor responses by the presentation of tumor antigens to lymphocytes. Tumor antigens are on the surface of inactivated tumor cells which are seeded inside the cryogel. For this, incorporate RGD peptides which provide adhesive sites to cells. The open interconnected pores allow the interaction between these cells with the DCs. PEG cryogels are also highly stretchable and shape memory materials because, after their compression, they return to their initial form. This allow the development of injectable vaccines.

### 7.3.1 Synthesis of Cryogels

Different cryogels compositions have been investigated in order to obtain a material which has interconnected and open macropores, is stretchable and is cell adhesive. For the sake of clarity, experimental matrixes are recalled from chapter 5.

The first type of cryogel that was investigated, was based on literature [17,35] results on methacrylated alginate and RGD peptide and developed with the collaboration of Prof. Paolo Sgarbossa (DII). The methacrylation reaction of sodium alginate was performed and optimized in order to obtain alginate with methacrylic groups. During the syntheses, sodium alginate and AEMA showed low solubility in the MES buffer. For this reason, the reagents were solubilised in MES before their addition to the reaction flask. This allowed to obtain a quite homogeneous solution in which the reaction could take place. However, the products that were obtained were not soluble in water because a gelation occurred. Figure 7.13 shows the inhomogeneous solution obtained after the methacrylation rection of sodium alginate.

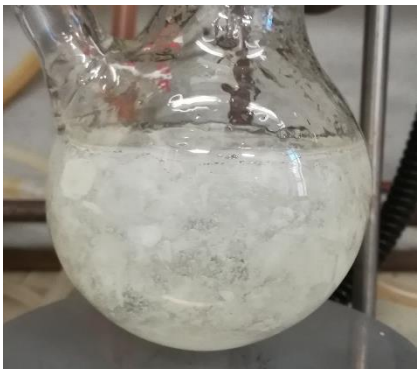

**Figure 7.13.** *Product of methacrylation reaction of sodium alginate.*

Therefore, other types of cryogels were then synthetized by the polymerization of 4-arm-PEG acrylate (PEG-Acr) and polyethylene glycol diacrylate (PEGDA). These two polymers were functionalized with RGD peptide and GELMA, in order to allow cell adhesion.

PEG acrylate cryogels were synthetized with RGD peptide, GELMA and both. The compositions are reported in table 7.14. Cryogels were obtained with a molar ratio between cysteine and acrylate of 1:4 and 1:8. In addition also the cryogel which was functionalised with both RGD and GELMA was obtained successfully. However, cryogels reported in table 7.15 didn't polymerize.

**Table 7.14.** *Composition of 7.5% PEG Acr and RGD cryogels, final volume solution 500 mL.*

| PEG 7.5% | PEG 20% in TEA [µL] | RGD 4% in TEA [µL] | TEA [µL] | APS 10% in $H_2O$ | TEMED [µL] |
|---|---|---|---|---|---|
| 1:4 C:A | 188.0 | 32.5 | 269.0 | 10.0 | 0.7 |
| 1:8 C:A | 188.0 | 16.3 | 285.0 | 10.0 | 0.7 |

**Table 7.15.** *Composition of 7.5% PEG Acr and GELMA cryogels, final volume solution 500 mL.*

| PEG 7.5% | PEG 20% in $H_2O$ [µL] | GELMA 8% in $H_2O$ [µL] | $H_2O$ [µL] | APS 10% in $H_2O$ | TEMED [µL] |
|---|---|---|---|---|---|
| 1% GELMA | 188.0 | 62.5 | 238.5 | 10.0 | 0.7 |
| 2% GELMA | 188.0 | 125.0 | 176.0 | 10.0 | 0.7 |

**Table 7.16.** *Composition of 7.5% PEG Acr, RGD and GELMA cryogels, final volume solution 500 mL.*

| PEG 7.5% | PEG 20% in TEA [µL] | RGD 4% in TEA [µL] | GELMA 10% in $H_2O$ [µL] | TEA [µL] | APS 10% in $H_2O$ | TEMED [µL] |
|---|---|---|---|---|---|---|
| 1:8 C:A | 188.0 | 11.3 | 2.5 | 287.5 | 10.0 | 0.7 |

PEGDA cryogels were functionalised with RGD peptide and GELMA with a molar ratio between cysteine and acrylate of 1:4 and 1:8, as reported in table 7.17. Also, in this case, the solution which included GELMA didn't polymerize and the cryogel wasn't obtained.

**Table 7.17.** *Composition of 5% PEGDA and RGD cryogels, final volume solution 500 mL.*

| PEGDA 5% | PEGDA 20% in TEA [µL] | RGD 4% in TEA [µL] | TEA [µL] | APS 10% in $H_2O$ | TEMED [µL] |
|---|---|---|---|---|---|
| 1:4 C:A | 125 | 32.5 | 332.0 | 10.0 | 0.7 |
| 1:8 C:A | 125 | 16.3 | 348.0 | 10.0 | 0.7 |

**Table 7.18.** *Composition of 5% PEGDA and GELMA cryogels, final volume solution 500 mL.*

| PEGDA 5% | PEGDA 20% in $H_2O$ [µL] | GELMA 8% in $H_2O$ [µL] | $H_2O$ [µL] | APS 10% in $H_2O$ | TEMED [µL] |
|---|---|---|---|---|---|
| 1:4 C:A | 125.0 | 62.5 | 301.8 | 10.0 | 0.7 |
| 1:8 C:A | 125.0 | 125.0 | 239.3 | 10.0 | 0.7 |

## 7.3.2 Characterization of cryogels

In order to study the structure of the synthetized cryogels, SEM photos were taken, in collaboration with Prof. Katia Brunelli (DII). The aim was verifying whether cryogels had open and interconnected pores of micrometric dimensions. The cryogels was lyophilized and then cut in order to investigate the internal microstructure. After lyophilization, the cryogels reduced their dimensions because water, which filled their microporous structure, was removed. In addition, the external surface was observed in order to verify if the micropores of the cryogel were open to external environment. The photos were taken with a magnification of 33x, 67x and 333x.

Figure 7.14 shows the SEM photos of the cross section and the external surface of the PEGDA-RGD cryogel. From these pictures it can be seen that the microstructure of the cross section is made of interconnected micropores and the external surface of the cryogel has the desired microstructure.

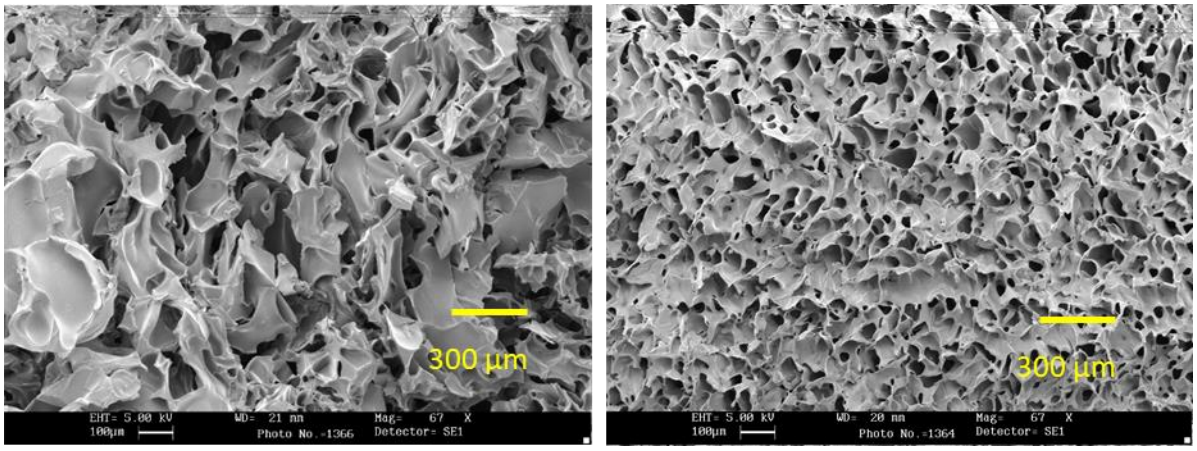


**Figure 7.14.** *SEM images of cross section (left) and external surface (right) of cryogel PEGDA 5%, RGD (67 x).*

Figure 7.15 shows the microstructure of the PEG-Acr functionalised with RGD peptide with a molar ratio of 1:4 (figures on the left) and 1:8 (figures on the right) and different magnifications: 33x (A1 and B1), 333 x (A2 and B2) and 67 x (A3, A4, B3, B4). The figures show that the internal microstructure of PEG acrylate cryogels are characterized by micro and interconnected pores. Figures A4 and B4 show the external surface of the two cryogels: it can be observed that these parts of the cryogels is closed by an external "skin".

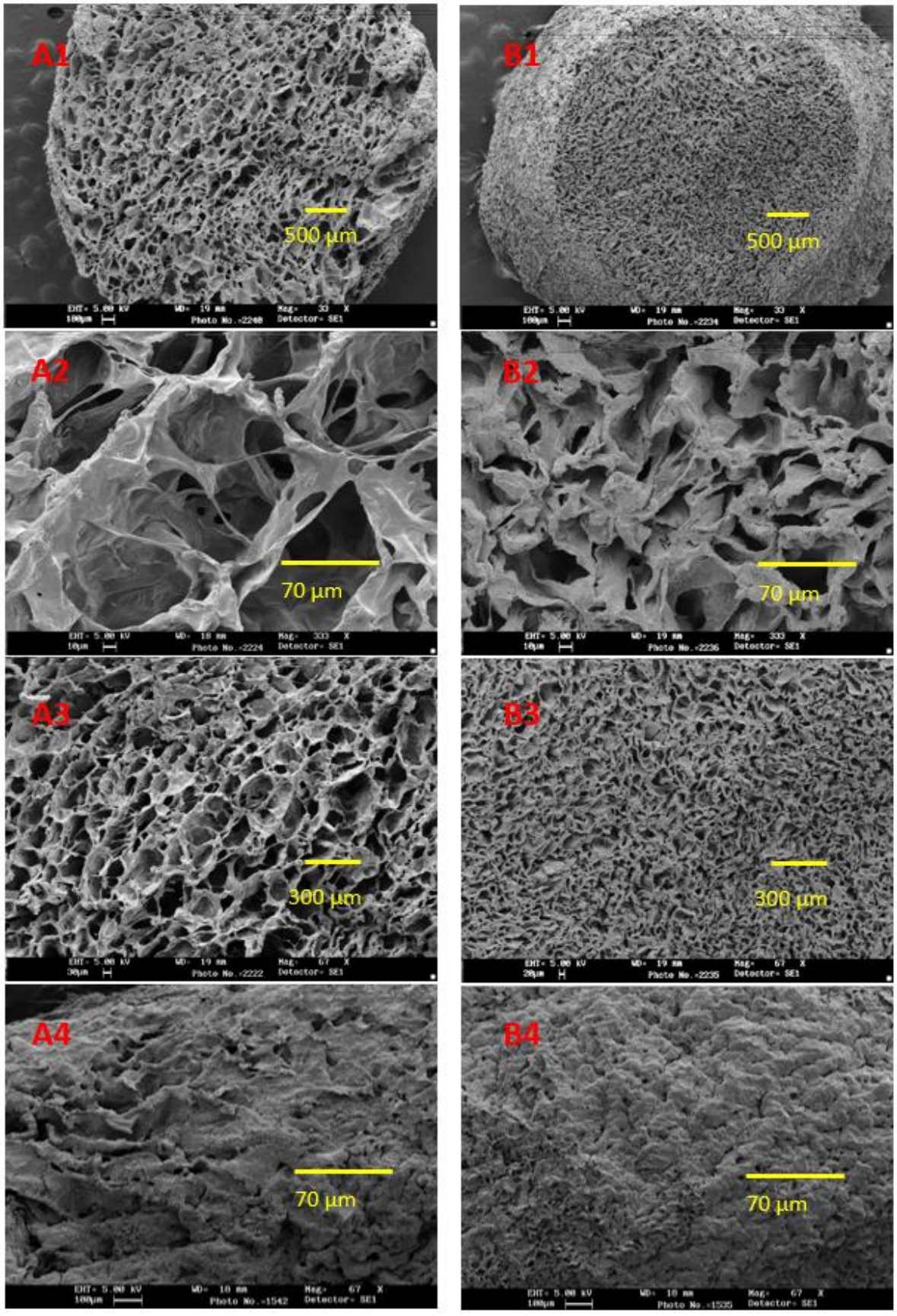


**Figure 7.15.** *SEM images of PEG cryogels 7.5%,1:4 RGD (A, left) and 1:8 RGD (B, right).*

Figure 7.16 shows that also the addition of a low amount of GELMA in the PEG cryogel doesn't affect the microstructure of the material and it is similar to the one of PEG acrylate with RGD.

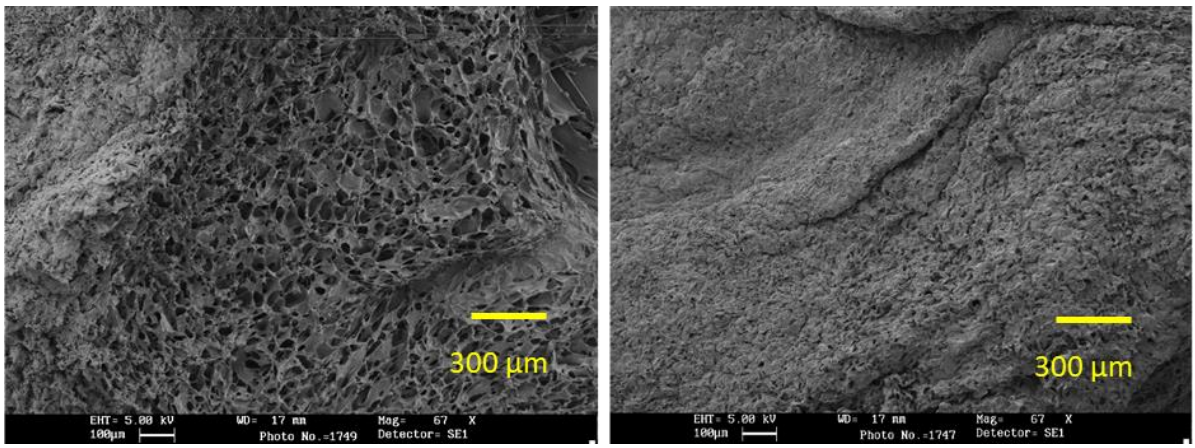


**Figure 7.16.** *SEM images of cross section (left) and external surface (right) of cryogel PEG 7.5%,1:8 RGD and GELMA (67 x).*

In order to observe the ability of the cryogels obtained to be deformed, PEGDA and PEG cryogels were tested. Figure 7.17 shows the compression of a PEGDA cryogel. When the cryogel is compressed, water exits from the open porosities of the material. After the compression, the cryogel recovers completely the deformation, returning to its initial shape. In addition, PEG-RGD cryogel were injected through a glass syringe, as can be observed in figure 7.19. During the injection, the cryogel reduced its volume and then it passed through the needle without breaking.

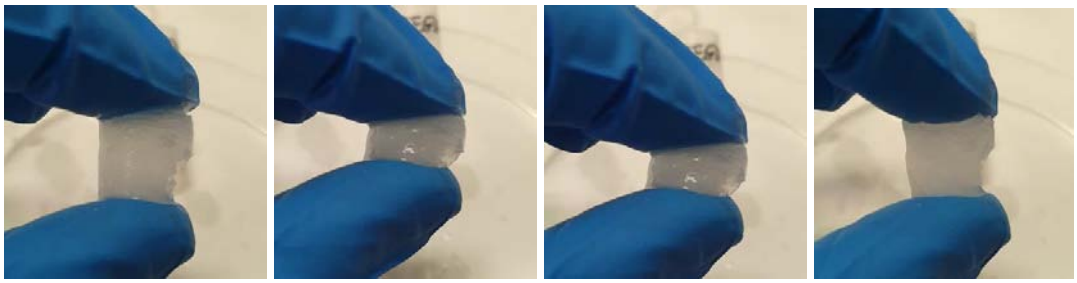

**Figure 7.17.** *Deformability and shape memory properties of PEGDA 5% cryogels.*

**Figure 7.18.** *Swelling of cryogels.*

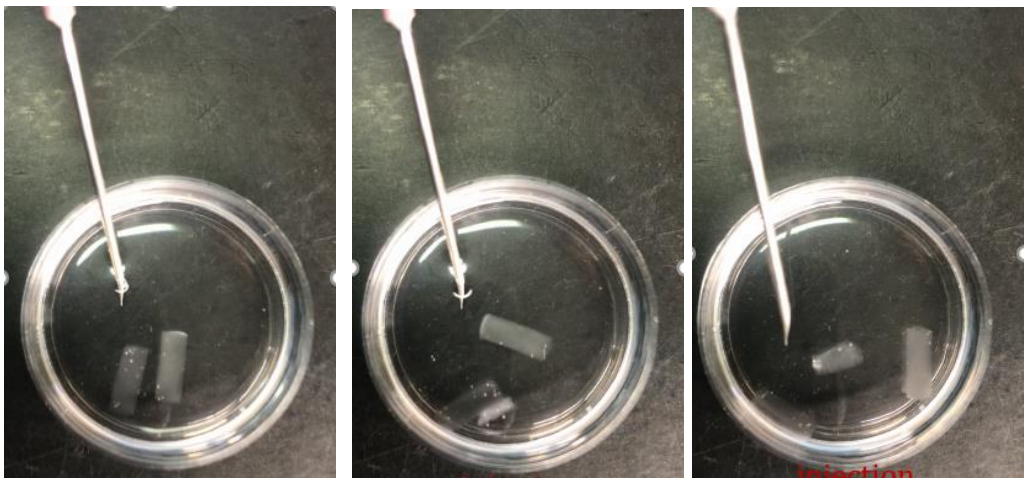

**Figure 7.19.** *Injectability test on PEG acrylate cryogel. On the left the cryogel is inside the syringe, in the centre can be seen the compressed cryogel after the injection and on the right the cryogel swelled after the injection.*

In conclusion, PEG cryogels functionalized with RGD by a molar ratio of 1:8 were synthetized successfully by a standardised and reproducible method. These cryogels have a microstructure with interconnected micro pores. In addition, these cryogels are sufficiently deformable and elastic to be used in biological applications.

## 7.4 Biological characterization

### Immunofluorescence on PAA and PEG hydrogels

The polyacrylamide hydrogels synthetized including hydroxy acrylamide and polyethylene glycol hydrogels were tested in order to biological validate them. In particular the samples were tested by immunofluorescence, and the mechanotransducers YAP/TAZ activity was evaluated. Figure 7.23 shows the results obtained by the staining of the seeded cells MCF10A on PAA hydrogels with hydroxy acrylamide. MCF10A are cell lines of tumor mammary glands. Primary antibody used are anti-YAP, secondary antibody used was Alexa Fluor 568 Goat Anti-rabbit IgG (red), F-actin was stained with Alexa Fluor 488 Phalloidin (green) and nuclei were stained

with DAPI (blue). The hydrogels tested are PAA-OH 1, 2, 3, 8, 9 and 10. Second line in figure 7.23 reports the red signals which allows to identify where the YAP/TAZ proteins are located into the cell. YAP/TAZ are localized in the cytoplasm if the cells are seeded on the soft hydrogel PAA-OH 1. An increase of the substrate stiffness localizes YAP/TAZ into the nuclei, as can be observed in the case of PAA-OH 10. The position of the nuclei of cells is identified by the blue signal. In addition, cells stretch if seeded on stiff substrates, as can be seen in fourth line. In fact, the green signal allows to observe actin filaments which allows to identify the shape of cells, since they are located in the cell edges. Cells seeded on soft hydrogels has a round shape and cells seeded on stiff hydrogels are stretched. Intermediate behaviours are observed in the other substrates with intermediate elastic moduli. These substrates induce stiffness-dependent responses in YAP/TAZ nuclear localization, as expected from literature and previous publications [11,12,56]. The scale of hydrogel compositions tested allowed to obtain a study biologically significant on the behaviour of cells.

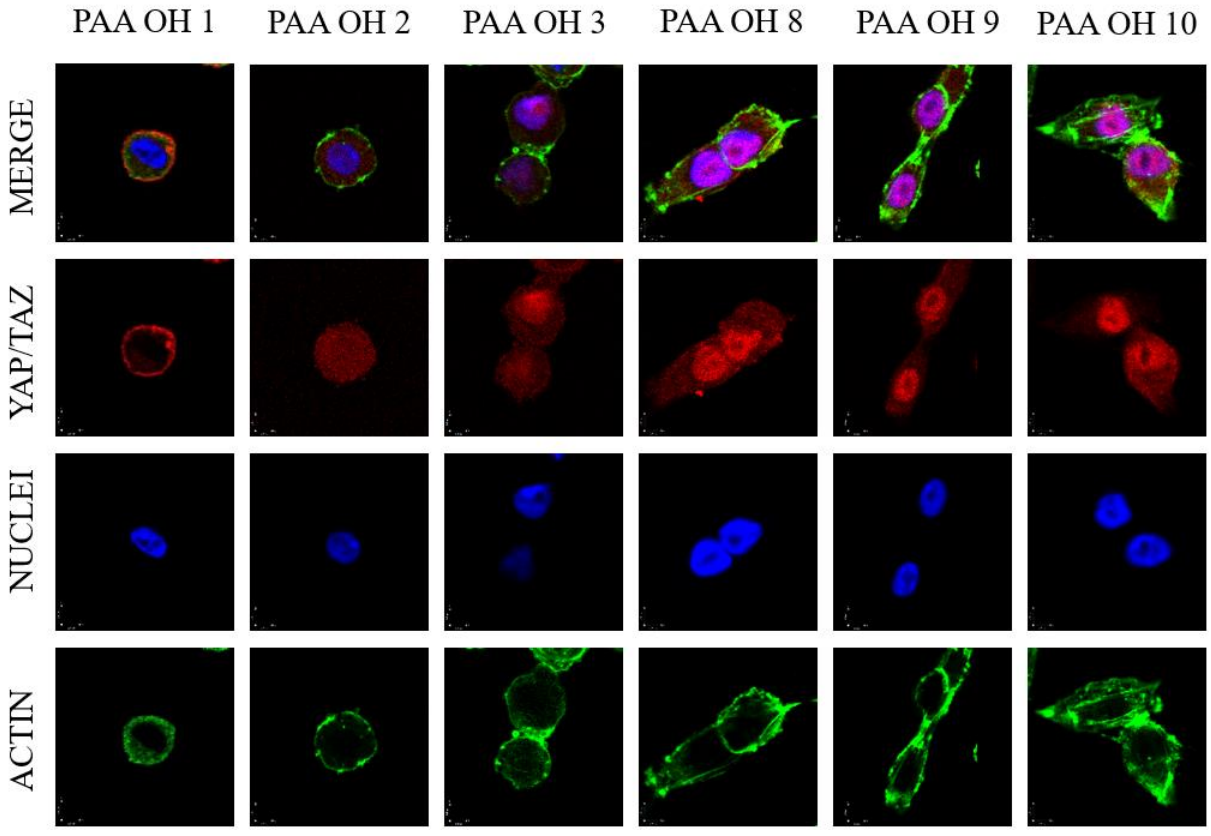


**Figure 7.23.** *Immunoassay results obtained by staining of MCF10A seeded on PAA hydrogels of different compositions.*

In addition, polyethylene glycol hydrogels were tested by immunofluorescence. The samples analysed were PEG-norbornene four arm hydrogels functionalised with a three millimolar concentration of RGD peptide. These hydrogels were synthetized by the method without the

premix of PEG and RGD solutions. Figure 7.24 shows that the mechanotransducers YAP/TAZ are in the cytoplasm in the soft PEG hydrogel on the left and are concentrated in the nucleus of the cell in the stiff substrate on the right. In addition, cells seeded on the soft hydrogel has a spherical shape and they stretch in the case of the stiff hydrogel with higher PEG concentration. Despite the good result with four arm PEG we decided to test 8 arm PEG as well so to obtain a wider range of stiffness and more freedom on the composition side. However, 8-arm PEG without a premix step shown high variability on the mechanical and biological results. In order to improve the reproducibility, PEG-norbornene eight arm hydrogels have been synthetized introducing a premixing step between PEG and RGD peptide in the protocol. These gels, however, couldn't be tested yet by immunofluorescence.

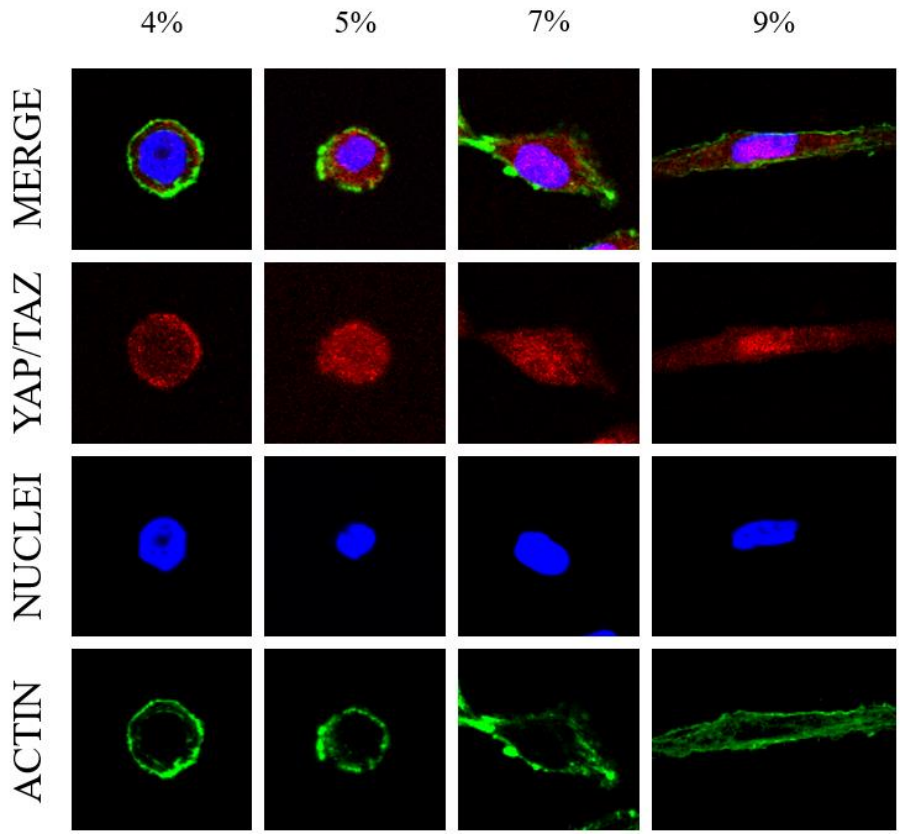


**Figure 7.24.** *Immunoassay results obtained by staining of MCF10A seeded on 4 arm PEG hydrogels of different compositions.*

## Preliminary characterization of Cryogels used as cancer vaccines

A preliminary biological test of a cryogel with the desired microstructure was performed. PEG cryogels functionalized with RGD peptide with a molar ration between cysteine and acrylate groups of 1:8 was seeded with inactivated D2A1 cells. The materials were incubated for 1.5 hours before to be implanted under skin in a BALB/c mouse. Figures 7.25, 7.26, 7.27 and 7.28

shows the photo of the seeded cryogels after thirteen days and after a month of implantation in the mouse. Purple dots, that can be noticed in these figures, are the nuclei of cells.

Cells attached well on the cryogel and it were homogeneously seeded within the volume. The implant of these cryogel was successful. The degradation of the cryogel in the mouse was slow, in fact the cryogels were found in the body also after a month. In addition, the microstructure of the cryogels with open and interconnected pores allowed the macrophages to enter the material. Some lymphocytes were also found on the external surface of the cryogel. The open micropores also allowed cells to enter and exit the cryogel. From the photo taken after a month of injection can be observed that cells increase their adhesion and are more spread on the material. The injection into the mouse body did not generate any inflammatory reaction, because of their biocompatibility.

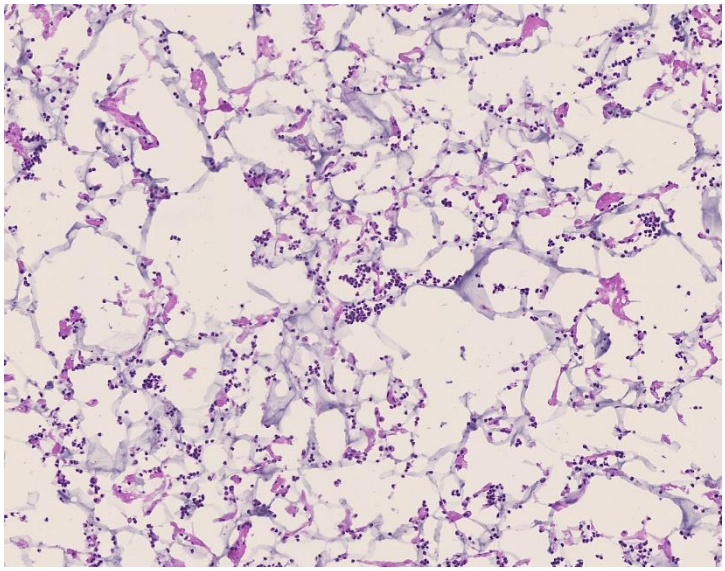

**Figure 7.25.** *PEG-RGD cryogel seeded with cells after 13 days, magnification 10x.*

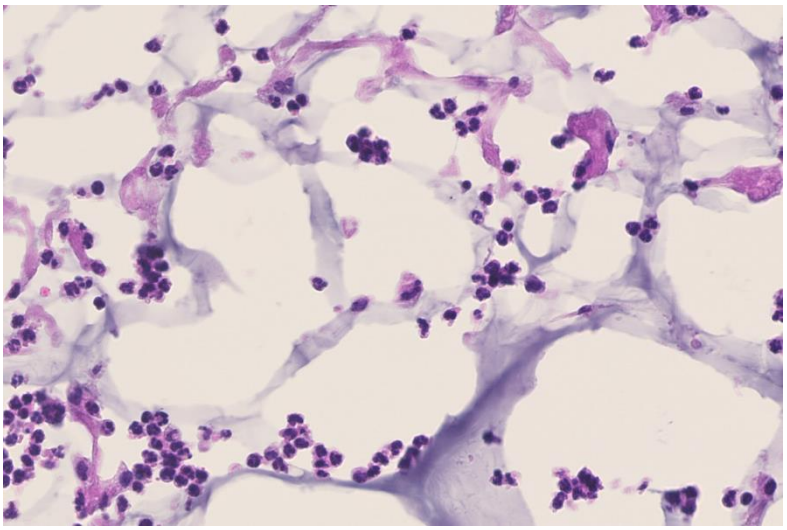

**Figure 7.26.** *PEG-RGD cryogel seeded with cells after 13 days, magnification 40x.*

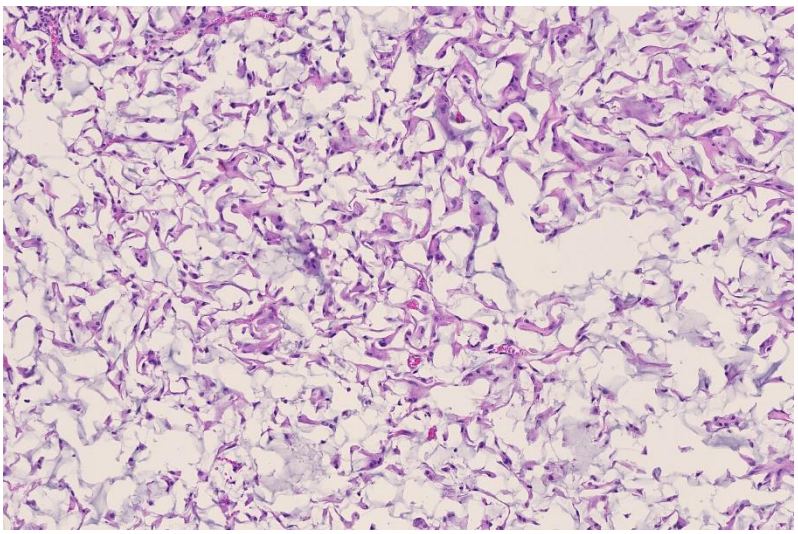

**Figure 7.27.** *PEG-RGD cryogel seeded with cells after 1 month, magnification 10x.*

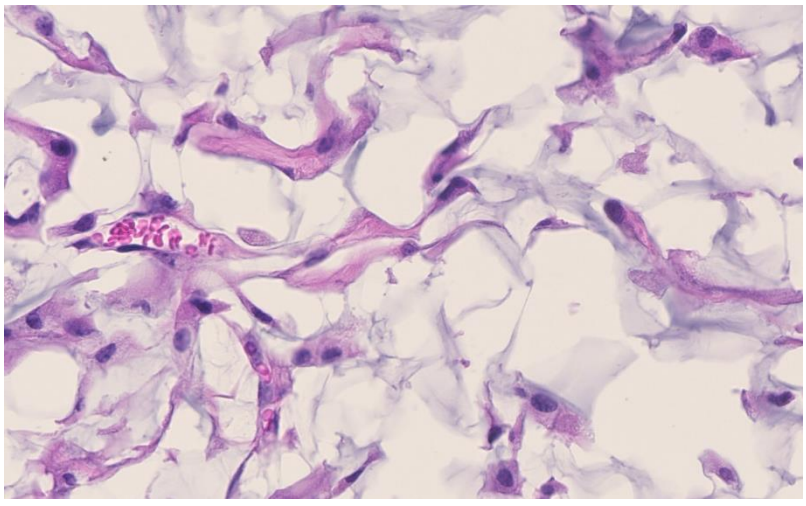

**Figure 7.28.** *PEG-RGD cryogel seeded with cells after 1 month, magnification 40x.*

# Conclusions

The aim of this work was the development and the optimisation of standardized and reproducible protocols for the synthesis and the characterisation of hydrogels with two purposes: mechanotransduction studies and development of cancer vaccines. For mechanotrasduction we focused attention on the development of easily and reproducible protocols that don't require special equipment, for both synthesis and characterization. These methods allowed us to prepare polyacrylamide (PAA) and polyethylene glycol (PEG) hydrogels for cell cultures with a range of mechanical properties, in particular elastic modulus from <1kPa to tens of kPa, useful to mimicking natural tissues. The tuning of elastic modulus was achieved varying the concentration and covalent crosslinking degree of the polymeric hydrogels. For PAA hydrogels different concentrations of acrylamide (from 4,0 to 8,5 wt%) and molar ratios of acrylamide/bisacrylamide were used, enabling the production of hydrogels with different elastic modulus. A critical issue of PAA hydrogels is that they need to be coated with adhesive proteins in order to be used as cell culture substrates. In this study, to improve and simplify the functionalization step respect to literature data, part of the acrylamide was substituted with N-Hydroxyethyl acrylamide, to increase and homogenize protein attachment at the surface of the PAA-OH hydrogels. Then, a method to synthetize PEG hydrogels with different mechanical properties for cell cultures was developed. These materials are advantageous compared to PAA hydrogels because they don't require the surface functionalization, allowing the incorporation of cell-adhesive ligands during the polymerization, which provide adhesion sites for cells. Multi-arm-PEG norbornene terminated macromers were used to prepare PEG hydrogels, using UV assisted thiol-ene click chemistry for both pre-react a single-cysteine terminated adhesive peptide (containing an FN-mimicking RGD sequence) and crosslink NB units with di-cysteine terminated crosslinking peptides. Both adhesive and crosslinking peptide amount can be stoichiometrically controlled with this chemistry, allowing a fine tuning not only of the hydrogel stiffness but also of the number of cell-adhesive ligands (RGD peptide). In fact, stoichiometrically varying their amount we were able to study the relevance of their density on the regulation of mechano-response of cells and so clarifying the relative contribution of pure stiffness sensing and degree of adhesiveness in regulating the mechanical behavior of cells. In stiffest hydrogels cells don't perceive much adhesive site density variation but pure stiffness; conversely, once stiffness is decreased the density of adhesive spots starts becoming essential, partly balancing the effect of a weaker mechanical signal at intermediate stiffness. However, a

threshold of stiffness is required to impart a minimum mechanical feedback necessary to maturate cell adhesion.

In order to determine the elastic modulus of synthetized PAA-OH and PEG-NB hydrogels, two standardized measurement methods were developed and optimized, macroindentation and micropipette aspiration. In contrast to the commonly used atomic force microscopy, rheology and uniaxial compression, the developed methods are simple, cheap, fast and easily reproducible. In the case of macroindentation method, an optimised model for the calculation of elastic modulus were developed in this study, since the different models reported in literature were based on assumptions which don't take into account all our experimental conditions. The developed model allows the calculation of elastic modulus in the case of large deformation and non-linear material considering the influence of the finite diameter and the finite height of the sample. The model was developed and implemented basing on both FEM finite element simulations and mathematical correlations. FEM simulations were used to evaluate the influence of boundary effects and non-linearities of hydrogel samples on the elastic modulus determined by them. Mathematical correlations allowed to obtain an analytical equation to calculate the elastic modulus more accurately respect to previous results reported in literature. The results achieved with macroindentation and micropipette aspiration on a gradient of PAA hydrogels were compared with the same measures obtained on the same PAA hydrogels with other three leading modalities of measuring hydrogel elastic modulus, so allowing to test the reliability of our methods. From the comparison we found a consistent matching of results, with a maximal 2-fold variations between elastic moduli calculated with the different techniques over the same gradient of rigidities, as such validating our proposed methods as reliable and straightforward mechanical methods to test hydrogel rigidity.

Synthetized hydrogels were tested by the macroindentation and the micropipette aspiration methods, in order to determine their elastic moduli. Elastic moduli of synthetized PAA-OH hydrogels that was measured and calculated by macroindentation ranged from 0,2 to 78 kPa. The values obtained by the micropipette aspiration agreed with the one obtained by macroindentation and ranged from 0,3 to 47 kPa. These values are slightly higher respect to those measured in PAA with the same mono- and bi-functional monomers amount. Elastic moduli of PEG-NB hydrogels were also measured using micropipette aspiration, showing values in the range from 0.03 to 9 kPa. This range of stiffness doesn't match that obtained with PAA-OH hydrogels. However, the relevance of biological results is comparable, as it offers the same cell behaviour, i.e. the same mechanotransduction effect. The biological behaviour was

evaluated by immunofluorescence analysis, that allows to analyse the influence of mechanical stimuli (hydrogel stiffness along with adhesiveness cue) on seeded cells. In particular, the localization of the universal YAP/TAZ mechanotransducers (two transcription factors that are mechanosensors) allowed quantitative and immediate read-outs of cellular mechanoresponsiveness to substrate stiffness. Cells seeded on soft hydrogels are round and presents YAP/TAZ localized in the cytoplasm and the ones seeded on progressively stiffer substrates are increasingly stretched and YAP/TAZ localized in their nuclei. Therefore, the achieved scales of PAA-OH and PEG-NB hydrogels tested allowed to induce a complete biologically significant behaviour of cells, because they induced stiffness-dependent responses on cells.

As further investigation, PEG cryogels were designed and synthetized as a material for the development of a cancer vaccine, to investigate if these biomaterials can be used in-vivo, maintain their cell adhesiveness and can be produced in a highly porous fashion to be accessible to the cell of the immune system. Different cryogels compositions have been investigated and characterized by SEM to investigate their microstructure. In particular, 4-arm-PEG acrylate cryogels functionalised by a ratio 1:8 with an RGD cell-adhesive peptide gave successfully results, showing interconnected and open macropores and cell-adhesiveness. This cryogels were successfully seeded with antigen presenting cells and implanted under skin in a mouse. The implantation didn't generate inflammatory reaction and the open and interconnected pores allowed macrophages to enter the cryogel. Moreover, these cryogels showed highly stretchability and shape memory, opening the possibility to use them as injectable vaccines.

Future works will be carried out by further testing of the reproducibility of the optimised method for both synthesis and hydrogel mechanical characterization. In addition, the range of stiffness and RGD concentration of these hydrogels may be expanded synthetizing more and less concentrated solutions, in order to used them with different types of cells which requires different range of relevant stiffness. In addition, thanks to the positive preliminary results achieved with cryogels for vaccine development, the immune response stimulated by cryogels seeded with antigen presenting cells will be tested.

# Bibliographic references


1. Kloxin AM, Tibbitt MW, Anseth KS. Synthesis of photodegradable hydrogels as dynamically tunable cell culture platforms. *Nat Protoc*. 2010;5(12):1867-1887. doi:10.1038/nprot.2010.139

2. Tse JR, Engler AJ. Preparation of hydrogel substrates with tunable mechanical properties. *Curr Protoc Cell Biol*. 2010;(SUPPL. 47):1-16. doi:10.1002/0471143030.cb1016s47

3. Paluch EK, Nelson CM, Biais N, et al. Mechanotransduction: Use the force(s). *BMC Biol*. 2015;13(1):1-14. doi:10.1186/s12915-015-0150-4

4. Jansen KA, Donato DM, Balcioglu HE, Schmidt T, Danen EHJ, Koenderink GH. A guide to mechanobiology: Where biology and physics meet. *Biochim Biophys Acta - Mol Cell Res*. 2015;1853(11):3043-3052. doi:10.1016/j.bbamcr.2015.05.007

5. Totaro A, Castellan M, Battilana G, et al. YAP/TAZ link cell mechanics to Notch signalling to control epidermal stem cell fate. *Nat Commun*. 2017;8(May):1-13. doi:10.1038/ncomms15206

6. Grevesse T, Versaevel M, Circelli G, Desprez S, Gabriele S. A simple route to functionalize polyacrylamide hydrogels for the independent tuning of mechanotransduction cues. *Lab Chip*. 2013;13(5):777-780. doi:10.1039/c2lc41168g

7. Halder G, Dupont S, Piccolo S. Transduction of mechanical and cytoskeletal cues by YAP and TAZ. *Nat Rev Mol Cell Biol*. 2012;13(9):591-600. doi:10.1038/nrm3416

8. Li Z, Lee H, Zhu C. Molecular mechanisms of mechanotransduction in integrin-mediated cell-matrix adhesion. *Exp Cell Res*. 2016;349(1):85-94. doi:10.1016/j.yexcr.2016.10.001

9. Janoštiak R, Pataki AC, Brábek J, Rösel D. Mechanosensors in integrin signaling: The emerging role of p130Cas. *Eur J Cell Biol*. 2014;93(10-12):445-454. doi:10.1016/j.ejcb.2014.07.002

10. Taylor MP, Koyuncu OO, Enquist LW. Subversion of the actin cytoskeleton during viral infection. *Nat Rev Microbiol*. 2011;9(6):427-439. doi:10.1038/nrmicro2574

11. Panciera T, Azzolin L, Cordenonsi M, Piccolo S. Mechanobiology of YAP and TAZ in physiology and disease. *Nat Rev Mol Cell Biol*. 2017;18(12):758-770. doi:10.1038/nrm.2017.87

12. Totaro A, Panciera T, Piccolo S. YAP/TAZ upstream signals and downstream responses. *Nat Cell Biol*. 2018;20(8):888-899. doi:10.1038/s41556-018-0142-z

13. Kim, S., Shah, S.B., Graney PL et al. Multiscale engineering of immune cells and lymphoid organs. *Nat Rev Mater*. 2019;4:355–378. https://doi.org/10.1038/s41578-019-0100-9.

14. Riley RS, June CH, Langer R, Mitchell MJ. Delivery technologies for cancer immunotherapy. *Nat Rev Drug Discov*. 2019;18(3):175-196. doi:10.1038/s41573-018-0006-z

15. The immune system Google books. https://books.google.it/books?id=Ph7ABAAAQBAJ&printsec=frontcover&hl=it&source=gbs_atb#v=onepage&q&f=false.

16. Wang H, Mooney DJ. Biomaterial-assisted targeted modulation of immune cells in cancer treatment. *Nat Mater*. 2018;17(9):761-772. doi:10.1038/s41563-018-0147-9

17. Bencherif SA, Sands RW, Bhatta D, et al. Injectable preformed scaffolds with shape-memory properties. *Proc Natl Acad Sci U S A*. 2012;109(48):19590-19595. doi:10.1073/pnas.1211516109

18. sciencedirect alginate. https://www.sciencedirect.com/topics/chemical-engineering/alginate.

19. Smeds KA, Grinstaff MW. Photocrosslinkable polysaccharides for in situ hydrogel formation. *J Biomed Mater Res*. 2001;54(1):115-121. doi:10.1002/1097-4636(200101)54:1<115::AID-JBM14>3.0.CO;2-Q

20. Shih TY, Blacklow SO, Li AW, et al. Injectable, Tough Alginate Cryogels as Cancer Vaccines. *Adv Healthc Mater*. 2018;7(10):1-26. doi:10.1002/adhm.201701469

21. Chou AI, Nicoll SB. Characterization of photocrosslinked alginate hydrogels for nucleus pulposus cell encapsulation. *J Biomed Mater Res - Part A*. 2009;91(1):187-194. doi:10.1002/jbm.a.32191

22. Yue K, Trujillo-de Santiago G, Alvarez MM, Tamayol A, Annabi N, Khademhosseini A. Synthesis, properties, and biomedical applications of gelatin methacryloyl (GelMA) hydrogels. *Biomaterials*. 2015;73:254-271. doi:10.1016/j.biomaterials.2015.08.045

23. GelMA. https://www.researchgate.net/figure/Synthesis-of-fish-gelatin-methacryloyl-GelMA-and-fabrication-of-photocrosslinked-GelMA_fig1_309001742.

24. Burdick JA, Chung C, Jia X, Randolph MA, Langer R. Controlled degradation and mechanical behavior of photopolymerized hyaluronic acid networks. *Biomacromolecules*. 2005;6(1):386-391. doi:10.1021/bm049508a

25. Liu SQ, Tay R, Khan M, Rachel Ee PL, Hedrick JL, Yang YY. Synthetic hydrogels for controlled stem cell differentiation. *Soft Matter*. 2009;6(1):67-81. doi:10.1039/b916705f

26. polymerization. https://www.sciencedirect.com/science/article/pii/S0091679X07830020.

27. Bhadani R, Mitra U. Synthesis and Characterization of Polyacrylamide Hydrogels. *Asian J Res Chem*. 2014;7(3):345-348.

28. Fedorchak GR, Kaminski A, Lammerding J. Cellular mechanosensing: Getting to the nucleus of it all. *Prog Biophys Mol Biol*. 2014;115(2-3):76-92. doi:10.1016/j.pbiomolbio.2014.06.009

29. Kandow CE, Georges PC, Janmey PA, Beningo KA. Polyacrylamide Hydrogels for Cell Mechanics: Steps Toward Optimization and Alternative Uses. *Methods Cell Biol*. 2007;83(07):29-46. doi:10.1016/S0091-679X(07)83002-0

30. Bruns J, McBride-Gagyi S, Zustiak SP. Injectable and Cell-Adhesive Polyethylene Glycol Cryogel Scaffolds: Independent Control of Cryogel Microstructure and Composition. *Macromol Mater Eng*. 2018;303(10):1-15. doi:10.1002/mame.201800298

31. Singh SP, Schwartz MP, Lee JY, Fairbanks BD, Anseth KS. A peptide functionalized poly(ethylene glycol) (PEG) hydrogel for investigating the influence of biochemical and biophysical matrix properties on tumor cell migration. *Biomater Sci*. 2014;2(7):1024-1034. doi:10.1039/c4bm00022f

32. Schultz KM, Anseth KS. Monitoring degradation of matrix metalloproteinases-cleavable PEG hydrogels via multiple particle tracking microrheology. *Soft Matter*. 2013;9(5):1570-1579. doi:10.1039/c2sm27303a

33. Singh SP, Schwartz MP, Tokuda EY, et al. A synthetic modular approach for modeling the role of the 3D microenvironment in tumor progression. *Sci Rep*. 2015;5(December):1-9. doi:10.1038/srep17814

34. Rogers ZJ, Bencherif SA. Cryogelation and cryogels. *Gels*. 2019;5(4):6-7. doi:10.3390/gels5040046

35. Bencherif SA, Sands RW, Ali OA, et al. Injectable cryogel-based whole-cell cancer vaccines. *Nat Commun*. 2015;6(May):1-13. doi:10.1038/ncomms8556

36. PEGDA. https://www.sigmaaldrich.com/catalog/substance/polyethyleneglycoldiacrylate123452657048911?lang=it&region=IT.

37. Zhang MG, Cao YP, Li GY, Feng XQ. Pipette aspiration of hyperelastic compliant materials: Theoretical analysis, simulations and experiments. *J Mech Phys Solids*. 2014;68(1):179-196. doi:10.1016/j.jmps.2014.03.012

38. Caccavo D, Cascone S, Lamberti G, Barba AA. Hydrogels: Experimental characterization and mathematical modelling of their mechanical and diffusive behaviour. *Chem Soc Rev*. 2018;47(7):2357-2373. doi:10.1039/c7cs00638a

39. Kloxin AM, Kloxin CJ, Bowman CN, Anseth KS. Mechanical properties of cellularly responsive hydrogels and their experimental determination. *Adv Mater*. 2010;22(31):3484-3494. doi:10.1002/adma.200904179

40. Zuidema JM, Rivet CJ, Gilbert RJ, Morrison FA. A protocol for rheological characterization of hydrogels for tissue engineering strategies. *J Biomed Mater Res - Part B Appl Biomater*. 2014;102(5):1063-1073. doi:10.1002/jbm.b.33088

41. tainstruments. www.tainstruments.com.

42. Yan C, Pochan DJ. Rheological properties of peptide-based hydrogels for biomedical and other applications. *Chem Soc Rev*. 2010;39(9):3528-3540. doi:10.1039/b919449p

43. Ahearne M, Yang Y, Liu K. Mechanical Characterisation of Hydrogels for Tissue Engineering Applications. *Tissue Eng*. 2008;4(June):1-16. http://www.oulu.fi/spareparts/ebook_topics_in_t_e_vol4/abstracts/ahearne.pdf.

44. Broitman E. Indentation Hardness Measurements at Macro-, Micro-, and Nanoscale: A Critical Overview. *Tribol Lett*. 2017;65(1):1-18. doi:10.1007/s11249-016-0805-5

45. Long R, Hall MS, Wu M, Hui CY. Effects of gel thickness on microscopic indentation measurements of gel modulus. *Biophys J*. 2011;101(3):643-650. doi:10.1016/j.bpj.2011.06.049

46. Frey MT, Engler A, Discher DE, Lee J, Wang YL. Microscopic Methods for Measuring the Elasticity of Gel Substrates for Cell Culture: Microspheres, Microindenters, and Atomic Force Microscopy. *Methods Cell Biol*. 2007;83(07):47-65. doi:10.1016/S0091-679X(07)83003-2

47. Yang Y, Bagnaninchi PO, Ahearne M, Wang RK, Liu KK. A novel optical coherence tomography-based micro-indentation technique for mechanical characterization of hydrogels. *J R Soc Interface*. 2007;4(17):1169-1173. doi:10.1098/rsif.2007.1044

48. Hu Y, You JO, Auguste DT, Suo Z, Vlassak JJ. Indentation: A simple, nondestructive method for characterizing the mechanical and transport properties of pH-sensitive hydrogels. *J Mater Res*. 2012;27(1):152-160. doi:10.1557/jmr.2011.368

49. Evans EA. Bending elastic modulus of red blood cell membrane derived from buckling instability in micropipet aspiration tests. *Biophys J*. 1983;43(1):27-30.

doi:10.1016/S0006-3495(83)84319-7

50. Aoki T, Ohashi T, Matsumoto T, Sato M. The pipette aspiration applied to the local stiffness measurement of soft tissues. *Ann Biomed Eng*. 1997;25(3):581-587. doi:10.1007/BF02684197

51. Hochmuth RM. Micropipette aspiration of living cells. *J Biomech*. 2000;33(1):15-22. doi:10.1016/S0021-9290(99)00175-X

52. Zhao R, Sider KL, Simmons CA. Measurement of layer-specific mechanical properties in multilayered biomaterials by micropipette aspiration. *Acta Biomater*. 2011;7(3):1220-1227. doi:10.1016/j.actbio.2010.11.004

53. Lin CC, Raza A, Shih H. PEG hydrogels formed by thiol-ene photo-click chemistry and their effect on the formation and recovery of insulin-secreting cell spheroids. *Biomaterials*. 2011;32(36):9685-9695. doi:10.1016/j.biomaterials.2011.08.083

54. Ding Y, Wang GF, Feng XQ, Yu SW. Micropipette aspiration method for characterizing biological materials with surface energy. *J Biomech*. 2018;80:32-36. doi:10.1016/j.jbiomech.2018.08.020

55. Dimitriadis EK, Horkay F, Maresca J, Kachar B, Chadwick RS. Determination of elastic moduli of thin layers of soft material using the atomic force microscope. *Biophys J*. 2002;82(5):2798-2810. doi:10.1016/S0006-3495(02)75620-8

56. Brusatin G, Panciera T, Gandin A, Citron A, Piccolo S. Biomaterials and engineered microenvironments to control YAP/TAZ-dependent cell behaviour. *Nat Mater*. 2018;17(12):1063-1075. doi:10.1038/s41563-018-0180-8

# Aknowledgements

# Ringraziamenti

A conclusione di questo lavoro che mi ha impegnano diversi mesi, vorrei ringraziare alcune persone che hanno avuto un ruolo fondamentale in questa esperienza. Innanzitutto, desidero ringraziare la Prof.ssa Giovanna Brusatin, mia relatrice, e Alessandro Gandin che mi hanno seguito e guidato nell'attività di laboratorio con quotidiana disponibilità. Inoltre, vorrei ringraziare il laboratorio del Prof. Stefano Piccolo con cui si è avuta una stretta collaborazione e che mi ha permesso in primo luogo di svolgere il lavoro di questa tesi di laurea. Voglio inoltre ringraziare la Prof.ssa Lucia Nicola, il Prof. Paolo Sgarbossa e la Prof. Katia Brunelli per il loro supporto professionale e i consigli dispensati. Ringrazio i miei genitori che mi hanno permesso di intraprendere questo percorso universitario e hanno creduto in me supportandomi in questi anni universitari. Infine, vorrei ringraziare Damiano, una persona speciale con cui ho affrontato questi mesi con felicità, forza ed entusiasmo.